

UNIVERSITY OF KWAZULU-NATAL
COLLEGE OF AGRICULTURE, ENGINEERING AND SCIENCE

**DESIGN AND PERFORMANCE ANALYSIS OF HYBRID
PHOTOVOLTAIC-THERMAL GRID CONNECTED SYSTEM
FOR RESIDENTIAL APPLICATION**

by

Ntumba Marc-Alain Mutombo

Dissertation submitted in fulfillment of the academic requirements for the degree of Master of Science in
Mechanical Engineering

Supervisor: Doctor Freddie L. Inambao

Co-Supervisor: Professor Glen Bright

20th November 2012

“As the candidate’s Supervisor I agree/~~do not agree~~ to the submission of this dissertation”. The supervisor must sign all copies after deleting which is not applicable.

.....

NAME OF SUPERVISOR SIGNATURE

DECLARATION 1 - PLAGIARISM

I, **Ntumba Marc-Alain Mutombo**, declare that:

1. The research reported in this dissertation, except where otherwise indicated, is my original research.
2. This dissertation has not been submitted for any degree or examination at any other university.
3. This dissertation does not contain other persons' data, pictures, graphs or other information, unless specifically acknowledged as being sourced from other persons.
4. This dissertation does not contain other persons' writing, unless specifically acknowledged as being sourced from other researchers. Where other written sources have been quoted, then:
 - a. Their words have been re-written but the general information attributed to them has been referenced.
 - b. Where their exact words have been used, then their writing has been placed in italics and inside quotation marks, and referenced.
5. This dissertation does not contain text, graphics or tables copied and pasted from the Internet, unless specifically acknowledged, and the source being detailed in the dissertation and in the References sections.

Signed

.....

DECLARATION 2 - PUBLICATIONS

DETAILS OF CONTRIBUTION TO PUBLICATIONS that form part and/or include research presented in this dissertation (include publications in preparation, submitted, *in press* and published and give details of the contributions of each author to the experimental work and writing of each publication).

Publication 1: ***Ntumba Marc-Alain Mutombo, Inambao F.L.***: Temperature Evaluation and Energy Estimation of Photovoltaic Module by Simulation, *Proceedings of 12th Botswana Institution of Engineers Biennial Conference, CD Rom, 14-16 September, 2011, Gaborone, Botswana, pp. 249-254.*

Publication 2: ***Ntumba Marc-Alain Mutombo and Freddie L. Inambao***: Photovoltaic Panel Temperature and Power Output Analysis Tool, *R & D Journal of the South African Institution of Mechanical Engineering 2012, 28, 12-20, (In Press)*

Publication 3: ***Ntumba Marc-Alain Mutombo, Dr Freddie Inambao and Prof Glen Bright***: Performance Analysis of Thermosyphon Hybrid Photovoltaic Thermal Collector, *Journal of Energy of Southern Africa, (Submitted and under review)*

In all these papers, I Ntumba Marc-Alain Mutombo was the main and corresponding author, whilst Dr Freddie L. Inambao and Prof Glen Bright were the co-authors and my research supervisor and co-supervisor, respectively.

Signed:

.....

ACKNOWLEDGEMENTS

I would particularly like to thank my supervisor Dr Freddie L. Inambao for his enthusiasm, encouragement, persistent support and guidance in all aspects throughout the whole research work. My gratitude is also due to Prof. Glen Bright who agreed to be my second supervisor, for his advice and guidance.

This dissertation is not only a result of my own devotion and determination, but is largely a credit to my wife Sidonie Mangabu, my sweet daughter Pricilla Mwa-Mujinga, my son Ethaniel Mutombo, my son Emmanuel Ilunga, my father Polycarpe Mutombo, my mother Therese Mujinga, my father-in-law Jean-Patrice Ilunga, my mother-in-law Bernadette Luendu, my brother Jean-Claude Mutombo, my brother Jean-Pierre Tshiunza, my friend Erick Bizala and my other relatives for their love, encouragement and support.

I would also like to acknowledge the financial assistance of the Centre for Engineering Postgraduate Studies (CEPS) for funding me during my stay at UKZN and in particular, Prof. Nelson M. Ijumba and Charlaine King. I would also like to express my heartfelt thanks to all my colleagues in the Green Energy Solutions Research Group (GES) for making helpful suggestions throughout the duration of my studies.

ABSTRACT

High output electrical energy is obtained from photovoltaic (PV) systems subject to high irradiance. However, at high irradiance, the efficiency of PV systems drops due to increase of the temperature of the systems. In order to improve the efficiency of photovoltaic systems, much effort has been spent on developing hybrid photovoltaic thermal (PVT) systems using water as a coolant to withdraw heat from solar modules.

This research is focused on the study of the behavior of hybrid PVT collectors using rectangular channel profiles which provide a large surface for heat exchange between PV panels and thermal collectors unlike the circular channel profile used in conventional PV systems. In hybrid PVT systems, coolant water circulates in a closed circuit by means of the thermosyphon phenomenon and the heat from this water is extracted from a storage tank and can be used in hot water systems instead of an electric geysers.

Numerical models of water velocity in channels due to the thermosyphon phenomenon and the temperature of solar modules was developed and a system was designed for modest Durban household demand. A simulation was run for specific summer and winter days comparing a conventional PV system and a hybrid PVT system. The results were very encouraging, and demonstrated that the equipment is capable of extending the PVT application potential in the domestic sector where more than 40% of electricity cost is heating water.

Key words: Hybrid solar collector; Thermosyphon; Photovoltaic; Array system; Household demand.

TABLE OF CONTENTS

CHAPTER ONE INTRODUCTION	1
1.1 Background.....	1
1.1.1 South Africa electricity production	1
1.1.2 Electricity crisis in South Africa	2
1.1.3 Electricity crisis strategic plan	2
1.1.4 Coal and environmental impact.....	3
1.1.5 South Africa solar irradiance and tilt angle.....	3
1.1.6 Hybrid photovoltaic thermal (PVT) module	4
1.2 Objectives of this research.....	6
1.3 Research questions	7
1.4 Dissertation layout	7
CHAPTER TWO SOLAR INSOLATION AND MODELING THEORIES	10
2.1 Solar insolation on tilted surface.....	10
2.2 Modeling theories	13
2.2.1 The differential continuity equation	13
2.2.2 The differential momentum equation	14
2.2.3 The differential energy equation	14
2.3 Solutions of differential equations	15
2.3.1 Fourier series.....	15
2.3.2 Numerical methods and finite difference method	16
CHAPTER THREE CONVENTIONAL PHOTOVOLTAIC SYSTEMS.....	19
3.1 Development of photovoltaic systems.....	19
3.2 Basic semiconductor physics	19
3.2.1 The Band Gap Energy	19
3.2.2 The p–n junction.....	20
3.3 Photovoltaic cells	22
3.3.1 A generic photovoltaic cell.....	22

3.3.2 Generalised equivalent circuit for a PV cell	26
3.4 Photovoltaic module.....	30
3.4.1 From cells to a module	31
3.4.2 Modeling of photovoltaic module	31
3.5 The PV I-V curve under standard test conditions (STC).....	32
3.6 Impacts of temperature and insolation on I-V curves	35
3.7 Determination of cell temperature and average efficiency	37
3.7.1 Determination of cell temperature.....	37
3.7.2. Calculation of average efficiency	38
 CHAPTER FOUR THERMOSYPHON PRINCIPLE AND FLUID VELOCITY IN RECTANGULAR CHANNELS	 40
4.1 Variation of density with temperature variation	40
4.2 Determination of velocity of the fluid in channels.....	42
 CHAPTER FIVE THERMOSYPHON HYBRID PHOTOVOLTAIC THERMAL SYSTEM ..	 47
5.1 Description and principle of operation of PVT systems.....	48
5.2 Determination of the thermal collector temperature	49
5.3 Determination of the temperature of the water storage tank.....	57
5.3.1 Tank geometry	57
5.3.2 Temperature of the water in the tank.....	58
 CHAPTER SIX PVT SYSTEM BEHAVIOR AGAINST VARIATION OF ENVIRONMENTAL PARAMETERS.....	 66
6.1 PVT system behaviors against the variation of insolation.....	66
6.2 The influence of ambient temperature on performance of the PVT system	69
6.3 PVT system behaviors against the variation of wind velocity.....	72
 CHAPTER SEVEN DESIGN OF THERMOSYPHON HYBRID GRID CONNECTED PHOTOVOLTAIC SYSTEM FOR DURBAN MODEST HOUSEHOLD	 75

7.1 Load determination	75
7.2 Grid connected photovoltaic array sizing	76
7.2.1 PV generator	76
7.2.2 Cable sizing and over-current protection	81
7.3 Thermal collector and water tank.....	88
7.3.1 The design of thermal absorber	88
7.3.2 Design of water tank.....	89
7.4 The Design summary	90
CHAPTER EIGHT GRID CONNECTED PVT SYSTEM SIMULATIONS.....	91
8.1 Description of dynamical simulation tool program.....	91
8.2 Simulation results.....	92
CHAPTER NINE GRID-CONNECTED PV AND PVT SYSTEMS ECONOMICS	98
9.1. Cost of PV and PVT systems and energy delivery	98
9.2 Loan terms and income tax	101
9.3 Systems finance	101
CHAPTER TEN CONCLUSION AND RECOMMENDATIONS.....	106
10.1 Conclusion	106
10.2 Recommendations	107
REFERENCES	109
APPENDICES	114
Appendix A: The Newton Raphson’s method.....	114
Appendix B: Heat transfer coefficients.....	115
Appendix C: Dimensionless coefficients	118

Appendix D: Eskom Residential Tariff.....	119
Appendix E: Q cells and Q PEAK Module characteristics	120
Appendix F: Sunny Boy 3000TL/ 4000TL / 5000TL Characteristics	124
Appendix G: NASA insolation data for Durban.....	126
Appendix H: Table 310.17 Allowable Ampacities of Single-Insulated Conductors Rated 0 Through 2000 Volts in Free Air, Based on Ambient Air Temperature of 30°C (86°F).....	128
Appendix I: NEC 240.6 Standard Ampere Ratings	131
Appendix J: Graphical results from simulation of PV and PVT arrays systems	132
Appendix K: Numerical results from simulation of PV and PVT arrays systems for particular days	135
Appendix L: Annual Cash Flow for Systems	143

LIST OF FIGURES

Figure 2.1: The extraterrestrial spectrum and the spectrum of a blackbody at 5800 K.	11
Figure 2.2: Light incident on a surface tilted to the horizontal	12
Figure 2.3: Finite difference formulation for time-dependent problems.....	17
Figure 2.4: The formulation of explicit and implicit methods	18
Figure 3.1: Photon energy against Wavelength	20
Figure 3.2: A p-n junction (a) When first brought together and (b) In steady-state	21
Figure 3.3: Illustration of the p-n junction of PV cell	22
Figure 3.4: Side view of solar cell and the conducting current.....	23
Figure 3.5: A simple equivalent circuit for a photovoltaic cell with load connected.....	23
Figure 3.6: Short-circuit current and Open-circuit voltage for a PV cell.....	24
Figure 3.7: Complex equivalent circuit for a PV cell	26
Figure 3.8: A simplified equivalent circuit for a PV cell	28
Figure 3.9: A typical laminated module structure.....	30
Figure 3.10: Photovoltaic cells, modules and an array	30
Figure 3.11: Q6LMX3 Solar cells wired in series at STC simulated with the Matlab model.....	31
Figure 3.12: PV module at different states.....	32
Figure 3.13: PV module and Load characteristic curves	33
Figure 3.14: Q PEAK PV module I-V and P-V characteristic curves at STC simulated with Matlab	33
Figure 3.15: Q PEAK PV module I-V curve at STC simulated with Matlab	34
Figure 3.16: Current-voltage characteristic curves for PV module under various irradiance levels at 25°C temperature and 1m/s wind velocity simulated with the Matlab	36
Figure 3.17: Current-voltage characteristic curves for PV module under various cell temperature levels at 1kW/m ² insolation and 1m/s wind velocity simulated with Matlab	36
Figure 3.18: Power-voltage curve of PV module at STC and power-voltage curve.....	37
Figure 4.1: Newtonian fluid flowing in rectangular channel	41
Figure 4.2: 3D view of velocity profile in channels simulated with Matlab.....	45
Figure 4.3: a-b and b-w views of water velocity profile in rectangular channels	46
Figure 5.1: Hybrid photovoltaic thermal system.....	47

Figure 5.2: PV module above thermal absorber.....	48
Figure 5.3: Cross-section view of the Photovoltaic Thermal absorber	49
Figure 5.4: PV module input and output energies.....	50
Figure 5.5: Upper channel wall input and output energies	52
Figure 5.6: Channel water input and output energies.....	54
Figure 5.7: A volume element of water in thermal collector channel.....	54
Figure 5.8: Tank divided into five nodes	58
Figure 5.9: Six nodes from five layers for the water tank.....	59
Figure 5.10: Exterior node 0 input and output energies.....	60
Figure 5.11: Interior node j input and output energies.....	61
Figure 5.12: Exterior node 5 input and output energies.....	62
Figure 6.1: PVT module behaviors for variation of solar irradiance at ambient temperature 25°C and wind speed 1m/s.....	66
Figure 6.2: Electrical efficiency behaviors for variation of solar irradiance at ambient temperature 25°C and wind speed 1m/s for PVT module compared to PV module	67
Figure 6.3: Maximum Power point behaviors for variation of solar irradiance at ambient temperature 25°C and wind speed 1m/s for PVT module compared to PV module	68
Figure 6.4: Water tank temperature for variation of solar irradiance at ambient temperature 25°C and wind speed 1m/s for PVT module.....	69
Figure 6.5: Cell temperature behaviors against the variation of ambient temperature for PV module and PVT module at 1000w/m ² insolation and 1m/s wind speed.....	70
Figure 6.6: Electrical efficiency behaviors against the variation of ambient temperature for PV module and PVT module at 1000w/m ² insolation and 1m/s wind speed	70
Figure 6.7: Water tank temperature for variation of ambient temperature for PV module and PVT module at 1000w/m ² insolation and 1m/s wind speed.....	71
Figure 6.8: Cell temperature behaviors for the variation of wind velocity for PV module and PVT module at 1000w/m ² insolation and 25°C ambient temperature	72
Figure 6.9: Electrical efficiency behaviors for the variation of wind velocity for PV module and PVT module at 1000w/m ² insolation and 25°C ambient temperature	73
Figure 6.10: Water tank temperature for the variation of wind velocity for PVT module at 1000W/m ² insolation and 25°C ambient temperature.....	73

Figure 7.1: Large grid-connected system using an individual inverter for each string	78
Figure 7.2: Electrical drawing of the system design for the Durban modest household demand	87
Figure 8.1: Environmental parameters for summer day of 04/12/2010	92
Figure 8.2: PV and PVT solar cell temperatures for summer day of 04/12/2010	93
Figure 8.3: PV and PVT arrays electrical efficiencies for summer day of 04/12/2010	94
Figure 8.4: Storage tank temperature for summer day of 04/12/2010	94
Figure 8.5: PV and PVT arrays MPP for summer day of 04/12/2010	95
Figure 9.1: Average cost of residential PV systems for Durban modest household demand	99
Figure 9.2: Average cost of residential PVT systems for Durban modest household demand ..	100
Figure 9.3: PV system and PVT system loan balance and loan interest over 20 years.....	104
Figure 9.4: PV system and PVT system variation of electricity cost over 20 years	104
Figure 9.5: PV system and PVT system tax savings over 20 years	105

LIST OF TABLES

Table 7.1: Daily electrical use and kWh used per month for modest household	76
Table 7.2: Array description	81
Table 7. 3: Wire sizing specification.....	86
Table 7.4: Switches and protection components for grid connected a PVT system for Durban modest household demand	88
Table 7.5: Hybrid Grid Connected PVT System Components	90
Table 8.1: Summary of the results from simulation for PV and PVT systems.....	97
Table 9.1: PV and PVT components cost	98
Table 9.2: The tax rates applicable to individuals for the tax year 2012/2013	101
Table 9.3: System electricity cost and net economic benefit in the first year	103

NOMENCLATURE

Roman

<i>A</i>	Ideal factor; surface, area [m^2]
<i>a</i>	Fourier coefficient for cosines functions
<i>b</i>	Fourier coefficient for sinus functions; higher of the channel [m]
<i>C</i>	Specific heat capacity [$\text{J}/(\text{kg } ^\circ\text{C})$]
<i>D</i>	Diffuse component of solar insolation on the horizontal surface [$\text{kWh}/\text{m}^2\text{day}$]
<i>d</i>	Day number [-]
<i>E</i>	Electrical energy output [W or W/m^2]
<i>E_g</i>	Band gap [eV]
<i>f</i>	Function
<i>G</i>	Global insolation on the horizontal ($\text{kWh}/\text{m}^2\text{day}$)
<i>g</i>	Acceleration due to gravity [m/s^2]
<i>H</i>	Heat [W/m^2]
<i>h</i>	Convective heat transfer coefficient [$\text{W}/\text{m}^2\text{K}$]
<i>I</i>	Current [A]
<i>k</i>	Boltzmann's constant [J/K]; conductive heat transfer coefficient [$\text{W}/(\text{m K})$]
<i>L</i>	Length [m]
<i>m</i>	Simplification coefficient of the numerator of the anti-derivative function of the left hand side of a differential equation of first order [-]; Positive integer
<i>n</i>	Positive integer

p	Pressure [N/m ²]
Q	Volume of the fluid discharged [m ³ /s]
q	Electron charge [C]
R	Resistance [Ω]
S	Direct component of solar insolation on the horizontal surface [kWh/m ² day]; Simplification coefficient of the numerator of right hand side of a differential equation of first order [-]
T	Period of Fourier function [1/s]; temperature [$^{\circ}$ C or K]
t	Time [s]
U	Overall heat transfer coefficient [W/m ² K]
V	Voltage [V]; volume [m ³]; velocity [m/s]
w	Component of velocity in z direction [m/s]
X	Function of x as variable
x	Rectangular coordinate in x direction
Y	Function of y as variable
y	Rectangular coordinate in y direction
z	Rectangular coordinate in z direction

Greek Symbols

α	Absorptivity [-]; altitude of the sun [$^{\circ}$]
β	Southern latitude [$^{\circ}$]; Temperature coefficient [1/K]; Volumetric thermal-expansion coefficient [1/K]

Γ	Ratio of reference efficiency per temperature coefficient [K]
γ	Solar irradiance coefficient [m^2/W]
δ	Declination of the sun [$^\circ$]; thickness [m]
Δ	Difference, increment
ε	Earth's inclination [$^\circ$]
η	Efficiency [%]
θ	Tilt angle [$^\circ$]
λ	Temperature coefficient [$1/\text{K}$]; coefficient of proportionality between current and irradiance [$\text{A m}^2/\text{W}$]; constant [-]
μ	Dynamic viscosity [kg/ms]
ξ	Dimensionless coefficient [-]
ρ	Density [kg/m^3]
τ	Transmittivity [-]

Subscripts

a	Ambient
abs	Absorbed
ac	Alternative current
b	Back
c	Solar cell
$cond$	Conducted
$conv$	Convected

<i>D</i>	Diametric
<i>d</i>	Diode
<i>dc</i>	Direct current
<i>eff</i>	Effective
<i>f</i>	Fluid
<i>g</i>	Glass; Gap
<i>h</i>	Height
<i>i</i>	Time step; Inlet; Interest [Rand]
<i>L</i>	Light
<i>lcw</i>	Lower channel wall
<i>m</i>	Maximum; mean
<i>o</i>	Reverse saturation; outlet
<i>oc</i>	Open-circuit
<i>p</i>	Parallel; Constant pressure [Pa]; Particular solution
<i>ph</i>	Photon
<i>r</i>	Reference
<i>rad</i>	Radiated
<i>s</i>	Series
<i>sc</i>	Short circuit
<i>sh</i>	Shunt
<i>T</i>	Tedlar
<i>t</i>	Tank

<i>trans</i>	Transmitted
<i>u</i>	Upper
<i>ucw</i>	Upper channel wall
<i>w</i>	Wind
<i>x</i>	x direction
<i>y</i>	y direction
<i>z</i>	z direction

Superscripts

<i>i</i>	Time step for implicit finite difference method
----------	-------------------------------------------------

ACRONYMS AND ABBREVIATIONS

AM	Air Mass
CE	Cost of Electricity
CRF	Capital Recovery Factor
ER	Energy Rebate
FDM	Finite Difference Method
FEM	Finite Element Method
FF	Fill Factor
FVM	Finite Volume Method
GDP	Gross Domestic Product
GRADRAD	Greater Durban Radiometric
HMDE	Highest Minimum Daily Energy
HYE	Highest Yearly Energy
IPVTS	Integrated Photovoltaic and Thermal Solar System
MatLab	Matrix Laboratory
MPP	Maximum Power Point
MPPT	Maximum Power Point Tracking
MTB	Marginal Tax Bracket
NARSA	National Energy Regulator South Africa
NCS	Net Cost of the System
NEB	Net Economic Benefit

NEC	National Electrical Code
NM	Non-Metallic
NOCT	Normal Operating Cell Temperature
PER	Public Electricity Rate
PF	Packing Factor
PN	pn junction
PPP	Purchasing Power Parity
PV	Photovoltaic
PVT	Photovoltaic Thermal
rms	root mean square
SC	System Cost
SEP	System Energy Predicted
SMA	System-, Mess-und Anlagentechnik (Control, Measuring and Equipment Technology)
SNP	System Nominal Power
STC	Standard Test Condition
SUNSIM	Sun Simulator
THHN	Thermoplastic Heat and Water-Resistant Nylon-coated
TS	Tax Savings

CHAPTER ONE

INTRODUCTION

1.1 Background

The International Energy Agency reported that in 2008 more than 1.5 billion people did not have access to electricity (1). Over 85% of this total are rural residents, with the majority of them living in remote areas of developing countries (2).

South African demand and production of electricity is covered in this chapter. The solar insolation available in the South African market, the optimum tilt angle for solar systems in South Africa and the evolution of Hybrid Photovoltaic Thermal systems are also covered. The chapter is completed with presentation of the objectives of this study, the research questions and the dissertation layout.

1.1.1 South Africa electricity production

In the next 25 years, the world electricity demand is expected to increase rapidly particularly in emerging countries. As one of lowest cost energy sources, coal is likely to remain one of the most important energy sources (3).

With a gross domestic product (GDP) of US\$ 495 billion based on purchasing power parity, South Africa is the most industrialized nation in Africa with a population of 48 million over 1.2 million km² (1). South Africa has vast natural resources of coal, gold and diamonds, and the country's use of electricity is the highest in Africa due to its mining industries (2).

Using its own coal resources and intensive public sector investment in generation and transmission, the price of electricity in South Africa is one of the lowest in the world (4). Even though the country is one of the most highly electrified country in Africa, only 75% of the population have regular access to electrical energy (2).

The South African public utility company Eskom which is the largest producer of electricity in Africa, is also ranked amongst the top seven utilities in the world producing electrical energy. Eskom operates a number of notable power stations including Kendal Power Station, one of the largest coal-fired power stations in the world (5). Unfortunately, this technology has significant environmental implications such as the depletion of natural resources, global environmental impacts and local/global pollution with adverse effects on human health and ecosystems (3).

1.1.2 Electricity crisis in South Africa

The provision of electrical energy in any society is an important public service, and can be seen as an essential right in the context of social equity and justice. Access to electricity promotes social integration and accessibility of other essential services. In South Africa where 40% of the population is poor, it is necessary to analyse the program of electrification for provision of universal access to electricity for poor and rich alike, and the impact this has on the economy (2).

Since 1994, the desire of the government to ensure universal access to electricity and the economic impact have increased South African electricity demand at the rate of 4% per year (4). By 2007, South Africa's electricity reserve (the difference between electricity generation and demand) had dropped from 25% in 2001 to between 8% and 10% (4). Since 2007, Eskom has been unable to meet the demand for electricity (6). This electricity over demand compared to supply had a negative impact on the South African government objective of growing the economy at 6% per year between 2010 and 2014 (4). In 2008, South Africa experienced a major electricity disaster. All fields of use endured black outs all over the country resulting in substantial economic loss. The National Energy Regulator of South Africa (NERSA) revealed that 50 billion Rands was lost to the economy because of the black outs (6).

1.1.3 Electricity crisis strategic plan

To improve the inadequate electricity capacity, Eskom planned to spend 343 billion Rands between 2008 and 2013. With the objective of boosting economic growth by increasing electricity demand by 4% per year, an extra 1.3 trillion Rands will be required by Eskom until 2025 to provide the infrastructure to meet the increasing demand (4).

To deal with electricity demand and supply and to support of energy conservation, Eskom and the government decided that electricity tariffs should be used as a strategic instrument. Based on forecasts, the demand for electricity will drop after the tariff increases promoted by Eskom and NERSA become a reality (6). In the third quarter of 2009, Eskom made representation to NERSA for an augmentation of the electricity tariffs to fund their present and future plans. At the end of September 2009, NERSA's decision was published: an approximate 25% increase of the electricity tariff per year over the next three years (7).

1.1.4 Coal and environmental impact

Rafey and Sovacool investigated the project for building Medupi coal fired power plant project and found that the plant would produce 4800MW of electricity but at the same time generate about 30 million annual metric tons of CO₂ which is equivalent to the greenhouse gas emission of the 63 lowest emitting countries combined (8).

The emission of pollutant gas and particles while producing energy from coal causes damage to the environment and society, not only in the areas surrounding the power plants but also faraway zones, including neighboring countries (9).

1.1.5 South Africa solar irradiance and tilt angle

The position of the sun in the sky changes over the course of the year. One of the ways to improve the efficiency of energy output of solar systems such as photovoltaic panels, solar water heaters and building thermal mass is to tilt the panels at the optimum angle according to the time of year (10).

South Africa's optimum tilt angle does not follow the latitudinal gradient. It increases from about 24° in the Northern part of the country towards Southeast, where it reaches values up to 35° (11). For Durban, Bellingham, Davies and Human propose the best angle for overall annual solar energy harvesting to be 35° to the horizontal (10).

There are two ways to position solar energy converter devices: the fixed system and the tracking system. The tracking system follows the daily displacement of the sun to maximize the solar insolation received while the fixed system is fixed at the same position for whole the year, either to deliver the highest yearly energy (HYE) e.g. grid-connected PV arrays or to deliver the highest minimum daily energy (HMDE) through the year e.g. for battery charging purposes.

For Durban, Becker proposes an optimal elevation tilt angle of 30° HYE (12). Zawilska and Brooks, recorded and analyzed solar radiometry and selected meteorological parameters for Durban over a full one-year period from January to December 2007, based on flat-plate collectors tilted at an angle equal to the latitude 29.867° south. They found a 13% increase in energy availability, confirming the value of an appropriate tilt angle in Durban (13).

1.1.6 Hybrid photovoltaic thermal (PVT) module

A photovoltaic system or PV system alone produces electrical energy by converting solar insolation reaching it. Less than 20% of insolation is converted into electricity. Part of the remaining insolation is converted into heat and part is reflect to the surroundings. The part converted into heat can be collected and used to produce hot water or warm air. A photovoltaic panel can be combined with a thermal absorber into one unit which is a hybrid photovoltaic thermal system or PVT system to produce both electricity and hot water/warm air.

Theoretical and experimental studies of PVT were carried out as early as the mid 1970s (14). In 1954 Chapin, Fuller and Pearson developed the first photovoltaic solar cell capable of converting enough solar insolation into electricity to run everyday electrical equipment. Later, Bell telephone laboratory made a silicon solar cell with 4% efficiency later improving efficiency to 11% (15).

The Institute of Energy Conversion was created at the University of Delaware (United States) in 1972 to design and develop the thin-film photovoltaic and solar thermal systems (16). In 1973, one of the world's first photovoltaic powered houses was made by the University of Delaware using a PVT hybrid system. The system was a roof-integrated array supplying excess electrical energy produced during the day to the utility and buying power at night from the utility. In

addition to electricity, the arrays acted as flat-plate thermal collectors, with fans blowing the warm air from over the arrays to phase change heat storage bins (16).

In 1976, Wolf analyzed the performance of a silicon solar array mounted inside a stationary flat plate collector using a lead-acid battery as the storage element (17). In 1979, Florschuetz presented a simple model for preliminary assessment of cooling system requirements for heat rejection from solar cells subjected to concentrated solar irradiation levels. Analysis of flat plate collectors from a Hottel-Whillier model for thermal collector was extended to the assessment of combined photovoltaic/thermal collectors and their efficiencies. Based on the extended model, examples of both thermal and electrical performance of a combined collector as a function of collector design parameters were presented and discussed (18).

In 1981, two separate one-dimensional analyses were developed for the prediction of the thermal and electrical performance of both liquid and air flat-plate photovoltaic/thermal (PVT) collectors (19). Four years later, several potentially useful features in the design of photovoltaic/thermal (PVT) collectors were explored in order to determine their effectiveness and interaction (20).

In 1994, the hybrid photovoltaic thermal system based on natural convection of water in a thermal absorber fitted with circular channel tubes was studied and experiments were conducted for several days on a thermal collector alone. A finite difference method (FDM) was used to model and simulate the performance of the thermal collector (21). In order to understand and evaluate the solar hybrid systems, an experimental study was performed (22). One year later, Garg performed the study of a hybrid forced circulation photovoltaic and thermal system and developed a mathematical model for the system using the finite difference method (23). The algorithms for making quantitative predictions on the performance of the system were established by Bergene and Lovvik after proposing a detailed physical model of a hybrid photovoltaic thermal system (24).

In 2001, Huang *et al.* studied the performance of an integrated photovoltaic and thermal solar system (IPVTS) compared to a conventional solar water heater and demonstrated the idea of an IPVTS design (25). In 2002, a hybrid PVT unit that simultaneously produced low temperature heat and electricity was made from the combination of mono crystalline silicon photovoltaic

cells with a polymer solar heat collector (26). Four numerical models were built for the simulation of the thermal yield of a combined PVT collector (27).

In 2003, Zondag evaluated nine different designs of combined PV thermal collectors in order to obtain a clearer view of the projected efficiency of the different concepts (28). The same year, Chow established an explicit dynamic model for a single-glazed flat plate water heating PVT collector based on the control volume finite difference approach (29), and Coventry and Lovegrove presented the methods that can be used to develop a ratio between electrical and thermal output energy for a domestic style PVT system (30).

Studies using finite element method (FEM), finite different method (FDM) or finite volume method (FVM) have been performed in different regions of the world with specific weather conditions and it has been shown that PVT collectors using rectangular channels are more efficient due to fact that they provide a large surface for heat exchange between the PV module and the thermal collector.

This study is a particular case in which a simulation was run with Durban meteorological conditions for two particular days with a single glazed thermosyphon flat-box absorber collector array using Fourier series for water flow velocity rate in absorber channels and a storage tank using implicit finite difference method (IFDM) for temperature calculation. This model was designed to simulate a PVT grid connected photovoltaic system for moderate household demand.

1.2 Objectives of this research

The overall objectives of this study were:

- To design a thermal collector and develop an analytical model of temperature for a hybrid PVT collector using rectangular channels;
- To develop an analytical model of the fluid velocity in rectangular collector channels due to thermosyphon;

- To evaluate the dynamic behaviors of a conventional PV module (Q.PEAK 250 solar module) against a hybrid PVT collector regarding change of irradiance, temperature and wind velocity for by means of simulation;
- To design and analyse the hybrid grid connected photovoltaic system for modest Durban household demand compared to a conventional PV system; and
- To evaluate the economic impact of a grid-connected PVT system for modest Durban household demand compared to a conventional PV system and utility grid.

1.3 Research questions

The key research questions addressed in this study are as follows:

- 1) What is the South African household energy demand?
- 2) What is the most energy-efficient and cost-effective way of matching photovoltaic systems?
- 3) What is the impact of a water cooling PV module in terms of electrical output energy for rectangular collector channels?
- 4) What is the impact of a PVT grid connected system on household energy demand compared to a conventional PV grid connected system and utility grid?

1.4 Dissertation layout

The dissertation is structured into ten chapters:

Chapter One presents the electricity needs in South Africa, the concept of photovoltaic hybrid system and previous research work in the area of PVT.

Chapter Two gives an introduction to different theories used for modeling of different parameters for simulations of PV and PVT systems.

In Chapter Three, various conventional PV systems are discussed. The electrical model, an electrical equivalent circuit representation of the model, the analytical model of the temperature and the impact of temperature on the conventional PV system output are presented.

Chapter Four presents the thermosyphon principle and fluid velocity in rectangular channels.

In Chapter Five, the thermosyphon hybrid photovoltaic thermal (PVT) system is presented. The chapter analyses the impact of using water to cool PV systems. The analytical model of solar cell temperature is established for this purpose.

Chapter Six presents the PVT behaviors with environmental parameters for the defined temperature model. Behaviors of PVT systems in terms of solar cell temperature, electrical efficiency and water temperature in the tank are determined respectively for variation of insolation, ambient temperature and wind velocity.

In Chapter Seven, the average load for modest Durban household is determined and a typical design of a thermosyphon hybrid grid-connected PVT system for modest Durban household demand is presented.

In Chapter Eight, simulations are carried out for a thermosyphon hybrid grid-connected PVT system for modest Durban household demand. The designed PVT system is compared to a PV system in terms of cell temperature, maximum power point, and electrical energy produced for four particular day weathers. The temperature of water in the tank is also determined.

Chapter Nine presents the thermosyphon hybrid grid-connected PVT system for modest Durban household demand economics. This chapter presents the economic impact of a grid-connected PVT system for modest Durban household demand compared to a conventional PV system. Systems trade-offs are worked out, the Rand per watt ambiguities determined, and the amortizing costs calculated.

In Chapter Ten, the main conclusions of the study are summarized. Based on the obtained results, the advantages and disadvantages of the studied systems in terms of energy output and economic gain are presented and directions for future research for better systems are proposed.

CHAPTER TWO

SOLAR INSOLATION AND MODELING THEORIES

This chapter presents the concept of solar insolation or irradiance which is a source to produce electrical and thermal energies, and introduces theories applied in the modeling of photovoltaic and hybrid photovoltaic systems for the purpose of simulation and analysis.

2.1 Solar insolation on tilted surface

It is difficult to understand the operation of an electricity production system based on photovoltaic system without basic knowledge of its energy source and the radiation received from the sun (31).

The flux of energy produced by the solar source reaching a surface per unit surface of an area is the insolation or solar irradiance. It is expressed in units of kWh/m²day for the average daily or monthly conditions at a given location. This quantity defines the maximum energy produced by a photovoltaic system for that particular location (32). More details about photovoltaic modules and arrays are given in Chapter Three.

The insolation from the sun can be converted into different forms of energy for the purpose of using a variety of technologies. When electrical energy is needed, the solar insolation can be converted into electricity by the use of photovoltaic technology such as grid-tied or stand-alone off grid. When heat is needed, the thermal systems can be used for cooking, melting, or heating, for example, and to produce hot water (33).

As solar radiation reaches the atmosphere of the earth, it is scattered, reflected and absorbed by atmospheric particles. As a result, only a portion of the solar radiation outside the earth's atmosphere, i.e. the extra-terrestrial radiation, actually reaches the surface of the earth. This portion, the extra-terrestrial radiation, varies from less than 50% to 70%, depending on the position of the sun and the clearness of the sky (31). Figure 2.1 presents the extra-terrestrial spectrum and the spectrum of a blackbody at 5800 K.

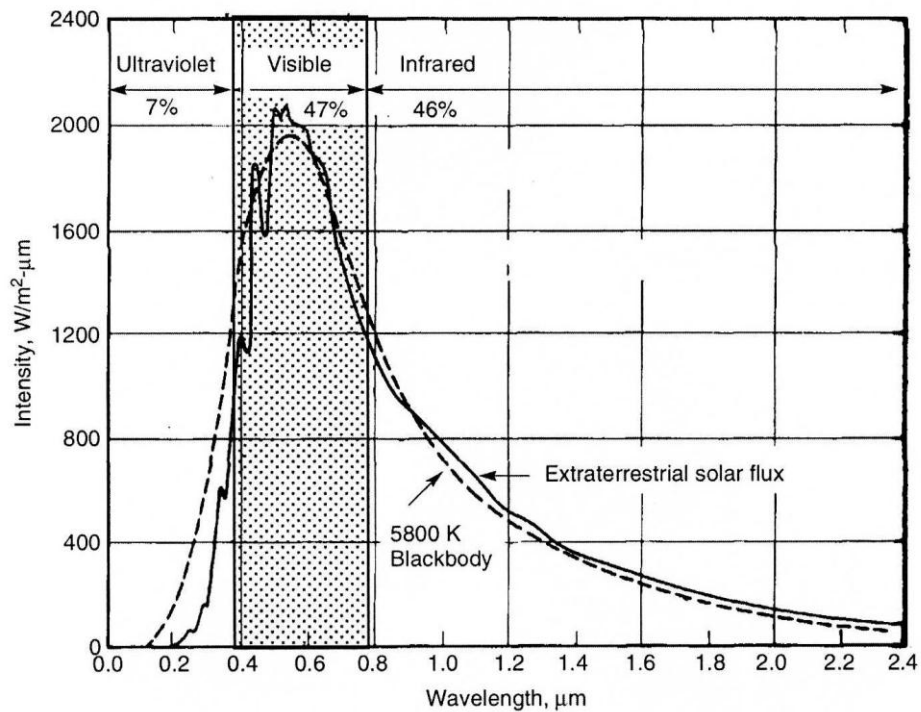


Figure 2.1: The extraterrestrial spectrum and the spectrum of a blackbody at 5800 K.

The total terrestrial solar flux hitting for instance the surface of a solar collector consists of three components: direct beam, diffuse and reflected radiation. Direct beam radiation is the radiation that passes in a straight line through the atmosphere; diffuse radiation is radiation scattered by atmospheric particles or moisture or reflected from clouds; and, reflected radiation is the radiation reflected from surfaces in front of the collector (31).

To maximize the amount of insolation received, collectors are installed at a certain angle to reduce the reflection of irradiance and minimize cosine losses (34). The photovoltaic panels are commonly tilted at a certain angle from the horizontal to receive the maximum amount of insolation. The insolation on the panels at the corresponding tilt angle is evaluated by separating the insolation into two components, the direct and the diffuse (35).

Where solar irradiance data is available in the form of direct and diffuse components, the approach below can be used to obtain the global insolation reaching the panels tilted at a certain angle θ from the horizontal (35).

Firstly, we can assume the diffuse component of insolation D does not depend on the tilt angle which is approximately right for tilt angles about or less than 45° .

Secondly, the direct component of insolation on the horizontal surface S is to be converted into the direct component S_θ that reaches the PV module tilted at angle θ to the horizontal as shown in Figure 2.2.

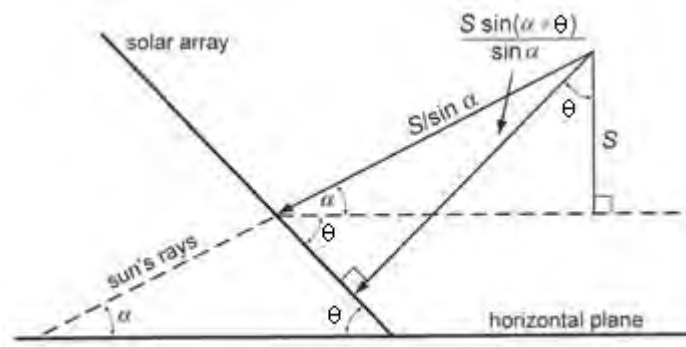


Figure 2.2: Light incident on a surface tilted to the horizontal

Consequently, we obtain:

$$S_\theta = \frac{S \sin(\alpha + \theta)}{\sin \alpha} \quad (2.1)$$

where α is the altitude of the sun (i.e. the angle between the sun and the horizontal) at noon, which is given by:

$$\alpha = 90 - \beta - \delta \quad (2.2)$$

where β is the southern latitude and δ is the declinaison of the sun as given by:

$$\delta \approx \varepsilon \sin \left[\frac{(d - 81)360}{365} \right] \quad (2.3)$$

where d is the day number starting with 1 January as $d = 1$ and $\varepsilon = 23.45^\circ$.

The global insolation on array is the sum of the direct component S_θ incident on a plane tilted at angle θ to the horizontal and the diffuse component D independent parameter of the tilt angle:

$$G = S_\theta + D \quad (2.4)$$

2.2 Modeling theories

Most physical and engineering phenomena are modelled based on differential equations. Partial differential equations are needed in order to solve for those quantities in the integrands that are not known, such as the velocity distribution in a pipe or the pressure distribution on an air foil. To solve a partial differential equation for the dependent variable, certain conditions are required, i.e. the dependent variable must be specified at certain values of the independent variables. If the independent variables are space coordinates, such as the velocity at the wall of a pipe, the conditions are called boundary conditions. If the independent variable is time, the conditions are called initial conditions (36).

The most useful equations in physical and engineering phenomena modeling are the differential continuity equation, the differential momentum equation and the differential energy equation in the study of fluid motion and heat and mass transfer.

2.2.1 The differential continuity equation

The differential continuity equation is established on the principle that the mass that flows into the element minus that which flows out must equal the change in mass inside the element (36).

This is expressed as:

$$\frac{\partial \rho}{\partial t} + \frac{\partial}{\partial x}(\rho u) + \frac{\partial}{\partial y}(\rho v) + \frac{\partial}{\partial z}(\rho w) = 0 \quad (2.5)$$

Equation (2.5) is often called the equation of continuity because in this, the density and velocity are continuum functions of space coordinates and no other assumptions are required (37). Thus, the fluid flow can be steady or unsteady, compressible or incompressible, viscous or frictionless.

2.2.2 The differential momentum equation

In this study, the fluid used is a Newtonian fluid. For a Newtonian fluid, the viscous stresses are proportional to the element strain rates and the coefficient of viscosity (37).

The Navier-Stokes equations for an incompressible Newtonian fluid flow are given by:

$$\left. \begin{aligned} \rho g_x - \frac{\partial p}{\partial x} + \mu \left(\frac{\partial^2 u}{\partial x^2} + \frac{\partial^2 u}{\partial y^2} + \frac{\partial^2 u}{\partial z^2} \right) &= \rho \frac{du}{dt} \\ \rho g_y - \frac{\partial p}{\partial y} + \mu \left(\frac{\partial^2 v}{\partial x^2} + \frac{\partial^2 v}{\partial y^2} + \frac{\partial^2 v}{\partial z^2} \right) &= \rho \frac{dv}{dt} \\ \rho g_z - \frac{\partial p}{\partial z} + \mu \left(\frac{\partial^2 w}{\partial x^2} + \frac{\partial^2 w}{\partial y^2} + \frac{\partial^2 w}{\partial z^2} \right) &= \rho \frac{dw}{dt} \end{aligned} \right\} \quad (2.6)$$

The differential momentum equation for a Newtonian fluid with constant density and viscosity contains three velocity components as the dependent variables (36). The three scalar Navier-Stokes equations and the continuity equation constitute the four equations that can be used to find the four variables u , v , w , and p , provided there are appropriate initial and boundary conditions (36).

2.2.3 The differential energy equation

The differential energy equation is needed if there are temperature differences on the boundaries or if viscous effects are so large that temperature gradients are developed in the flow (36).

For an unsteady, incompressible, viscous, heat conducting flow Newtonian fluid at rest or with negligible velocity the differential energy equation is (37):

$$\frac{\partial T}{\partial t} + u \frac{\partial T}{\partial x} + v \frac{\partial T}{\partial y} + w \frac{\partial T}{\partial z} = \frac{k}{\rho C_v} \left(\frac{\partial^2 T}{\partial x^2} + \frac{\partial^2 T}{\partial y^2} + \frac{\partial^2 T}{\partial z^2} \right) \quad (2.7)$$

This is called the heat-conduction equation in applied mathematics and is valid for solids and fluids at rest.

2.3 Solutions of differential equations

Analytical solutions for differential equations are difficult in practice. For solving differential equations, many techniques have been developed. In the early nineteenth century, Joseph Fourier, while studying the problem of heat flow, developed a cohesive theory of such series (38). In many practical problems, it is impossible to compute the analytical solutions, since the data is known only on a set of discrete points. To remedy this situation, we may forgo the search for an analytical solution in favor of a numerical solution. By discretizing a problem, we can come up with an algorithm or a formula that can be used to generate numerical values of the solution at a discrete set of points (39).

2.3.1 Fourier series

With the Fourier series, we are interested in expanding a function in terms of the special set of functions $1, \cos x, \cos 2x, \cos 3x, \sin x, \sin 2x, \sin 3x$.

Fourier Series are fundamental to the description of important physical phenomena for diverse fields, such as mechanical and acoustic vibrations, heat transfer, planetary motion, optics, signal processing, electromagnetism and statistics (39).

In general, a function f satisfying the identity:

$$f(x) = f(x + T) \quad (2.8)$$

For all x , where $T > 0$, T is called a period of function f . If f is non-constant, we define the fundamental period, or simply, the period of f to be the smallest positive number T for which equation (2.8) holds.

Using equation (2.8) repeatedly, we get:

$$f(x) = f(x + T) = f(x + 2T) = \dots = f(x + nT) \quad (2.9)$$

Hence if T is a period, then nT is also a period for any integer $n > 0$.

The Fourier series or Fourier expression corresponding to $f(x)$ is given by:

$$\frac{a_0}{2} + \sum_{n=1}^{\infty} \left(a_n \cos \frac{n\pi x}{L} + b_n \sin \frac{n\pi x}{L} \right) \quad (2.10)$$

where the Fourier coefficients a_n and b_n are:

$$\left. \begin{aligned} a_n &= \frac{1}{L} \int_{-L}^L f(x) \cos \frac{n\pi x}{L} dx \\ b_n &= \frac{1}{L} \int_{-L}^L f(x) \sin \frac{n\pi x}{L} dx \end{aligned} \right\} \quad (2.11)$$

The Fourier coefficients are integrals. These are obtained by starting with the series (2.10) and employing the following properties called orthogonality conditions:

$$\left. \begin{aligned} \int_{-L}^L \cos \frac{m\pi x}{L} \cos \frac{n\pi x}{L} dx &= 0 \text{ if } m \neq n \text{ and } L \text{ if } m = n \\ \int_{-L}^L \sin \frac{m\pi x}{L} \sin \frac{n\pi x}{L} dx &= 0 \text{ if } m \neq n \text{ and } L \text{ if } m = n \\ \int_{-L}^L \sin \frac{m\pi x}{L} \cos \frac{n\pi x}{L} dx &= 0 \text{ Where } m \text{ and } n \text{ can assume} \\ &\text{any positive integer values} \end{aligned} \right\} \quad (2.12)$$

2.3.2 Numerical methods and finite difference method

Several ways are provided by mathematics to get a numerical solution to scientific problems by using numerical methods. The most common numerical methods used are:

- The finite element method;
- The finite difference method;

- The boundary element method; and
- The energy balance or control volume method.

Each method has its own advantages and disadvantages, and each is used in practice (40).

This study is concerned more with heat and mass transfer problems and each of the numerical methods enumerated above can be used to obtain the numerical formulation of the problems. The finite difference method is used in this dissertation due to its flexibility and simplicity of computation. The finite difference method formulation of a heat transfer problem is realized by selecting a sufficient number of points in the region called the nodal points or nodes and apply the energy balance method on the volume elements centred about the nodes (40).

The formulation of the transient heat conduction by finite difference method is based on the energy balance that represents the variation of the tensor in term energy of the element of volume in the interval of time Δt . The formulation of finite difference methods for time-dependent problems involve discrete points in time as well as space as represented in Figure 2.3.

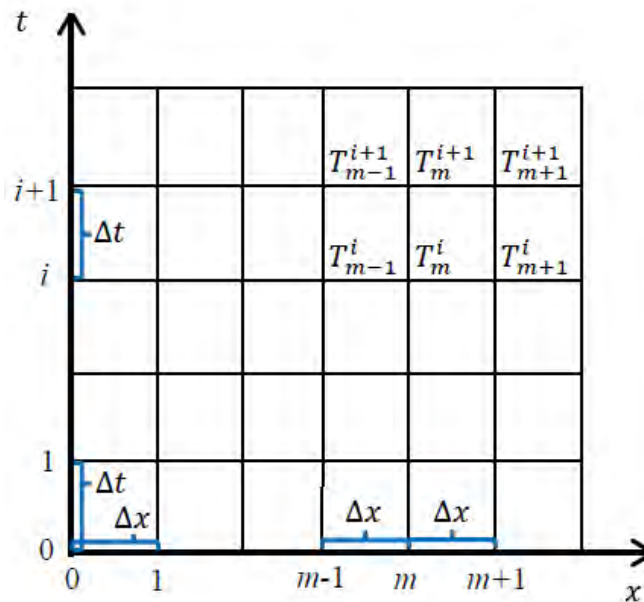
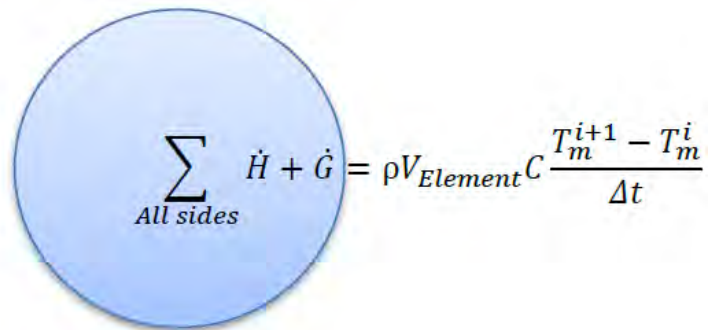


Figure 2.3: Finite difference formulation for time-dependent problems

The heat transfer and heat generation terms are displayed at step I in the explicit method and at step $i+1$ in the implicit method. The implicit method is fundamentally stable and one value of Δt can be used at this step as time (40). Figure 2.4 represents the formulation of explicit and implicit methods which differ at the time step (previous or new) at which the heat transfer and heat generation terms are displayed.

If expressed at $i+1$: Implicit method



$$\sum_{All\ sides} \dot{H} + \dot{G} = \rho V_{Element} C \frac{T_m^{i+1} - T_m^i}{\Delta t}$$

If expressed at i : Explicit method

Figure 2.4: The formulation of explicit and implicit methods

For a general node m , the implicit finite difference formulation is expressed as:

$$\sum_{Allsides} \dot{Q}^{i+1} + \dot{G}_{element}^{i+1} = \rho V_{element} C \frac{T_m^{i+1} - T_m^i}{\Delta t} \quad (2.13)$$

where:

T_m^i Temperature of node m at time $t_i = i\Delta t$

T_m^{i+1} Temperature of node m at time $t_{i+1} = (i+1)\Delta t$

$T_m^{i+1} - T_m^i$ Temperature change of the node during the time interval Δt between the time steps i and $i+1$.

CHAPTER THREE

CONVENTIONAL PHOTOVOLTAIC SYSTEMS

3.1 Development of photovoltaic systems

Photovoltaic systems (or PV systems) are semiconductor devices that convert part of the incident solar radiation directly into electrical energy (41).

In 1839, Edmund Becquerel caused a voltage to appear by illuminating a metal electrode in a weak electrolyte solution. The history of photovoltaics began with the Becquerel discovery. Almost 40 years later, the photovoltaic effect in solids was studied for the first time by Adams and Day in 1876 and thereafter cells were made of selenium which proved to be of 1% to 2% efficiency. Later in 1923, in what turned out to be a breakthrough in modern electronics and in photovoltaics in particular, a method to grow perfect silicon crystals was developed by Czochralski, a scientist from Poland. By the dawn of 1940s the first generation of single-crystal silicon based photovoltaics was made by using the Czochralski process which continues to dominate the industry to this date. Presently, the technique is widely used in the photovoltaic (PV) industry for almost all applications. The demand for photovoltaic applications has pushed up the renewable energy market and by 2002 600MW per year was being produced around the world with an increase of over 40% annually. In comparison to global wind power, the demand for PV was 10 times greater (42).

3.2 Basic semiconductor physics

Photovoltaic systems use semiconductors to convert sunlight into electrical energy. The genesis for most of the world's current generation of photovoltaic devices, in addition to almost all semiconductors, is pure crystalline silicon (42).

3.2.1 The Band Gap Energy

Photons with enough wavelength and high enough energy can produce in the photovoltaic material electrons by breaking free atoms that hold them. In the presence of an electric field, the

electrons produced by the photons can be move through a metallic contact where they can generate an electric current (42).

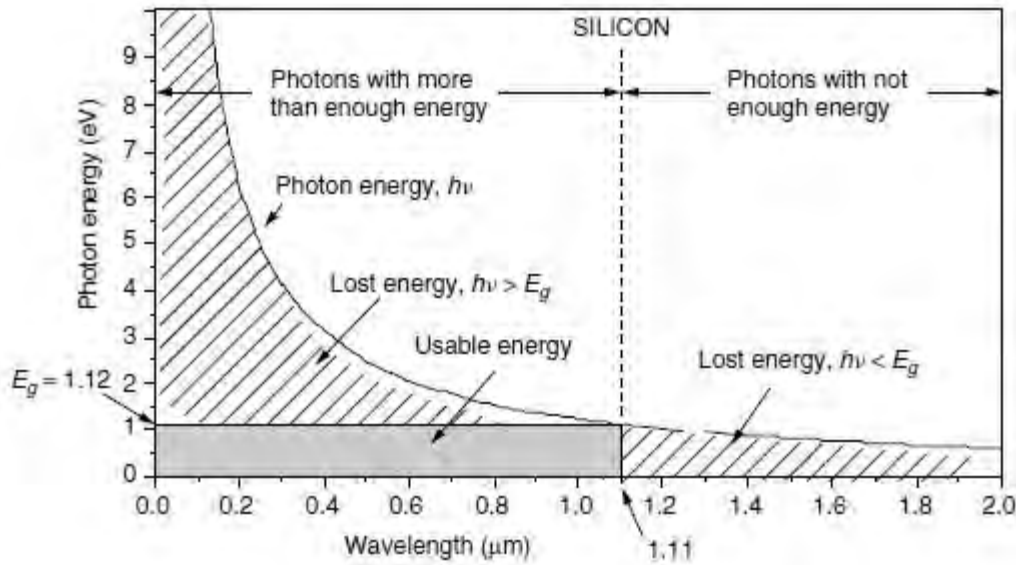


Figure 3.1: Photon energy against Wavelength (42)

To free an electron from the silicon material, a photon must have sufficiently energy to escape from its own nucleus. That energy which must be greater than the energy due to the electrostatic force that ties it to the nucleus is called the band-gap E_g and for silicon material is 1.12 eV (42). Figure 3.1 shows the photon energy against wavelength for silicon material. It can be seen that the diagram is divided into two parts. At a wavelength is less than $1.11 \mu\text{m}$ the photon energy is more than the band-gap and a photon has enough energy to escape from its own nucleus, resulting in a loss of energy. When a wavelength is more than $1.11 \mu\text{m}$, the photon energy is less than the band-gap and the photon cannot free itself from its nucleus. There is also a lot of energy which cannot be used. The only usable energy is represented by the area limited by the wavelength of $1.11 \mu\text{m}$ and a photon energy of 1.12 eV.

3.2.2 The p–n junction

As long as solar insolation reaches the solar cells, photons with energies above the band-gap free electrons from free atoms in the silicon material and produce hole-electron pairs. At any time, those holes and electrons can recombine and cause both charges to disappear. To avoid electrons

falling back into holes, an electric field is created in photovoltaic material by establishing two opposed regions within the semiconductor, one with n-type material built with pure silicon contaminated with a very small quantity of a trivalent element from column III of the periodic chart and p-type material built with pure silicon contaminated with pentavalent atoms from column V. By putting together the p side and the n side, the p-n junction is created and the electric field obtain at the junction will push electrons in one direction and holes in the other and the recombination of holes and electrons is avoided (42).

When n-type material is put next to p-type material, the conventional p-n junction diode is obtained between them as shown in Figure 3.2.

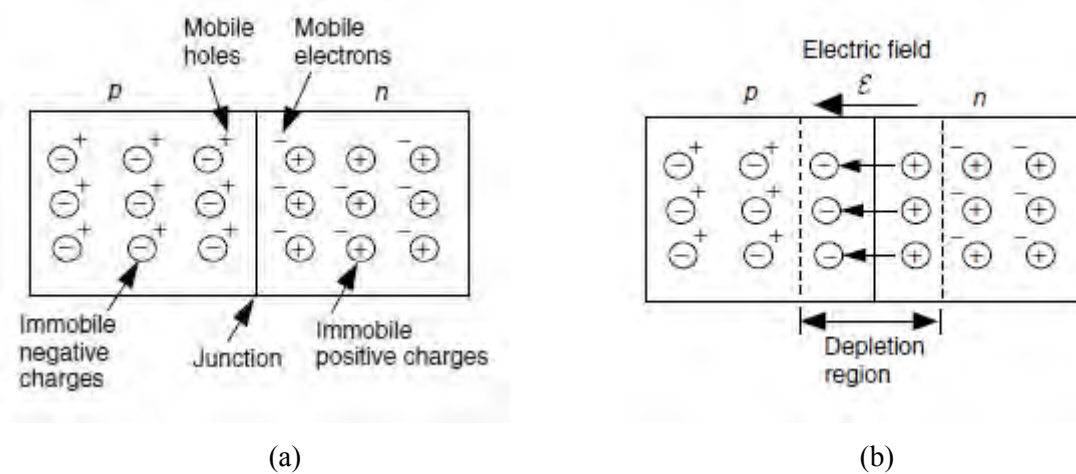


Figure 3.2: A p-n junction (a) When first brought together and (b) In steady-state (42)

The Shockley diode equation (3.1) illustrates the voltage-current characteristic curve for the *p-n* junction diode:

$$I_d = I_0(e^{qV_d/kT} - 1) \quad (3.1)$$

where:

- I_d Current flowing into the diode (A)
- V_d Voltage across the diode terminals (V)
- I_0 Reverse saturation current (A)
- q Electron charge (1.602×10^{-19} C)

- k Boltzmann's constant (1.381×10^{-23} J/K) and
 T Junction temperature (K)

In some circumstances, the Shockley diode equation is adjusted with an ideality factor, which considers diverse mechanisms responsible for moving transporters across the junction.

The equation (3.1) becomes:

$$I_d = I_0(e^{qV_d/AkT} - 1) \quad (3.2)$$

where superscript A is the ideality factor which is 1 if the transport process is purely diffusion, and approximately 2 if it is recombination in the depletion region (42).

3.3 Photovoltaic cells

3.3.1 A generic photovoltaic cell

In photovoltaic material, if the hole-electron pairs produced by photons from insolation reach the vicinity of the p-n junction, the motion of those particles creates an electrical field in the depletion region. The p-side accumulates holes and the n-side accumulates electrons which produces a voltage that is used to circulate current from between PV module and load (42).

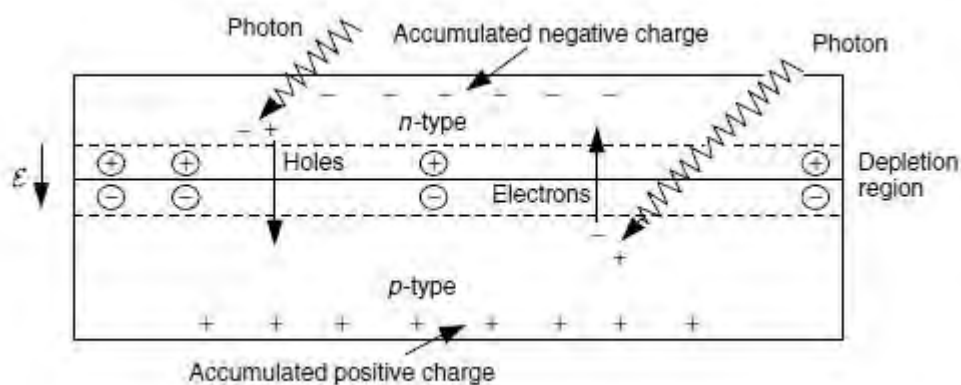


Figure 3.3: Illustration of the p-n junction of PV cell (42)

Consider solar cell lighting by solar insolation. If a load is connected to a photovoltaic cell through a connecting wire at electrical contacts on the n-side and the p-side as shown in Figure 3.4, electrons flow from the n-side to the p-side through the connecting wire. That flux of electrons generates a current which circulates from the p-side to the n-side in the circuit (42).

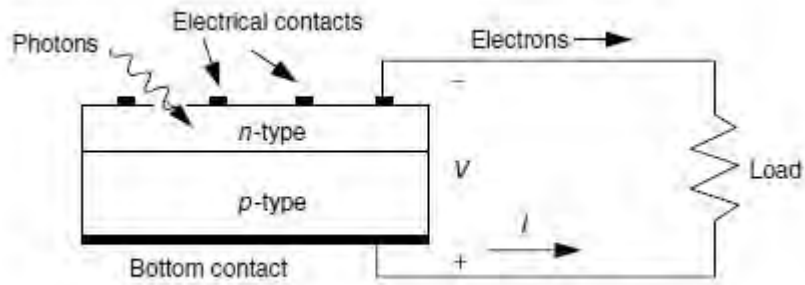


Figure 3.4: Side view of solar cell and the conducting current

A simple equivalent circuit of a solar cell generating electrical energy is represented by a real diode in parallel with an ideal current source as represented in Figure 3.5. The current delivered by the ideal source is proportional to the flux of insolation received by the solar cell (42).

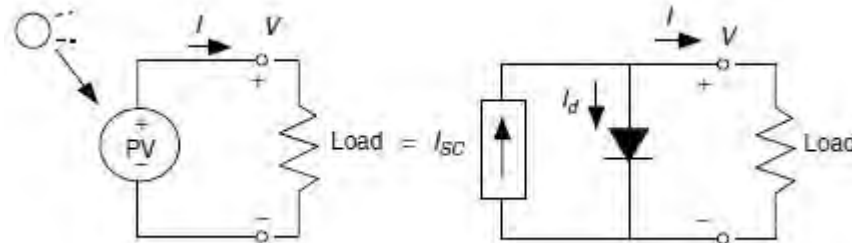


Figure 3.5: A simple equivalent circuit for a photovoltaic cell with load connected

The modeling of a solar cell is based on two important conditions for the actual PV and for its equivalent circuit from which the short-circuit current and the open-circuit voltage are defined.

- (1) When the leads of the equivalent circuit for the PV cell are short-circuited together, there is no current flow in the real diode since V_d is equal to 0; so all the current from the ideal source I_{ph} flows through the shorted leads. The amount of the ideal current source itself must be equal to the current that flows when the terminals are short-circuited together which is I_{sc} . It is the highest value of the current generated by cell (43):

$$I_{ph} = I_{sc} \quad (3.3)$$

- (2) The open-circuit voltage, V_{oc} is the voltage across the terminals when the leads are left open. It corresponds to the voltage drop across the diode when it is traversed by the current I_{ph} , namely, when the generated current is $I=0$ (43).

Applying Kirkhoff current law to the nodes, we can write a current equation for the equivalent circuit of the PV cell shown in Figure 3.5, as follows:

$$I = I_{sc} - I_d \quad (3.4)$$

The equations (3.2) and (3.4) give:

$$I = I_{sc} - I_0(e^{qV_d/AkT} - 1) \quad (3.5)$$

The reverse saturation current I_0 of a diode is constant under constant temperature and can be determined by displaying the open-circuit condition as shown in Figure 3.6.

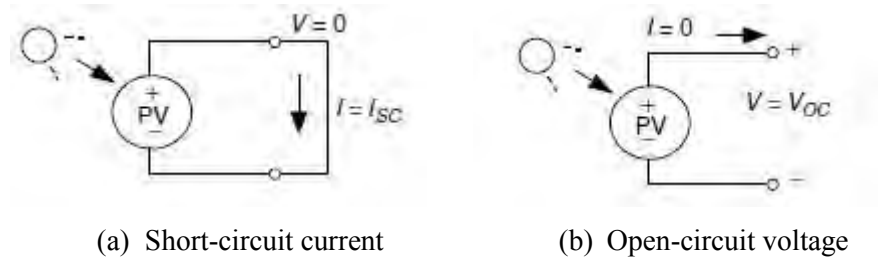


Figure 3.6: Short-circuit current and Open-circuit voltage for a PV cell

For $I=0$, we obtain from equation (3.5):

$$I_{sc} = I_0(e^{qV_{oc}/AkT} - 1) \quad (3.6)$$

The reverse saturation current of diode I_0 at the reference temperature is given by the equation:

$$I_0 = \frac{I_{sc}}{(e^{qV_{oc}/AkT} - 1)} \quad (3.7)$$

When the leads from the PV cell are left open, I is equal to 0 and using equation (3.7) we obtain the open-circuit voltage V_{oc} :

$$V_{oc} = \frac{AkT}{q} \ln \left(\frac{I_{sc}}{I_o} + 1 \right) \quad (3.8)$$

The values of I_{sc} and V_{oc} and the performance of solar cells in datasheets are obtained under the standard test condition (STC) for insolation $G_0=1000\text{W/m}^2$ at the air mass (AM) of 1.5. The short-circuit current of the module is assumed proportional to irradiance which slightly increases with cell temperature. This comes from a decrease in band gap and an improvement of minority-carrier lifetimes (44).

For insolation $G \neq G_0$, short-circuit current I_{sc} generated by the photon at G irradiance at given temperature is obtained by the following equation:

$$I_{sc}(T, G) = \left(\frac{G}{G_0} \right) I_{sc}(T) \quad (3.9)$$

where $I_{sc}(T)$ is the short-circuit current at the temperature T , given by:

$$I_{sc}(T) = I_{sc}(STC)[1 + \beta_I(T - 25^\circ\text{C})] \quad (3.10)$$

Open-circuit voltage strongly decreases linearly with the temperature (44) as per the following equation:

$$V_{oc}(T, G) = V_{oc}(STC) - \beta_V(T - 25^\circ\text{C}) \quad (3.11)$$

where β_I and β_V are the temperature coefficients of the current and the voltage respectively.

For V_{oc} , the irradiance dependence is buried in T . The reverse current I_o is also temperature dependant and the I_o at a given temperature T is calculated from the following equation:

$$I_o(T) = I_{oref} \left(\frac{T}{T_{ref}} \right)^{\frac{3}{A}} e^{\frac{-qE_g}{Ak} \left(\frac{1}{T} - \frac{1}{T_{ref}} \right)} \quad (3.12)$$

where:

I_o Reverse saturation current at temperature T (A)

I_{oref} Reverse current at STC (A)

T Junction temperature (K)

T_{ref} Reference temperature (K)

q Electron charge (1.602×10^{-19} C)

E_g Band-gap (1.12 eV)

A Ideality factor

k Boltzmann's constant (1.381×10^{-23} J/K)

3.3.2 Generalised equivalent circuit for a PV cell

As specified above, the circuit in Figure 3.5 represents an equivalent circuit of an ideal photovoltaic cell. With this typology, the load will not receive power as long as any of its cells are shaded. It is also important to note that there is a loss of energy due to contact resistance and the resistance of the solar cells themselves. To deal with all those situations, a parallel resistance R_p is inserted into the equivalent circuit (Figure 3.7) to deal with the loss due to shading of solar cells and a series resistance R_s is inserted into the circuit in order to deal with the loss due to contact resistance related to the bond between the cell and its wire leads, and the solar cells themselves (42).

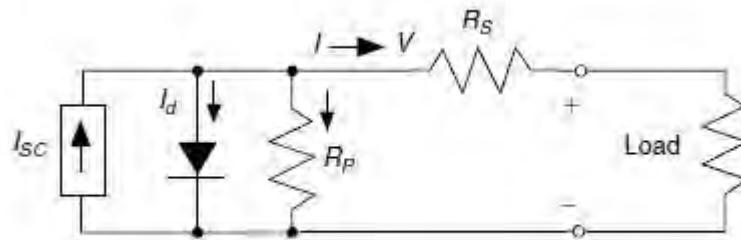


Figure 3.7: Complex equivalent circuit for a PV cell

With both series and parallel circuits considered, the generalized PV equivalent circuit is given in Figure 3.7. The following equation gives the current-voltage characteristic curve of the real PV cell.

$$I = I_{sc} - I_0 \left(e^{q \left(\frac{V + IR_s}{AkT} \right)} - 1 \right) - \left(\frac{V + IR_s}{R_p} \right) \quad (3.13)$$

where:

- I Cell current (the same as the module current) (A)
- I_{sc} Short circuit current which is equal to photocurrent (A)
- I_0 Dark saturation current (A)
- q Electronic charge (1.602×10^{-19} C)
- k Boltzmann's constant (1.381×10^{-23} J/K)
- A Idealizing factor
- T Cell temperature (K)
- V Cell voltage (V)
- R_s Shunt resistance (Ω)
- R_p Parallel resistance (Ω)

Employing the sign convention shown in Figure 3.7 and relating Kirchhoff's Current Law to the node above the diode, we can deduce that:

$$I_{sc} = I + I_d + I_p \quad (3.14)$$

where:

- I_d Diode current (A)
- I_p Parallel resistance current (A)

Rearranging and substituting the Shockley diode equation (3.2) into equation (3.14) at 25°C, we obtain:

$$I = I_{sc} - I_0(e^{38.9V_d} - 1) - \left(\frac{V_d}{R_p}\right) \quad (3.15)$$

where V_d is the diode voltage (V).

With an assumed value of V_d in a spreadsheet, current I can be found from equation (3.15).

The voltage across an individual cell can be found from equation (3.16):

$$V = V_d - IR_s \quad (3.16)$$

The effect of parallel resistance is less important in a PV module compared to series resistance, and it will become visible only in the larger systems where a number of PV modules are connected in parallel to produce a huge current (41). By setting the parallel resistance R_p to ∞ , we obtain the solar cell equivalent circuit one-diode model shown in Figure 3.8.

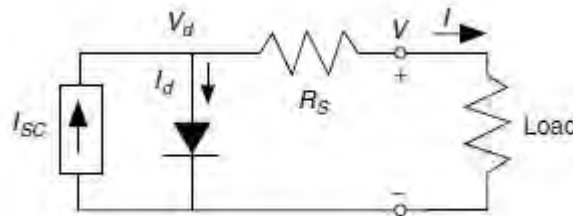


Figure 3.8: A simplified equivalent circuit for a PV cell

From equation (3.13), the current is given by the following equation:

$$I = I_{sc} - I_0 \left(e^{q \left(\frac{V + IR_s}{AkT} \right)} - 1 \right) \quad (3.17)$$

where:

I	Cell current (the same as the module current) (A)
I_{sc}	Short circuit current which is equal to photocurrent (A)
I_o	Dark saturation current (A)
q	Electronic charge (1.602×10^{-19} C)
k	Boltzmann's constant (1.381×10^{-23} J/K)
A	Idealizing factor
T	Cell temperature (K)
V	Cell voltage (V)
R_s	Shunt resistance (Ω)

The equation for R_s is derived by differentiating the equation (3.17) and then rearranging it in terms of R_s :

$$R_s = -\frac{dV}{dI} - \frac{AkT/q}{I_o e^{q\left(\frac{V+IR_s}{AkT}\right)}} \quad (3.18)$$

At the open circuit, the voltage $V = V_{oc}$ and the current $I=0$ so that equation (3.18) gives the value of R_s as:

$$R_s = -\left.\frac{dV}{dI}\right|_{V_{oc}} - \frac{AkT/q}{I_o e^{\frac{qV_{oc}}{AkT}}} \quad (3.19)$$

where:

$-\left.\frac{dV}{dI}\right _{V_{oc}}$	Slope of the I - V curve at the V_{oc} obtained from the I - V curve in the solar cell datasheet
V_{oc}	Open-circuit voltage of cell, found in the solar cell datasheet.

3.4 Photovoltaic module

The voltage produced by an individual solar cell is 0.5V to 0.6V which is too little for an application. To get useful and adequate voltage, cells are wired in series, all encased in tough, weather-resistant packages which is the PV module. A typical laminated module structure is shown in Figure 3.9.

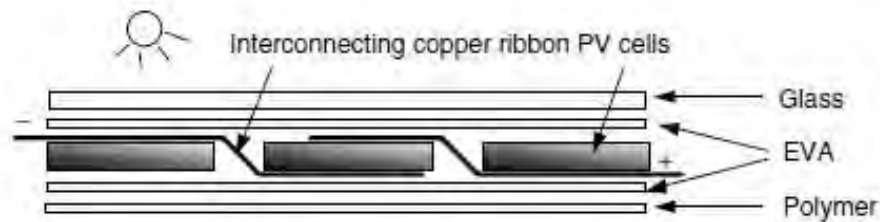


Figure 3.9: A typical laminated module structure

Multiple modules also can be connected in series to increase voltage and in parallel to increase current, the output product of which is power. Such arrangement of modules are referred to as an *array* as shown in Figure 3.10 (42).

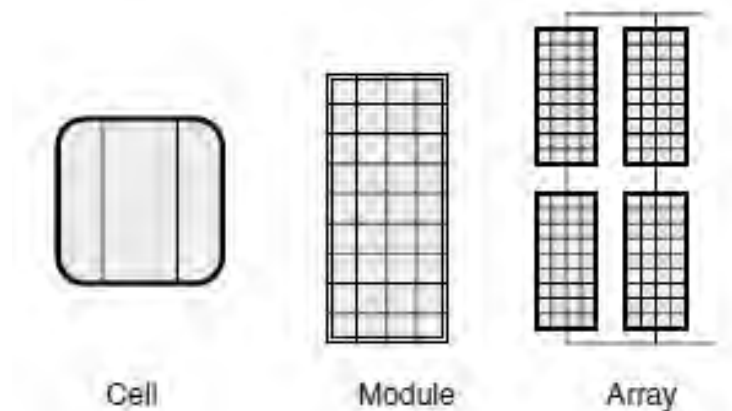


Figure 3.10: Photovoltaic cells, modules and an array

3.4.1 From cells to a module

When solar cells are wired in series, they all carry the same current, but at any given current their voltages add together. Figure 3.11 shows the variation of voltage with a number of cells wired in series in a module at standard test conditions (STC).

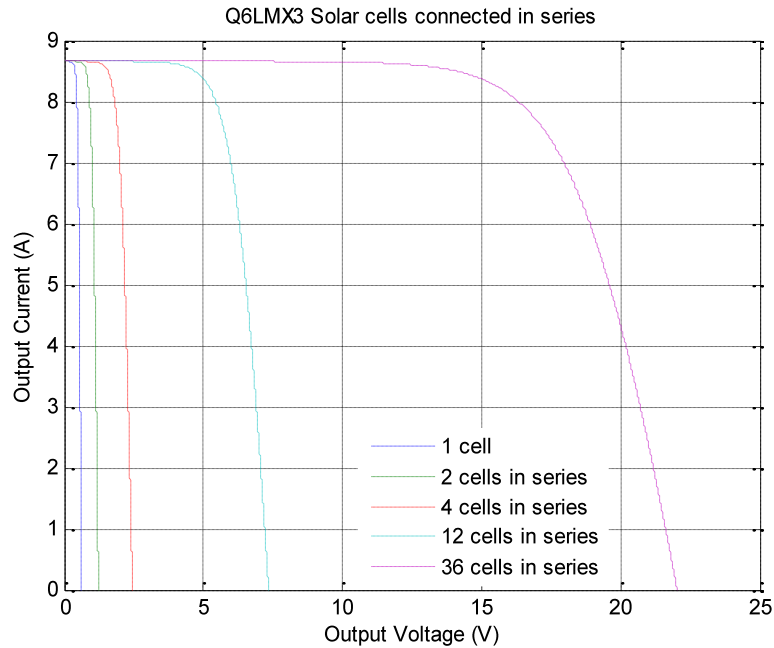


Figure 3.11: Q6LMX3 Solar cells wired in series at STC simulated with the Matlab model

The overall module voltage V is determined by multiplying equation (3.16) by the number n of cells in the module which gives the equation:

$$V = n(V_d - IR_S) \quad (3.20)$$

3.4.2 Modeling of photovoltaic module

As PV cells are wired in series to produce module voltage, the strategy of modeling the PV module is the same as modeling solar cells. The only difference is that voltages produced are divided by the number of cells in the PV module. Other parameters remain the same. The photovoltaic can therefore be modelled using equations (3.17) and (3.18).

The introduction of a series resistance in the model makes the numerical solution of the current equation unsolvable, reference to equation (3.17). An approximate solution to this equation is obtained by using the Newton Raphson method which converges quickly for positive as well as for negative current values (45) (for more details, see Appendix A).

3.5 The PV I-V curve under standard test conditions (STC)

Consider a PV module to be connected to the load. Before the load is connected, there is not load at the terminals of the PV module, the circuit is open. At any insulation, there is not current in the circuit, the module produces only an open voltage V_{oc} and the electric power is zero as seen in Figure 3.12(a). When the two terminals are short circuited as shown in Figure 3.12(b), the voltage V is zero, a short-circuit current I_{sc} circulates in the circuit and the electric power is also zero. When the load is connected to the PV module terminals, a current I flows in the circuit at voltage V and the electric power E delivered by the PV module to the load is the product of the voltage V and the current I (42).

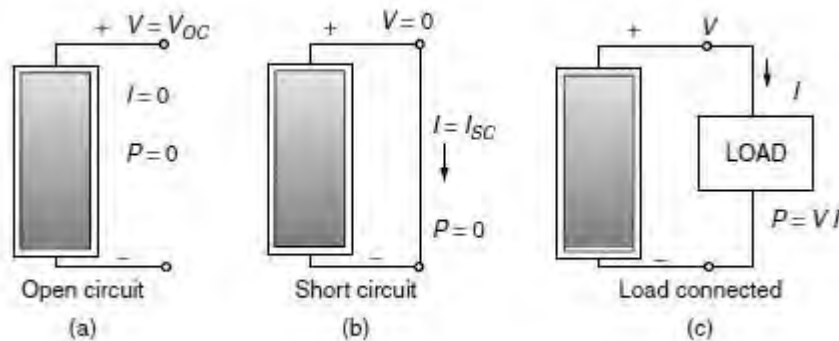


Figure 3.12: PV module at different states

To find out the value of the power delivered by the module to the load, the I-V characteristic curve of the PV module and the I-V characteristic of the load are represented in the same coordinate system axis at the same scale. The intersection of the I-V curve of the PV module and the I-V curve of the load produce the operating point of the PV system for that particular load as shown in Figure 3.13 (42).

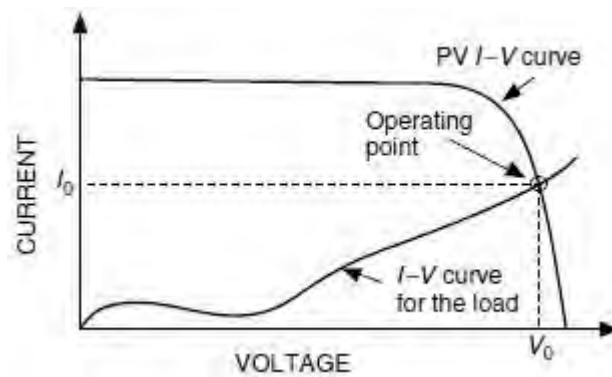


Figure 3.13: PV module and Load characteristic curves

In the design of a PV array and in the determination of PV modules, important parameters for solar cells and PV modules are provided by manufacturers. Those parameters are represented in Figure 3.14. In this figure, curves of current against voltage and electrical power against voltage are represented.

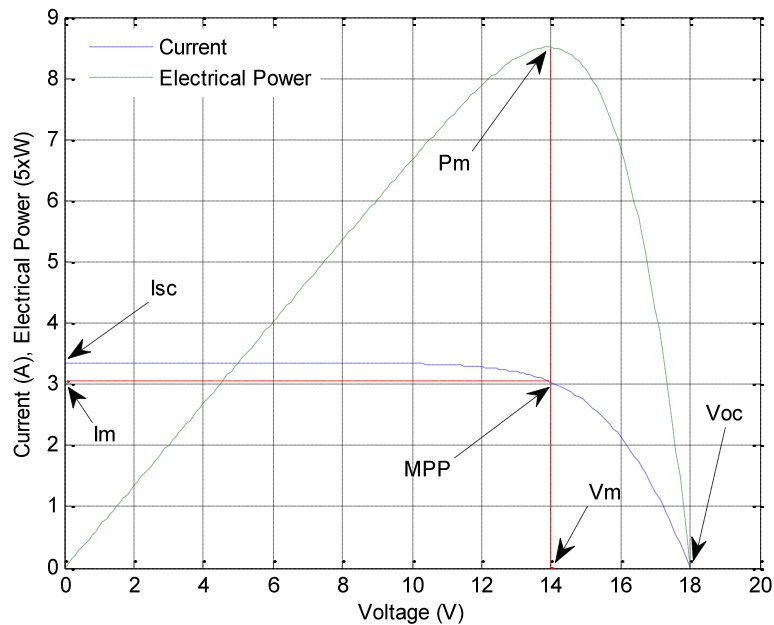


Figure 3.14: Q PEAK PV module I-V and P-V characteristic curves at STC simulated with Matlab

It can be seen that for a particular PV module, the power is zero to the two extremities of the power-voltage curve. The left point with the power equal to zero is the short-circuit point where

the voltage is zero and the current is equal to the short-circuit current I_{sc} and the right point with the power equal to zero is the open-circuit point, the current I is zero and the voltage is equal to the open-circuit voltage V_{oc} . The electric power is the maximum at a point at the knee of the power-voltage curve where the tangent dE/dV is zero. This point represents the maximum power point (MPP) (42). The values of voltage and current corresponding to this point are the maximum voltage V_m and the maximum current I_m . The maximum power is obtained from equation (3.21):

$$E_m = I_m V_m \quad (3.21)$$

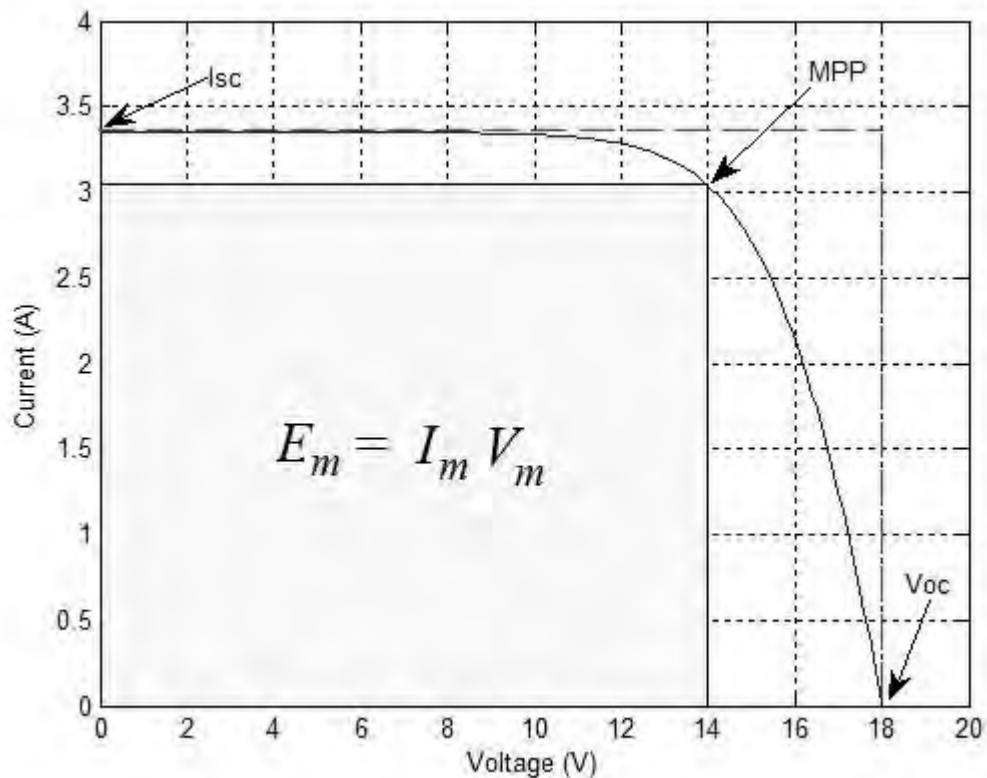


Figure 3.15: Q PEAK PV module I-V curve at STC simulated with Matlab

The maximum power point (MPP) is also determined by founding the biggest rectangle that will fit below the I-V curve as shown in Figure 3.15 as the electric power is defined as the product of

voltage and the current, and the surface of the rectangle corresponds to the maximum power E_m (42).

The ratio of the maximum power that can be delivered to the load and the product of I_{sc} and V_{oc} are often used to characterize module performance and is called the *fill factor* (FF) which is a measure of the real I-V characteristic. It is expressed as:

$$FF = \frac{E_m}{V_{oc}I_{sc}} = \frac{I_m V_m}{V_{oc}I_{sc}} \quad (3.22)$$

where:

E_m Maximum electric power (W)

V_m Maximum voltage (V)

I_m Maximum current (A)

V_{oc} Open-circuit voltage (V)

I_{sc} Short-circuit current (A)

Its value is higher than 0.7 for good cells (43). Fill factors around 70-75% for crystalline silicon solar modules are typical, while for multi-junction amorphous-Si modules, it is closer to 50–60% (42).

3.6 Impacts of temperature and insolation on I-V curves

Solar insolation and temperature have an impact on I-V curves of the PV module. When insolation increases, the short-circuit current increases in direct proportion while the open-circuit voltage increases by half of the previous increase for the same increment of the insolation. This trend can be seen in Figure 3.16 in which the behaviours of a PV module under various irradiance levels at ambient temperature of 25°C and wind speed of 1m/s are presented (42).

When cell temperature increases, the open-circuit voltage decreases considerably while the short-circuit current increases slightly as shown in Figure 3.17. Therefore, perhaps, this explains why photovoltaic performance is much better on cold, clear days than hot ones.

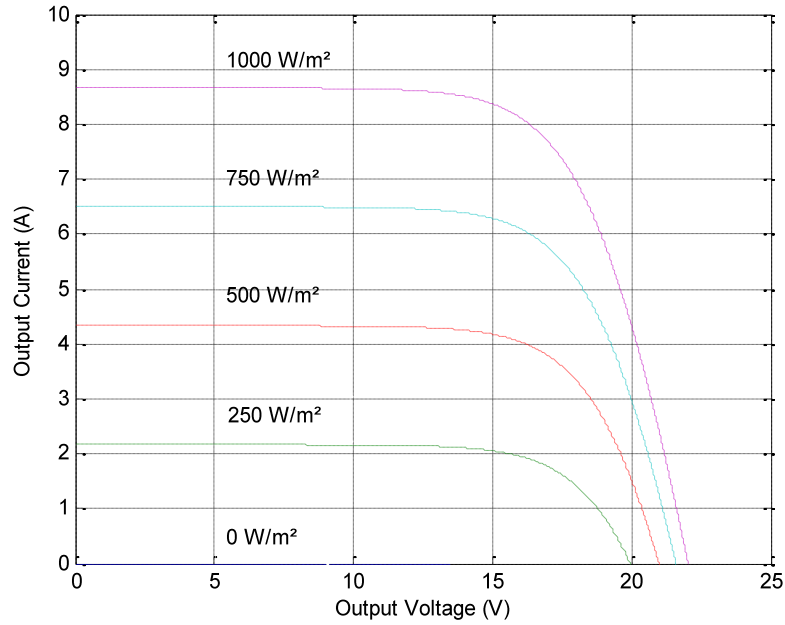


Figure 3.16: Current-voltage characteristic curves for PV module under various irradiance levels at 25°C temperature and 1m/s wind velocity simulated with the Matlab

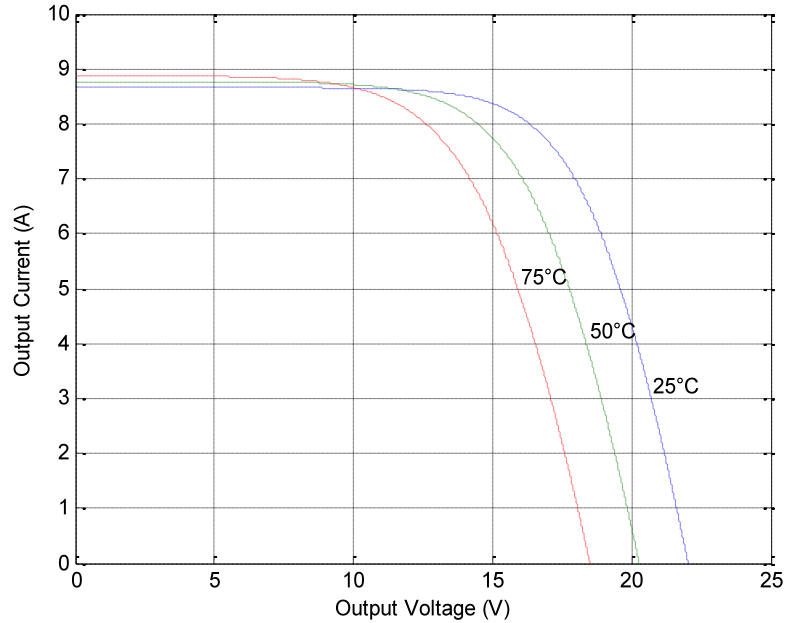


Figure 3.17: Current-voltage characteristic curves for PV module under various cell temperature levels at 1kW/m² insolation and 1m/s wind velocity simulated with Matlab

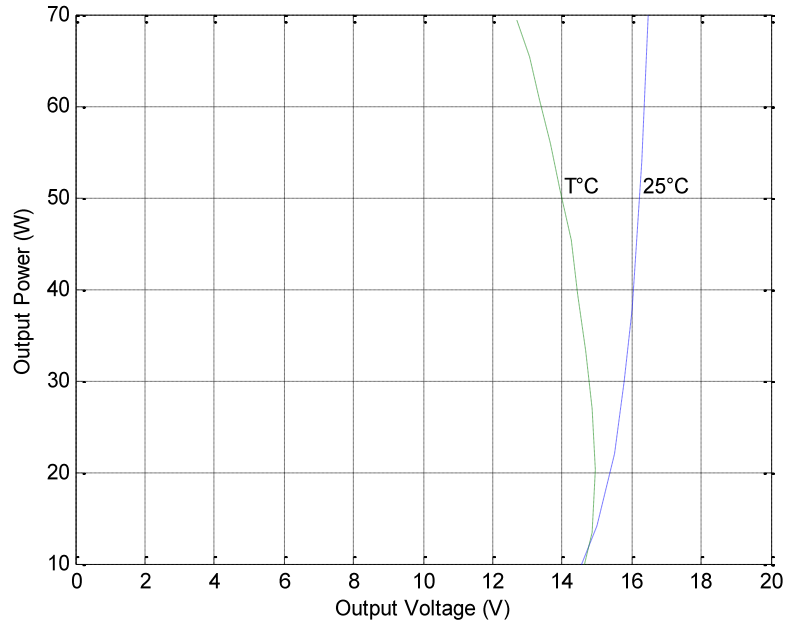


Figure 3.18: Power-voltage curve of PV module at STC and power-voltage curve of PV module under various cell temperature levels simulated with Matlab

For crystalline silicon cells, for each increase of one degree Celsius in temperature, the open-circuit voltage decreases by about 0.37% and the short-circuit current increases roughly by 0.05%. The consequence of this heating up of solar cells is that the MPP rises slightly and moves to the left with the MPP dropping about 0.5% per degree Celsius resulting in a significant shift in performance as cell temperature changes (42) as shown in Figure 3.18. These effects must be considered in any model for photovoltaic module efficiency.

3.7 Determination of cell temperature and average efficiency

Cell temperature has a negative impact on the efficiency of the PV module and must be curbed. In this section, cell temperature and its relation with efficiency is discussed.

3.7.1 Determination of cell temperature

The influence of temperature on I-V characteristics and consequently on the electrical efficiency of the PV module has been presented. Therefore it is important to determine the temperature of

the PV module which is the same as the temperature of solar cells for any analysis of its performance. The most common manner to do that is by using the Normal Operating Cell Temperature (NOCT) (46). The NOCT is the cell temperature in module lighting by the insolation of 0.8kW/m² at ambient temperature of 20°C and wind speed of 1m/s. The NOCT value is given by manufacturers of solar cells (42). The temperature of the PV module at different conditions is determined using the expression below:

$$T_c = T_a + \frac{NOCT - 20}{0.8} G \quad (3.23)$$

where:

- T_c Cell temperature (°C)
- T_a Ambient temperature (°C)
- G Solar insolation (kW/m²)

3.7.2. Calculation of average efficiency

The most common model of efficiency is given by the following equation:

$$\eta = \eta_r [1 - \beta_c (T_c - T_r) + \gamma \text{Log} G_o] \quad (3.24)$$

where:

- η_r Reference module efficiency
- T_r Reference temperature of 25°C
- G_o Solar insolation of 1000W/m²
- γ Solar irradiance coefficient of the PV module (m²/W)
- β_c Temperature coefficient of the PV module (1/K)
- T_c Cell temperature which depends on the environmental conditions (°C)

Most often this equation is obtained with $\gamma = 0$ (47). Then the equation (3.24) gives Evans-Florschuetz correlation below:

$$\eta = \eta_r [1 - \lambda (T_c - T_r)] \quad (3.25)$$

PV module electrical energy, E , as function of temperature is given by:

$$E = \eta AG \tag{3.26}$$

where A is the PV module surface (m^2).

The prediction of PV module performance in terms of electrical power output in the field which is the deviation from the standard test conditions as reported by the manufacturers is modelled in a manner similar to the above (48).

CHAPTER FOUR

THERMOSYPHON PRINCIPLE AND FLUID VELOCITY IN RECTANGULAR CHANNELS

This chapter presents details of the behavior of liquid due to variation of density with temperature, and the modeling of fluid velocity in absorber rectangular channels.

4.1 Variation of density with temperature variation

Heat added to a fluid increases its temperature, causes a density drop and induces flow (49). The factor that describes this phenomenon is called the volumetric thermal-expansion coefficient:

$$\beta = -\frac{1}{\rho} \left(\frac{\partial \rho}{\partial T} \right)_p \quad (4.1)$$

where:

ρ Density of the fluid in absorber channels (kg/m³)

T Temperature of the fluid in absorber channels (°C or K)

p pressure in the channels (Pa)

For small variations, β can be approximated by:

$$\beta = -\frac{1}{\rho} \left(\frac{\Delta \rho}{\Delta T} \right)_p \quad (4.2)$$

At the mean temperature T_m , the mean density is ρ_m and β is given by:

$$\beta = -\frac{1}{\rho_m} \frac{\rho - \rho_m}{T - T_m} \quad (4.3)$$

By rearranging equation (4.3), we obtain:

$$\rho = \rho_m - \beta \rho_m (T - T_m) \quad (4.4)$$

Considered a Newtonian fluid with constant properties heated from the top, flowing in z direction in a rectangular channel as shown in Figure 4.1. The fluid velocity is given by:

$$V = (0, 0, w(x, y)) \quad (4.5)$$

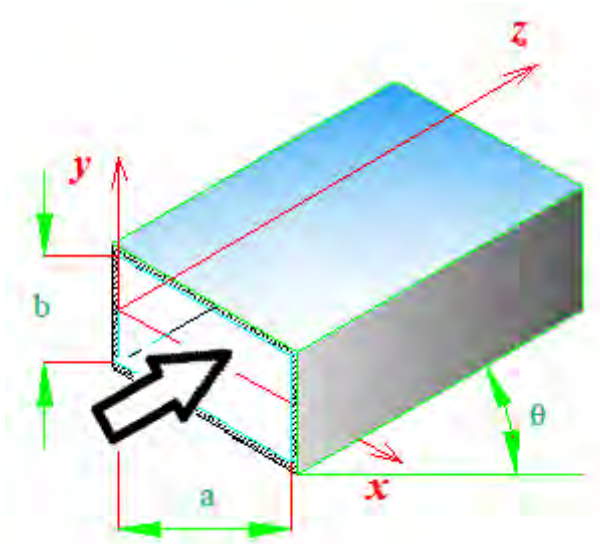


Figure 4.1: Newtonian fluid flowing in rectangular channel

Assuming that the system is at steady state, viscous dissipation and neglecting the edge effects, equation (2.5) becomes:

$$\frac{\partial w}{\partial z} = 0 \quad (4.6)$$

The x temperature dependence is not significant so that T becomes a function of y and equation (2.7) gives:

$$\frac{d^2 T}{dy^2} = 0 \quad (4.7)$$

In this case, boundary conditions are $T = T_{lcw}$ at $y = -0.5b$ and $T = T_{ucw}$ at $y = 0$

where:

T_{lcw} Temperature of lower channel wall ($^{\circ}\text{C}$)

T_{ucw} Temperature of upper channel wall (°C)

a Width of the channel (m)

b High of the channel (m)

Solving equation (4.7) and applying the boundary conditions, we get:

$$T - T_m = \frac{T_{ucw} - T_{lcw}}{b} y \quad (4.8)$$

where T_m is the mean temperature or a reference temperature given by:

$$T_m = \frac{T_{ucw} + T_{lcw}}{2} \quad (4.9)$$

Substituting equation (4.8) into equation (4.4) gives:

$$\rho = \rho_m - \beta \rho_m \frac{T_{ucw} - T_{lcw}}{b} y \quad (4.10)$$

4.2 Determination of velocity of the fluid in channels

As defined before, the channel profile has been considered to be rectangular. The velocity of the fluid can be determined by using continuity equations, energy equations and thermal energy equations. With the fluid velocity given by equation (4.6), we obtain from Navier-Stokes equations (2.6) the following equations:

$$-\frac{\partial p}{\partial x} = 0 \quad (4.11a)$$

$$-\frac{\partial p}{\partial y} + \rho g_y = 0 \quad (4.11b)$$

$$-\frac{\partial p}{\partial z} + \mu \left(\frac{\partial^2 w}{\partial x^2} + \frac{\partial^2 w}{\partial y^2} \right) + \rho g_z = 0 \quad (4.11c)$$

With $w=0$ at $-0.5a \leq x \leq 0.5a$, equation (4.11c) can be solved by separation of variables. The solution is given by:

$$w = w_p + X(x)Y(y) \quad (4.12)$$

where w_p is a particular solution and can be obtained by considering the case of the fluid flow between two parallel plates, so that equations (4.11a, 4.11b, and 4.11c) become:

$$-\frac{\partial p}{\partial x} = 0 \quad (4.13a)$$

$$0 = \frac{\partial p}{\partial y} - \rho g_y \quad (4.13b)$$

$$\mu \frac{\partial^2 w_p}{\partial y^2} = \frac{\partial p}{\partial z} - \rho g_z \quad (4.13c)$$

Solving equation (4.13c) with respect to boundary conditions $w_p = 0$ for the upper surface of the channel at $y = b$ and the lower surface of the channel at $y = 0$, we obtain the particular solution:

$$w_p = \frac{1}{2\mu} \left(\frac{\partial p}{\partial z} - \rho g_z \right) (y^2 - by) \quad (4.14)$$

And equation (4.12) becomes:

$$w = \frac{1}{2\mu} \left(\frac{\partial p}{\partial z} - \rho g \cos \theta \right) (y^2 - by) + X(x)Y(y) \quad (4.15)$$

Applying second partial derivation about x and y to equation (4.15), we obtain:

$$\frac{1}{Y} \frac{d^2 Y}{dy^2} = -\frac{1}{X} \frac{d^2 X}{dx^2} = -\lambda^2 \quad (4.16)$$

where λ is a dimensionless constant.

We then solve equation (4.16) and apply no-slip boundary conditions and symmetry in the direction of x . To meet the remaining condition, λ must be equal to $n\pi/a$, where n is any positive integer then applying to equation (4.15), the sum of Fourier series and the orthogonality conditions for sine, we obtain:

$$w = \frac{1}{2\mu} \left(\frac{\partial p}{\partial z} - \rho g_z \right) \left[(y^2 - ay) + \sum_{n=1}^{\infty} A_n \sin \frac{n\pi y}{b} \cosh \frac{n\pi x}{a} \right] \quad (4.17)$$

The value of the density ρ obtained in equation (4.10) gives:

$$\frac{\partial p}{\partial z} - \rho g_z = \frac{\partial p}{\partial z} - g_z \rho_m + \beta \rho_m g_z \frac{T_{ucw} - T_{lcw}}{b} y \quad (4.18)$$

Since the viscous terms are functions of at most y , and from the equations (4.13a) and (4.13b), p must be independent of x and linear in y , $\frac{\partial p}{\partial z}$ must be constant (50).

$$\frac{\partial p}{\partial z} = \frac{dp}{dz} \quad (4.19)$$

A pressure gradient $\frac{dp}{dz}$ in the system exists because the fluid has a non-zero density (49).

Therefore from hydrostatics:

$$\frac{dp}{dz} = \rho_m g_z \quad (4.20)$$

and

$$g_z = g \cos \theta \quad (4.21)$$

where:

g Acceleration due to gravity (m/s²)

θ Tilted angle of the PV module

From equation (4.10) and equation (4.15) we obtain:

$$\frac{\partial p}{\partial z} - \rho g_z = \beta \rho_m g \cos \theta \frac{T_{ucw} - T_{lcw}}{b} y \quad (4.22)$$

Equation (4.17) becomes:

$$w = \frac{1}{2\mu} \beta \rho_m g \cos \theta \frac{T_{ucw} - T_{lcw}}{b} y \left[(y^2 - ay) + \sum_{n=1}^{\infty} A_n \sin \frac{n\pi y}{b} \cosh \frac{n\pi x}{a} \right] \quad (4.23)$$

And coefficient A_n is obtained from equation (4.24) below:

$$A_n = \frac{\int_0^a (ya - y^2) \sin \frac{n\pi y}{a} dy}{\cosh \frac{n\pi b}{a} \int_0^a \sin^2 \frac{n\pi y}{a} dy} = \frac{4a^2}{n^3\pi^3} [1 - (-1)^n] \cosh \frac{n\pi b}{a} \quad (4.24)$$

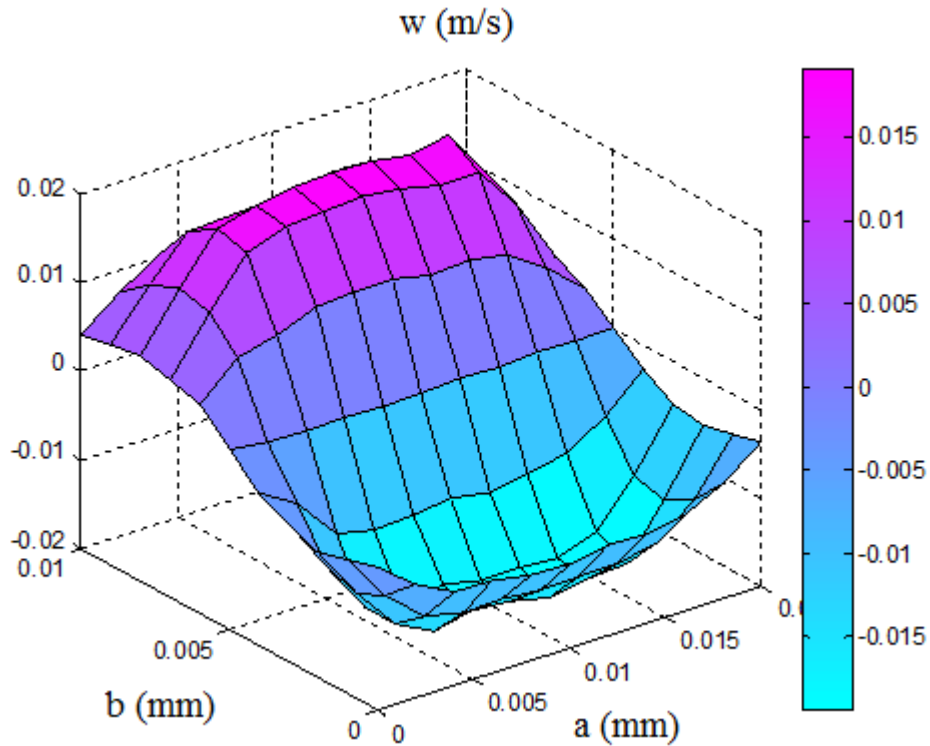


Figure 4.2: 3D view of velocity profile in channels simulated with Matlab

Figure 4.2 presents the profile of water velocity due to the thermosyphon phenomena in rectangular channels. It can be that the maximum velocity is obtained in the middle of each half of channel height and the average value of the velocity is the same for both parts although moving in opposite directions as illustrated in Figure 4.3.

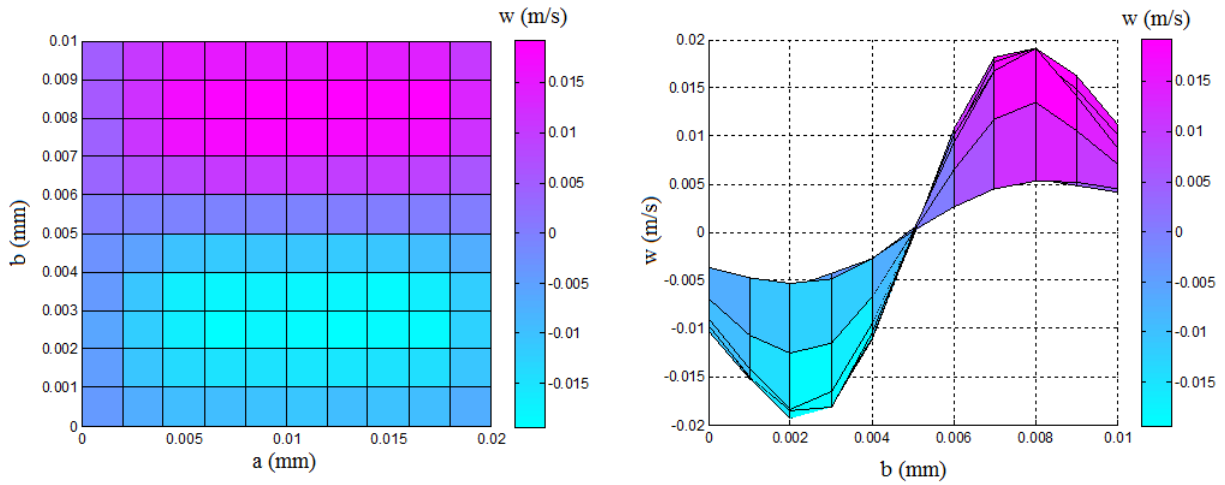


Figure 4.3: a-b and b-w views of water velocity profile in rectangular channels

The volume of the fluid discharged is given by equation (4.25) as:

$$Q = \int_0^b \int_{-0.5a}^{0.5a} w dx dy \quad (4.25)$$

With w given by equation (4.23), equation (4.25) for the volume discharged becomes:

$$Q = \beta \rho_m g \cos \theta \frac{T_{ucw} - T_{lcw}}{2\mu b} \times \left[-\frac{a^3 b^2}{12} + \sum_{n=1}^{\infty} A_n \frac{a^2}{n^2 \pi^2} (1 - (-1)^n) \left[b \sinh \frac{n\pi b}{a} + \frac{a}{n\pi} \left(1 - \cosh \frac{n\pi b}{a} \right) \right] \right] \quad (4.26)$$

Temperature coefficient β , mean density ρ_m , and dynamic viscosity μ vary slightly with temperature. Dimension parameters remain constant. From equation (4.26), the volume discharge depends more on the temperature difference between the upper channel wall temperature and the lower channel temperature.

CHAPTER FIVE

THERMOSYPHON HYBRID PHOTOVOLTAIC THERMAL SYSTEM

In Chapter Three we have shown that not only the ambient temperature has an impact on cell temperature, but also the solar insolation. The impact of the insolation on the PV module is due to the fact that the photovoltaic module converts only a small amount of insolation into electricity. The remainder of energy is transformed to heat (42). To improve its efficiency, a PV module must be cooled. The aim of this research is to cool the PV module with water by means of the thermosyphon principle i.e. by collecting heat from a PV module to a water storage tank for hot water use.

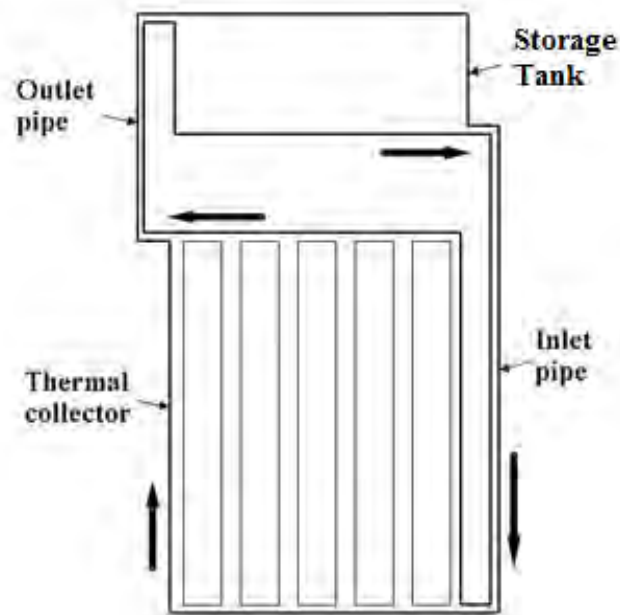


Figure 5.1: Hybrid photovoltaic thermal system

5.1 Description and principle of operation of PVT systems

The PVT system is constituted with a thermal collector plate, a water tank exchanger and inlet and outlet pipes as illustrated in Figure 5.1.

The thermal collector is constituted with front glazing, PV encapsulation, a thermal absorber plate and insulation as illustrated in Figure 5.2.

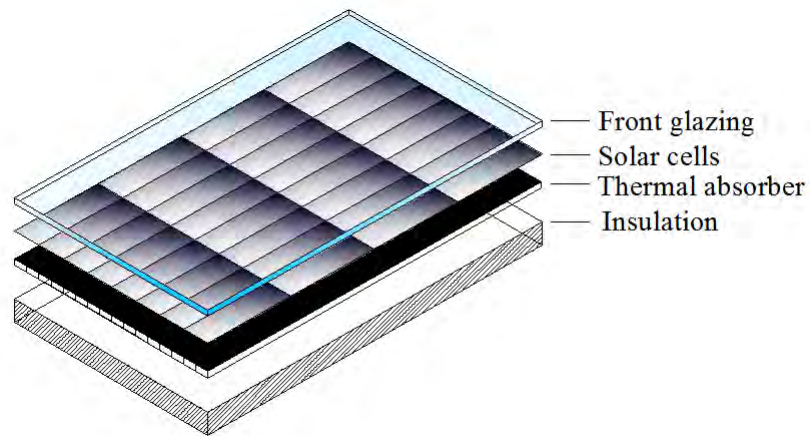


Figure 5.2: PV module above thermal absorber

Heat from PV cells is extracted by water flowing by natural convection in thermal absorber channels. Water is heated as the sun shines on the PV system, expands slightly, becomes lighter and is pushed through the collector outlet to the top of tank exchanger by cold water from the tank exchanger. The cold water enters the bottom of the collector by means of gravity and rises to the heat exchanger as it is warmed by means of the thermosyphon principle.

The PV module has been described and the effects of temperature and irradiance changes have been presented in Chapter Three.

A thermal absorber is added at the back side of the PV module to cool it and collect thermal energy. It is constituted by means of an assembly of flow modules with flat box flow channels in which water flows by natural convection. To allow water circulation by natural convection, the

thermal absorber is insulated at the bottom to avoid heat being exchanged with the external environment on the back side. A cross-section view of the PVT collector is presented in Figure 5.3.

Dimensions of the thermal absorber are the heat transfer surface area A_C and the thickness δ . The surface area A_C of the thermal absorber is approximately equal to the area of PV module defined by cell manufacturers that can be calculated using dimensions of solar cells or modules given in the associated datasheets and packing factor.

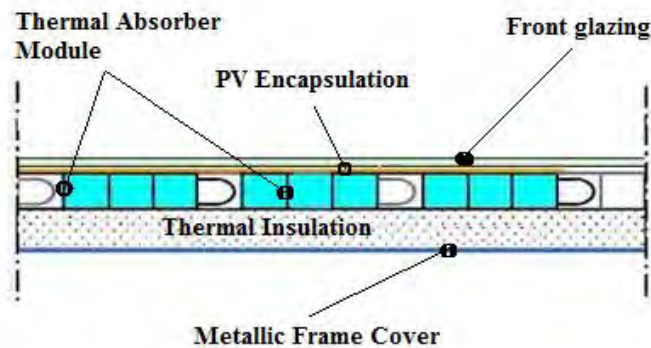


Figure 5.3: Cross-section view of the Photovoltaic Thermal absorber

5.2 Determination of the thermal collector temperature

To obtain temperatures for different components of the thermal collector, the energy balance for each component is introduced.

For the PV module:

The total insolation, G , from the sun to the collector is divided into solar irradiance G_c received by solar cells and solar irradiance G_T received by the tedlar. Part of this energy is converted to electricity E and the other part is transferred as heat H_{c-a} to ambient from the front glazing and H_{c-ucw} to upper thermal absorber channel surface as illustrated in Figure 5.4.

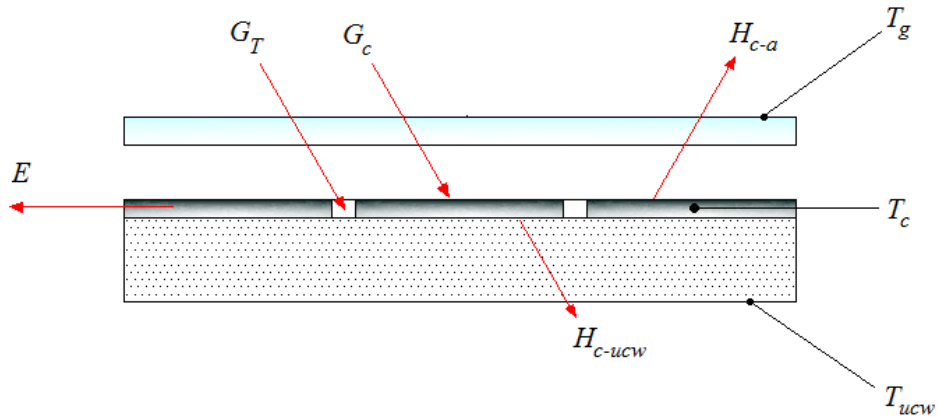


Figure 5.4: PV module input and output energies

Applying the energy balance to the element of surface dA of the module, we obtain:

$$G_c dA + G_T dA = H_{c-a} dA + H_{c-ucw} dA + E dA \quad (5.1)$$

or

$$G_c + G_T = H_{c-a} + H_{c-ucw} + E \quad (5.2)$$

where G_c is the irradiance on PV cells and is given by:

$$G_c = PF \tau_g \alpha_c G \quad (5.3)$$

where PF is the packing factor, τ_g is transmissivity of the front glass and α_c is absorptivity of solar cells.

The irradiance on tedlar, G_T is given by:

$$G_T = (1 - PF) \tau_g \alpha_T G \quad (5.4)$$

where α_T is the transmissivity of tedlar.

The heat transferred from solar cells to ambient by the top of the module H_{c-a} is given by:

$$H_{c-a} = U_{c-a}(T_c - T_a) \quad (5.5)$$

where U_{c-a} is the overall heat transfer coefficient from solar cells to ambient (W/m²K), T_c is solar cells temperature (°C) and T_a is the ambient temperature (°C).

The heat transferred from solar cells to the upper channels wall H_{c-ucw} , given by:

$$H_{c-ucw} = U_{c-ucw}(T_c - T_{ucw}) \quad (5.6)$$

where U_{c-ucw} is the overall heat transfer coefficient from the solar cells to the upper thermal absorber channel surface (W/m²K) and T_{ucw} is the temperature of the upper thermal absorber channel surface (°C).

The electrical energy produced by the module E is given by:

$$E = \eta_c PF \tau_g \alpha_c G \quad (5.7)$$

The solar module efficiency η_c is obtained from equation (5.8) below:

$$\eta_c = \eta_r [1 - \beta_c (T_c - T_r)] \quad (5.8)$$

where:

η_r Solar module reference efficiency or solar module efficiency at Standard Test Conditions (STC)

β_c Solar cell temperature coefficient (1/K)

Replacing the module efficiency into equation (5.7) by equation (5.8), the output electrical energy from the PV module becomes:

$$E = \eta_r PF \tau_g \alpha_c G - \Gamma PF \tau_g \alpha_c G (T_c - T_r) \quad (5.9)$$

where is Γ is given in Appendix C.

From equations (5.2), (5.3), (5.4), (5.5), (5.6) and (5.9) solar cell temperature is expressed as:

$$T_c = \frac{\tau_{eff}G + U_{c-a}T_a - U_{c-r}T_r + U_{c-ucw}T_{ucw}}{U_{c-a} + U_{c-ucw} - U_{c-r}} \quad (5.10)$$

Coefficients U_{c-a} , U_{c-ucw} , U_{c-r} and τ_{eff} are given in Appendix B.

For the upper channel wall (ucw):

The upper channel wall or surface receives heat H_{c-ucw} from solar cells and transfers it to water in channels of thermal absorber as heat H_{ucw-f} as illustrated in Figure 5.5.

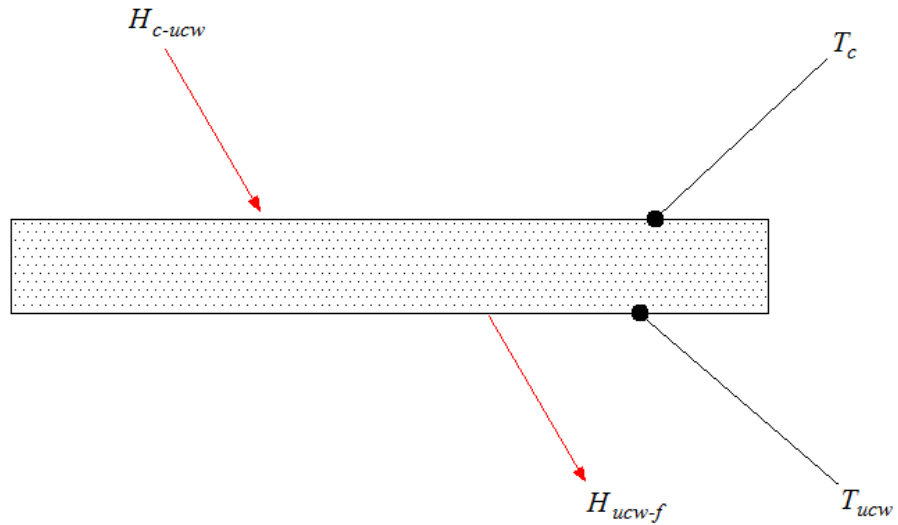


Figure 5.5: Upper channel wall input and output energies

Applying the energy balance to the element of surface dA of the upper channel wall (ucw), we obtain:

$$H_{c-ucw}dA = H_{ucw-f}dA \quad (5.11)$$

or

$$H_{c-ucw} = H_{ucw-f} \quad (5.12)$$

where the heat transferred from the upper channel wall to the water flowing in thermal absorber channels H_{ucw-f} , given by:

$$H_{ucw-f} = h_f(T_{ucw} - T_f) \quad (5.13)$$

where h_f is the channel water convective heat transfer coefficient (W/m²K) given in Appendix B.

From equations (5.6), (5.12) and (5.13), we obtain:

$$U_{c-ucw}T_c - (h_f + U_{c-ucw})T_{ucw} + h_fT_f = 0 \quad (5.14)$$

where T_f is the temperature of water in the thermal absorber channels.

From equations (5.10) and (5.14), we obtain the temperature T_{ucw} of the upper channel surface, given by:

$$T_{ucw} = \frac{\xi_{cu}\tau_{eff}G + \xi_{cu}(U_{c-a}T_a - U_{c-r}T_r) + h_fT_f}{h_f + U_{c-ucw}(1 - \xi_{cu})} \quad (5.15)$$

where the coefficient ξ_{cu} is the solar cell upper wall dimensionless coefficient, given in Appendix C.

For the water flowing through water ducts:

The heat removed from the upper channel surface by the water flowing in thermal absorber channels is H_{ucw-f} .

Water enters the channel at temperature T_i and leaves at temperature T_o at the velocity $(0,0,w(x,y))$ given by equation (4.5). A certain quantity of heat removed by water from the PV module is H_{ff} and another quantity of heat is transferred to the ambient from the back surface of the thermal collector depending on the back surface insulation is H_{f-a} as illustrated in Figure 5.6.

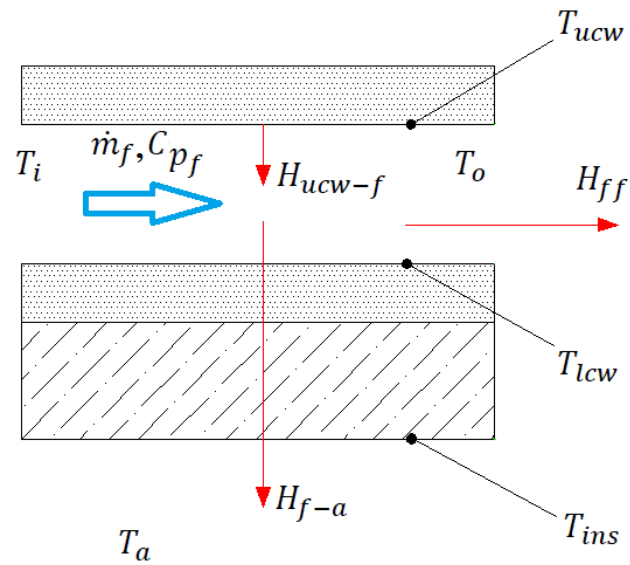


Figure 5.6: Channel water input and output energies

Consider a volume element of water dV , illustrated in Figure 5.7, flowing in the channel at the temperature dT_f with the velocity w_f .

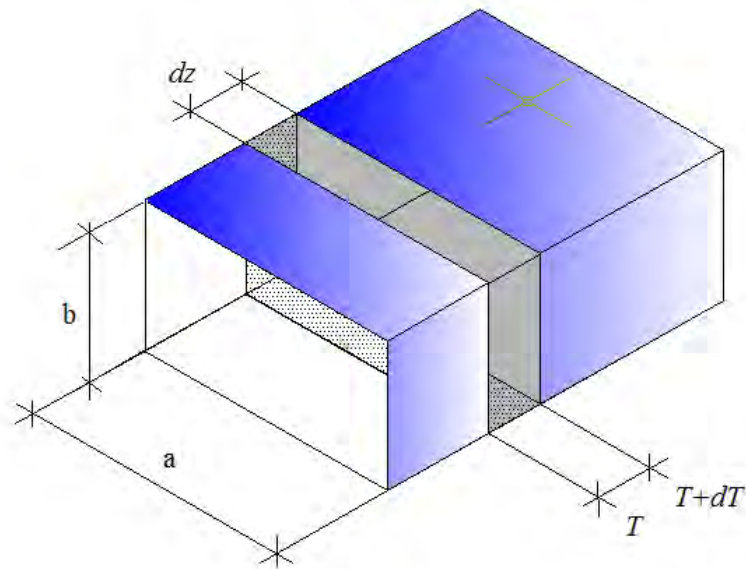


Figure 5.7: A volume element of water in thermal collector channel

Applying the energy balance to the element of volume dV of the water in the channel wall, we obtain:

$$H_{ucw-f} = H_{f-a} + H_{ff} \quad (5.16)$$

The heat transferred from the channel water to the ambient from the back surface of the element H_{f-a} , is given by:

$$H_{f-a} = U_{f-a}(T_f - T_a)a dz \quad (5.17)$$

The heat removed from upper channel wall by the flowing water for an element of volume dV , H_{ff} , is given by:

$$H_{ff} = \rho_f \omega_f abc_{pf} dT_f \quad (5.18)$$

From equations (5.13), (5.18) and (5.19), we obtain:

$$\frac{dT_f}{dz} + \frac{U_{f-a} + h_f(1 - \xi_{cu})}{b\rho_f\omega_f c_{pf}} T_f = \frac{\xi_{fu}\xi_{cu}(\tau_{eff}G + U_{c-a}T_a - U_{c-r}T_r) + U_{f-a}T_a}{b\rho_f\omega_f c_{pf}} \quad (5.19)$$

where:

b Height of the channel (m)

ρ_f Density of water (kg/m³)

c_{pf} Specific heat of the water (J/kgK)

U_{f-a} Channel fluid ambient overall heat transfer coefficient (W/m²K)

ξ_{fu} Upper wall dimensionless coefficient of the water (-)

The state coefficients are given in Appendix C.

Equation (5.19) is a not an homogeneous first order differential equation and it can be solved by assuming that:

$$r = U_{f-a} + h_f(1 - \xi_{cu}) \quad (5.20)$$

$$s = \xi_{fu}\xi_{cu}(\tau_{eff}G + U_{c-a}T_a - U_{c-r}T_r) + U_{f-a}T_a \quad (5.21)$$

$$m = b\rho_f\omega_f c_{pf} \quad (5.22)$$

At $z = 0$, the temperature T_f of the fluid is equal to the inlet temperature T_i . We obtain from equation (5.19):

$$T_f = \frac{s}{r} + \left(T_i - \frac{s}{r}\right) \exp\left(-\frac{r}{m}z\right) \quad (5.23)$$

The output water temperature T_o is obtained with $z = L$ and is given by:

$$T_o = \frac{s}{r} + \left(T_i - \frac{s}{r}\right) \exp\left(-\frac{r}{m}L\right) \quad (5.24)$$

The average fluid temperature \bar{T} in the thermal collector is obtained by integrate equation (5.23) for z equal 0 to L and divide the result per L the length L of the channel:

$$\bar{T}_f = \frac{1}{L} \int_0^L T_f dz \quad (5.25)$$

That gives:

$$\bar{T}_f = \frac{1}{L} \left[\frac{sL}{r} + \frac{m}{r} \left(T_i - \frac{s}{r}\right) \left(1 - \exp\left(-\frac{r}{m}L\right)\right) \right] \quad (5.26)$$

From equations (5.24) and (5.26), the average fluid temperature becomes:

$$\bar{T}_f = \frac{1}{rL} [sL + m(T_i - T_o)] \quad (5.27)$$

The average temperature of the upper channel wall is obtained from equation (5.15) and equation (5.27):

$$\bar{T}_{ucw} = \frac{\xi_{cu}\tau_{eff}G + \xi_{cu}(U_{c-a}T_a - U_{c-r}T_r) + h_f\bar{T}_f}{h_f + U_{c-ucw}(1 - \xi_{cu})} \quad (5.28)$$

where:

ξ_{cu} Solar cell upper channel wall dimensionless coefficient (-)

τ_{eff} Effective transmittivity (-)

G Solar insolation (W/m²)

U_{c-a} Overall heat transfer between solar cells and ambient temperature from the top (W/m²K)

U_{c-r} Overall heat transfer between solar cells and ambient temperature from the top (W/m²K)

U_{c-ucw} Overall heat transfer between solar cells and upper channel wall (W/m²K)

h_f Water convective heat transfer coefficient (W/m²K)

T_a Ambient temperature (°C)

T_r Reference temperature (= 25°C)

And the average cell temperature is obtained from equation (5.10) and equation (5.28):

$$\bar{T}_c = \frac{\tau_{eff}G + U_{c-a}T_a - U_{c-r}T_r + U_{c-ucw}\bar{T}_{ucw}}{U_{c-a} + U_{c-ucw} - U_{c-r}} \quad (5.29)$$

5.3 Determination of the temperature of the water storage tank

The temperature of water in the storage tank is obtained by dividing the tank into five layers and applying the finite difference method to each layer. The average temperature of water in the tank is the sum of temperatures of layers over the number of layers.

5.3.1 Tank geometry

Most tanks used are cylindrical and for a cylindrical tank, we have two surfaces of heat exchange.

The two areas A_D (the top and bottom the cylinder) perpendicular to the cylinder axis shown in Figure 5.8 are given by:

$$A_D = \pi \frac{D_t^2}{4} \quad (5.30)$$

where D_t is the diameter of the tank (m)

And the area A_h parallel to the cylinder axis is given by:

$$A_h = \pi D_t h_t \quad (5.31)$$

where h_t is the height of the tank (m)

The volume V_t of the tank is obtained from the relation below:

$$V_t = A_D h_t \quad (5.32)$$

5.3.2 Temperature of the water in the tank

The heat transferred to water in the tank is transient heat conduction, the temperature of water changing with position and time. For the specific case of a hybrid PVT system, a solar hot water storage tank is used to store heat from the thermal collector.

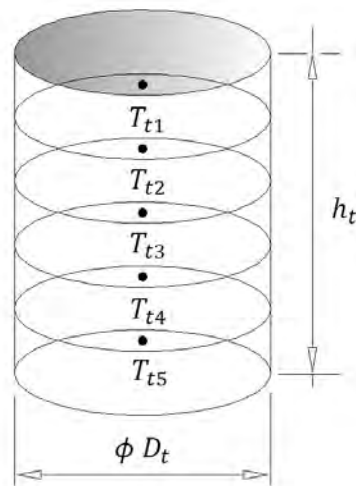


Figure 5.8: Tank divided into five nodes

The variation of the temperature is only in one direction from the tank inlet to the tank outlet. Numerical methods based on finite difference are used to obtain the numerical value of the temperature of water in the tank. The finite difference method has already been introduced in Chapter Two.

Consider storage divided into five equal layers of temperature T_{ij} with j equal 1 to 5 as shown in Figure 5.8. From this division, six nodes from 0 and 5 are obtained with nodes 0 and 5 as boundary nodes and nodes 1, 2, 3, 4 as interior nodes as shown in Figure 5.9.

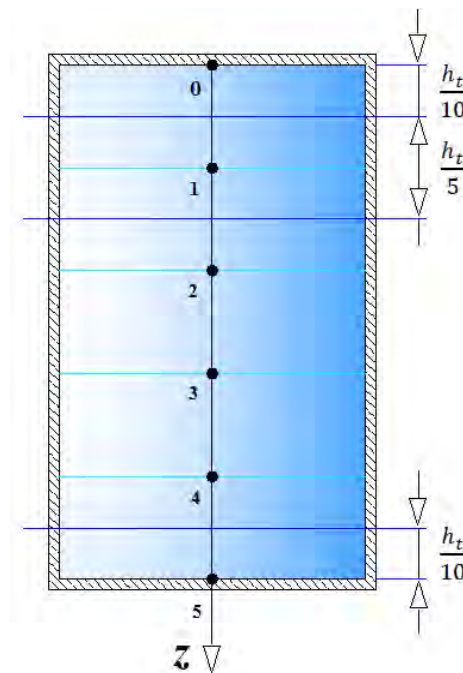


Figure 5.9: Six nodes from five layers for the water tank

Applying the finite difference method to each node of the tank, we obtain:

For the top layer, $j=1$:

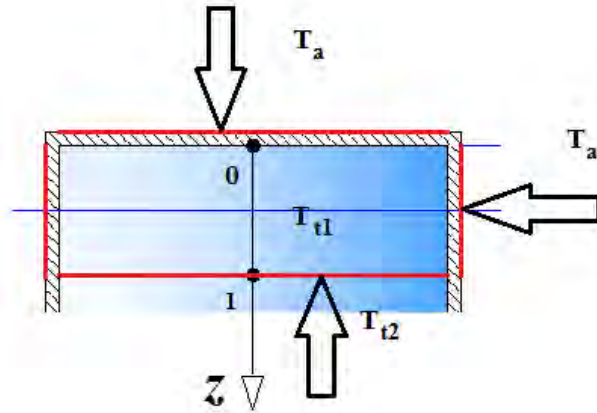


Figure 5.10: Exterior node 0 input and output energies

The energy balance applied to layer 1 gives:

$$\frac{1}{5}V_t\rho_f c_f \frac{dT_{t1}}{dt} = \dot{m}_f c_f (T_o - T_{t1}) + \frac{5k_f}{h_t} A_D (T_{t2} - T_{t1}) + U_{a-t} \left(\frac{A_h}{5} + A_D \right) (T_a - T_{t1}) \quad (5.33)$$

where:

\dot{m}_f Mass flow rate in the thermal absorber channel (kg/s)

T_{t1} Temperature of water in the tank at node 1 (°C)

T_{t2} Temperature of water in the tank at node 2 (°C)

k_f Thermal conductive heat transfer coefficient for the water (W/mK)

U_{a-t} Water tank ambient overall heat transfer coefficient (W/m²K)

The variation of the temperature $\frac{dT_{t1}}{dt}$ can be approximated by $\frac{T_{t1}^{i+1} - T_{t1}^i}{\Delta t}$, so that equation (5.33) is rewritten as:

$$V_t \rho_f c_f \left(\frac{T_{t1}^{i+1} - T_{t1}^i}{\Delta t} \right) = 5\dot{m}_f c_f (T_o - T_{t1}) + \frac{25k_f}{h_t} A_D (T_{t2} - T_{t1}) + U_{a-t} (A_h + 5A_D) (T_a - T_{t1}) \quad (5.34)$$

or

$$V_t \rho_f c_f T_{t1}^{i+1} - V_t \rho_f c_f T_{t1}^i = \left[-5\dot{m}_f c_f \Delta t - 25 \frac{k_f}{h_t} A_D \Delta t - U_{a-t} (A_h + 5A_D) \Delta t \right] T_{t1} + 25 \frac{k_f}{h_t} A_D \Delta t T_{t2} + 5\dot{m}_f c_f \Delta t T_o + U_{a-t} (A_h + 5A_D) \Delta t T_a \quad (5.35)$$

Applying the implicit finite difference method, equation (2.13) and equation (5.35) gives:

$$\left[V_t \rho_f c_f + 5\dot{m}_f c_f \Delta t + 25 \frac{k_f}{h_t} A_D \Delta t + U_{a-t} (A_h + 5A_D) \Delta t \right] T_{t1}^{i+1} - 25 \frac{k_f}{h_t} A_D \Delta t T_{t2}^{i+1} = 5\dot{m}_f c_f \Delta t T_o^{i+1} + V_t \rho_f c_f T_{t1}^i + U_{a-t} (A_h + 5A_D) \Delta t T_a \quad (5.36)$$

where T_{tj}^i is the temperature of water in the tank at the node j at time t^i

For interior layers

Consider an interior layer j :

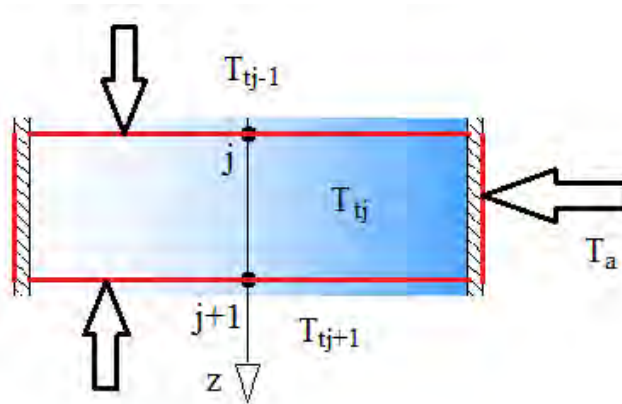


Figure 5.11: Interior node j input and output energies

The energy balance applied to the layer j gives:

$$\begin{aligned} \frac{1}{5} V_t \rho_t c_t \frac{dT_{tj}}{dt} &= \dot{m}_f c_t (T_{t(j-1)} - T_{tj}) + \frac{5k_t}{h_t} A_D (T_{t(j-1)} - T_{tj}) \\ &+ \frac{5k_f}{h_t} A_D (T_{t(j+1)} - T_{tj}) + \frac{1}{5} U_{a-t} A_h (T_a - T_{tj}) \end{aligned} \quad (5.37)$$

or

$$\begin{aligned} V_t \rho_t c_t T_{tj}^{i+1} - V_t \rho_t c_t T_{tj}^i &= 5 \left(\dot{m}_f c_t + \frac{5k_t}{h_t} A_D \right) \Delta t T_{t(j-1)} \\ -5 \left(\dot{m}_f c_t + \frac{10k_t}{h_t} A_D + U_{a-t} \frac{A_h}{5} \right) \Delta t T_{tj} &+ \frac{25k_f}{h_t} A_D \Delta t T_{t(j+1)} + U_{a-t} A_h \Delta t T_a \end{aligned} \quad (5.38)$$

Applying the implicit finite difference method to equation (5.38), we obtain:

$$\begin{aligned} -5 \left(\dot{m}_f c_t + \frac{5k_t}{h_t} A_D \right) \Delta t T_{t(j-1)}^{i+1} &+ \left[V_t \rho_t c_t + 5 \left(\dot{m}_f c_t + \frac{10k_t}{h_t} A_D + U_{a-t} \frac{A_h}{5} \right) \Delta t \right] T_{tj}^{i+1} \\ - \frac{25k_t}{h_t} A_D \Delta t T_{t(j+1)}^{i+1} &= V_t \rho_t c_t T_{tj}^i + U_{a-t} A_h \Delta t T_a \end{aligned} \quad (5.39)$$

with $j = 2, 3$ and 4 .

For the bottom layer, $j = 5$

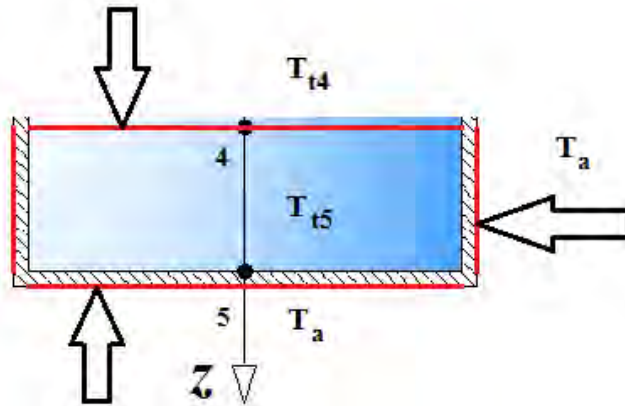


Figure 5.12: Exterior node 5 input and output energies

The energy balance applied to layer 5 gives:

$$\frac{1}{5}V_t\rho_t c_t \frac{dT_{t5}}{dt} = \dot{m}_f c_t (T_{t4} - T_{t5}) + \frac{5k_t}{h_t} A_D (T_{t4} - T_{t5}) + U_{a-t} \left(\frac{A_h}{5} + A_D \right) (T_a - T_{t5}) \quad (5.40)$$

The variation of the temperature $\frac{dT_{t5}}{dt}$ can be approximated to $\frac{T_{t5}^{i+1} - T_{t5}^i}{\Delta t}$, so that equation (5.40) is rewritten as:

$$\begin{aligned} V_t\rho_t c_t \left(\frac{T_{t5}^{i+1} - T_{t5}^i}{\Delta t} \right) &= 5\dot{m}_f c_t (T_{t4} - T_{t5}) + \frac{25k_t}{h_t} A_D (T_{t4} - T_{t5}) \\ &+ U_{a-t} (A_h + 5A_D) (T_a - T_{t5}) \end{aligned} \quad (5.41)$$

or

$$\begin{aligned} V_t\rho_t c_t T_{t5}^{i+1} - V_t\rho_t c_t T_{t5}^i &= \left[-5\dot{m}_f c_t \Delta t - 25 \frac{k_t}{h_t} A_D \Delta t - U_{a-t} (A_h + 5A_D) \Delta t \right] T_{t5} \\ &+ 5 \left(\dot{m}_f c_t + \frac{5k_t}{h_t} A_D \right) \Delta t T_{t4} + 5U_{a-t} \left(\frac{A_h}{5} + A_D \right) \Delta t T_a \end{aligned} \quad (5.42)$$

Applying the implicit finite difference method, equation (2.13) and equation (5.42) gives:

$$\begin{aligned} -5 \left(\dot{m}_f c_t + \frac{5k_t}{h_t} A_D \right) \Delta t T_{t5}^{i+1} + \left[V_t\rho_t c_t + 5 \left(\dot{m}_f c_t + \frac{5k_t}{h_t} A_D + U_{a-t} \left(\frac{A_h}{5} + A_D \right) \right) \Delta t \right] T_{t5}^{i+1} \\ = V_t\rho_t c_t T_{t5}^i + 5U_{a-t} \left(\frac{A_h}{5} + A_D \right) \Delta t T_a \end{aligned} \quad (5.43)$$

Assuming that:

$$\varepsilon = V_t\rho_t c_t + 5 \left(\dot{m}_f c_t + \frac{10k_t}{h_t} A_D + U_{a-t} \frac{A_h}{5} \right) \Delta t \quad (5.44)$$

From equations (5.36), (5.39) and (5.43) we obtain the system of equations below in matrix form:

$$AT = B \quad (5.45)$$

where:

The temperature vector is given by:

$$T = \begin{bmatrix} T_{t1}^{i+1} \\ T_{t2}^{i+1} \\ T_{t3}^{i+1} \\ T_{t4}^{i+1} \\ T_{t5}^{i+1} \end{bmatrix} \quad (5.46)$$

The vector B is given by:

$$B = \begin{bmatrix} 5\dot{m}_f c_f \Delta t T_o^{i+1} + V_t \rho_t c_t T_{t1}^i + 5U_{a-t} \left(\frac{A_h}{5} + A_D \right) \Delta t T_a \\ V_t \rho_t c_t T_{t2}^i + U_{a-t} A_h \Delta t T_a \\ V_t \rho_t c_t T_{t3}^i + U_{a-t} A_h \Delta t T_a \\ V_t \rho_t c_t T_{t4}^i + U_{a-t} A_h \Delta t T_a \\ V_t \rho_t c_t T_{t5}^i + 5U_{a-t} \left(\frac{A_h}{5} + A_D \right) \Delta t T_a \end{bmatrix} \quad (5.47)$$

And the matrix A given by (5.48) is the matrix of coefficients of temperatures of different layers at time $i+1$:

$$A = \begin{pmatrix} \varepsilon + 5 \left(U_{a-t} - \frac{5k_t}{h_t} \right) A_D \Delta t & -\frac{25k_t}{h_t} A_D \Delta t & 0 & 0 & 0 \\ -5 \left(\dot{m}_f c_t + \frac{5k_t}{h_t} A_D \right) \Delta t & \varepsilon & -\frac{25k_t}{h_t} A_D \Delta t & 0 & 0 \\ 0 & -5 \left(\dot{m}_f c_t + \frac{5k_t}{h_t} A_D \right) \Delta t & \varepsilon & -\frac{25k_t}{h_t} A_D \Delta t & 0 \\ 0 & 0 & -5 \left(\dot{m}_f c_t + \frac{5k_t}{h_t} A_D \right) \Delta t & \varepsilon & -\frac{25k_t}{h_t} A_D \Delta t \\ 0 & 0 & 0 & -5 \left(\dot{m}_f c_t + \frac{5k_t}{h_t} A_D \right) \Delta t & \varepsilon + 5 \left(U_{a-t} - \frac{5k_t}{h_t} \right) A_D \Delta t \end{pmatrix} \quad (5.48)$$

CHAPTER SIX

PVT SYSTEM BEHAVIOR AGAINST VARIATION OF ENVIRONMENTAL PARAMETERS

Environmental parameters have great impact on output energy and efficiency of photovoltaic systems. The important environmental parameters that influence the performance of PV systems are solar irradiance, ambient temperature and wind velocity. The simulation results based on models developed in Chapter Five are achieved for each environmental parameter, and PVT module behaviors are compared to PV module behaviors.

6.1 PVT system behaviors against the variation of insolation

The most important environmental parameter is the solar irradiance due to the fact that the PV panel converts light from the sun into electrical and thermal energies. Figure 6.1 and Figure 6.2 show the PVT system behaviors against the variation of insolation.

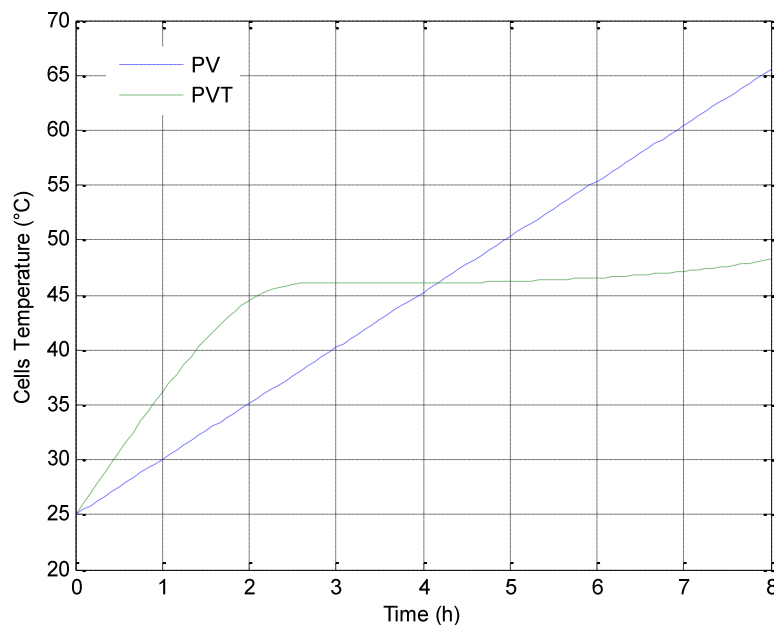


Figure 6.1: PVT module behaviors for variation of solar irradiance at ambient temperature of 25°C and wind speed of 1m/s

Figure 6.1 represents the variation of PV module temperature and PVT module temperature with solar insolation for 8 hours of exposure to the sunlight. For solar insolation varying from $0\text{W}/\text{m}^2$ to $1200\text{W}/\text{m}^2$, it can be seen that cell temperature for a conventional PV module varies linearly from 25°C to 65°C while for a PVT module temperature varies linearly from 25°C to 45°C for the 2 first hours then remains constant between 45°C and 48°C for the remaining time.

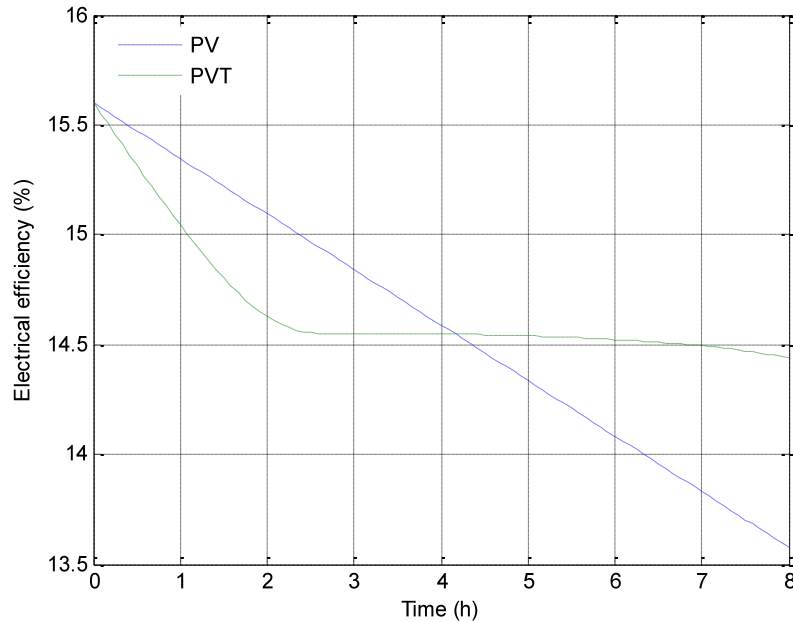


Figure 6.2: Electrical efficiency behaviors for variation of solar irradiance at ambient temperature 25°C and wind speed $1\text{m}/\text{s}$ for PVT module compared to PV module

Due to the increase in temperature of the module with solar insolation, the electrical efficiency of a conventional PV module decreases linearly from the STC values of 15.6% to 13.58% while the PVT module efficiency decreases linearly from 15.6% to 14.57% for the 2 first hours then remains constant between 14.44% and 14.57% for the remaining time as shown in Figure 6.2 above.

From Figure 6.3, it can be seen that the Maximum Power Point (MPP) of the PVT module is at the left of MPP of the conventional PV module for insolation below $600\text{W}/\text{m}^2$ due to water in the channels that constitutes a thermal resistance between solar cells and ambient on the back side of the thermal collector. Above $600\text{W}/\text{m}^2$, water density in thermal absorber channels decreases and the thermosyphon phenomenon occurs.

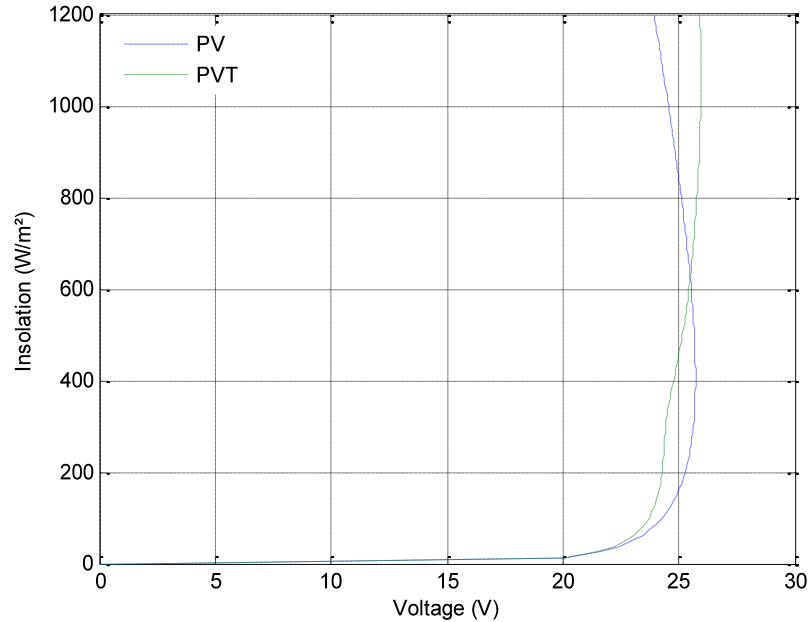


Figure 6.3: Maximum Power point behaviors for variation of solar irradiance at ambient temperature 25°C and wind speed 1m/s for PVT module compared to PV module

The MPP curve for the PVT module shifts to the right of the PV module MPP curve so that at the same insolation, more power can be obtained from the PVT module than from the PV module. This demonstrates the advantage of PVT systems compared to conventional PV systems, especially at higher insolation.

The water tank temperature remains constant at 25°C for the first 2 hours then increases from 25°C to 38.56°C following the positive exponential law as seen in Figure 6.4.

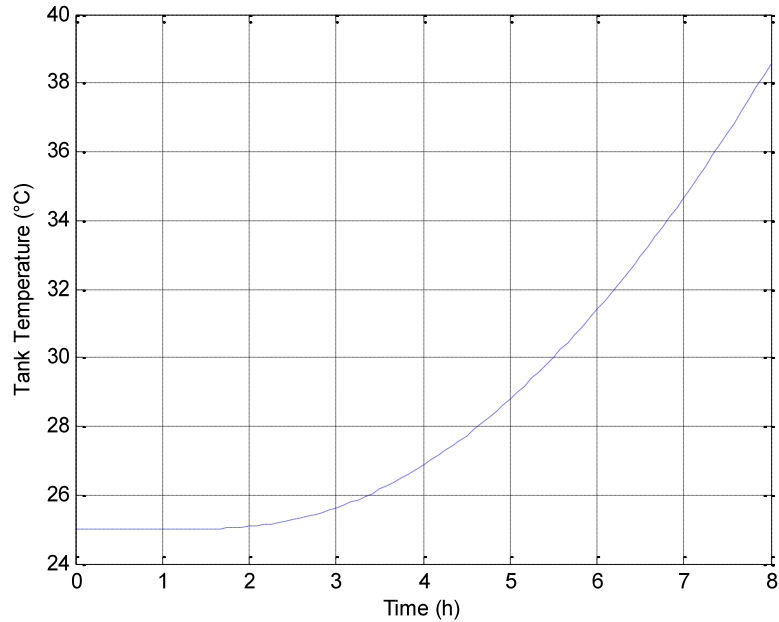


Figure 6.4: Water tank temperature for variation of solar irradiance at ambient temperature 25°C and wind speed 1m/s for PVT module

6.2 The influence of ambient temperature on performance of the PVT system

The other important parameter that influences the efficiency of the PV module is ambient temperature. Consider the case of ambient temperature varying from 15°C to 35°C for constant insolation of 1000W/m² at 1m/s wind velocity for 8 hours.

For a constant value of insolation and wind velocity, it can see from Figure 6.5 that cell temperature for conventional PV module increases linearly from 48.75°C to 68.75°C with ambient temperature. For PVT module on the other hand, due to sudden exposure of PVT module to high solar insolation, the cell temperature decreases from 89.39°C to 41.78°C accompanied by oscillation behaviors due to under damped solution of equation (5.19).

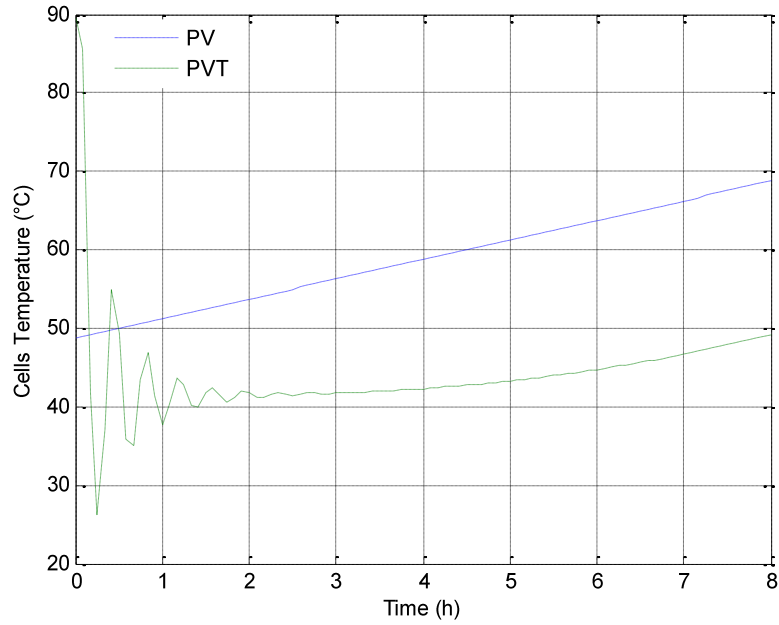


Figure 6.5: Cell temperature behaviors against the variation of ambient temperature for PV module and PVT module at $1000\text{W}/\text{m}^2$ insolation and $1\text{m}/\text{s}$ wind speed

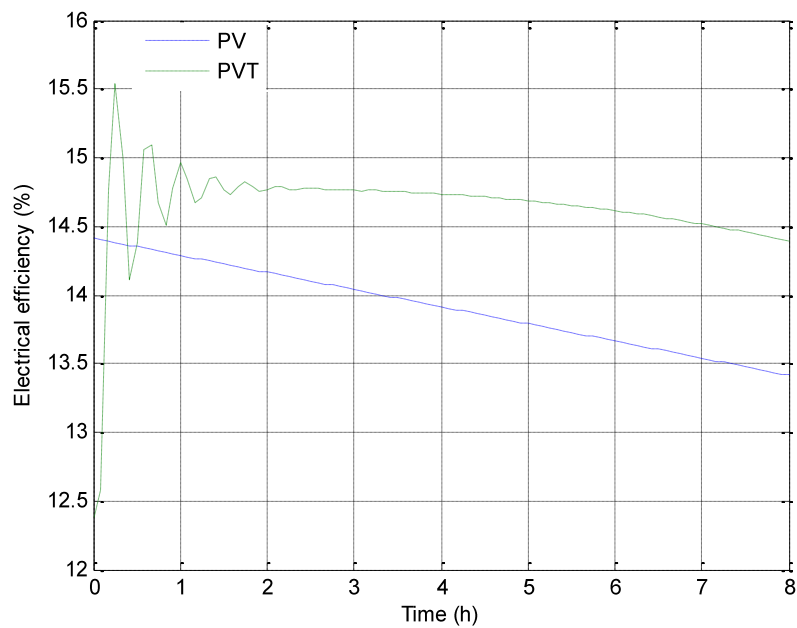


Figure 6.6: Electrical efficiency behaviors against the variation of ambient temperature for PV module and PVT module at $1000\text{W}/\text{m}^2$ insolation and $1\text{m}/\text{s}$ wind speed

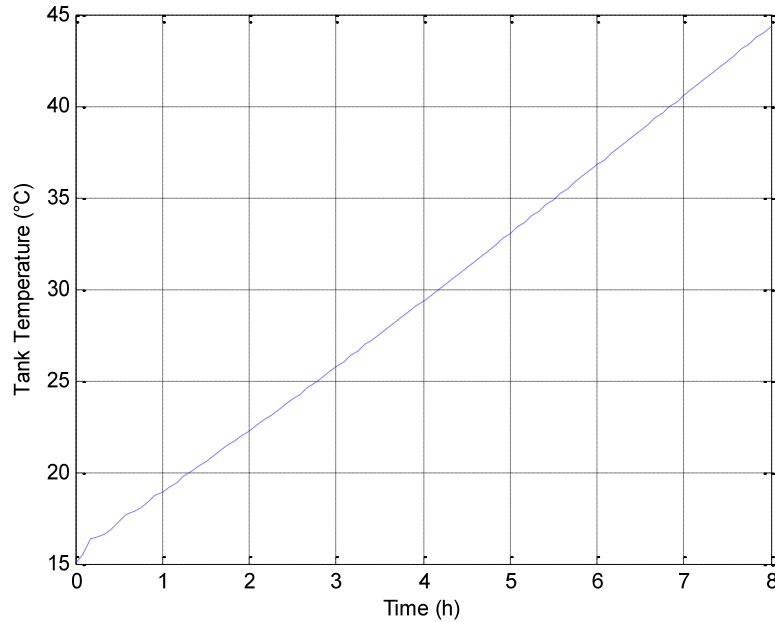


Figure 6.7: Water tank temperature for variation of ambient temperature for PVT module at 1000W/m² insolation and 1m/s wind speed

Oscillation behavior of cell temperature is justified by the natural response of water temperature in the channels to the thermal shock for the 3 first hours as seen in Figure 6.5. For the remaining five hours, the cell temperature increases from 41.78°C to 49.22°C following the positive exponential function.

The PV module efficiency decreases linearly from 14.41% to 13.42% while the PVT module increases from 12.39% to 14.76% accompanied by oscillation for the first three hours due to temperature behaviour explained above then following the negative exponential from 14.76% to 14.39% for the rest of time as shown in Figure 6.6.

The water tank temperature increases linearly with the ambient temperature from 15.02°C to 44.34°C as seen in Figure 6.7.

6.3 PVT system behaviors against the variation of wind velocity

The other environmental parameter that has the impact on PV module efficiency is the wind. The heat produced by solar cells is removed from the top and back sides by the wind. If the wind velocity increases, more heat is removed from the module to the ambient.

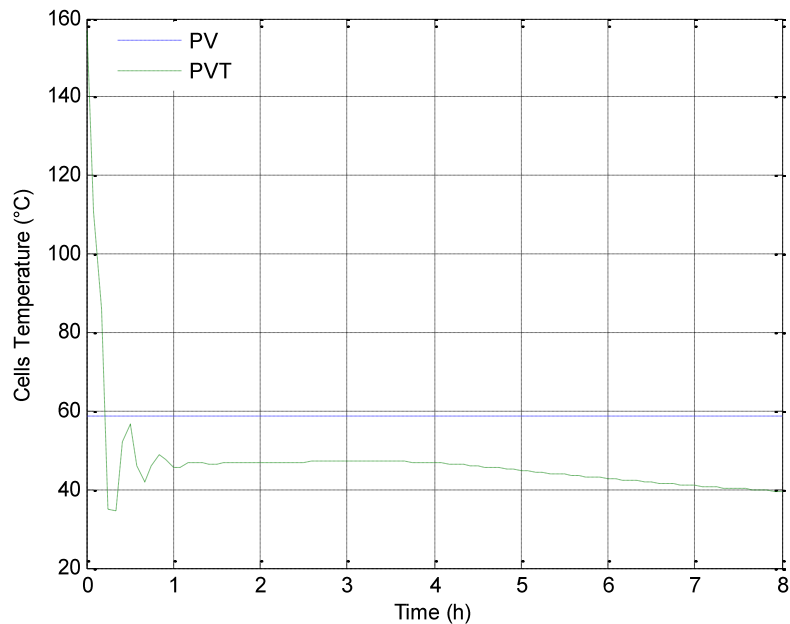


Figure 6.8: Cell temperature behaviors for the variation of wind velocity for PV and PVT modules at insolation of $1000\text{W}/\text{m}^2$ and ambient temperature of 25°C

Consider a variation of wind velocity from $0\text{m}/\text{s}$ to $12\text{m}/\text{s}$. Figure 6.8 shows the cell temperature behaviors for the variation of wind velocity for PV module and PVT module at insolation of $1000\text{W}/\text{m}^2$ and ambient temperature of 25°C . The PV temperature remains constant at 58.75°C while the PVT temperature decreases from 156.8°C to 46.74°C accompanied by oscillation behaviors explained in section 5.5.2 for the first hours then remains constant between 46.64°C and 46.74°C the three next hours, then decreases from 46.64°C to 39.51°C .

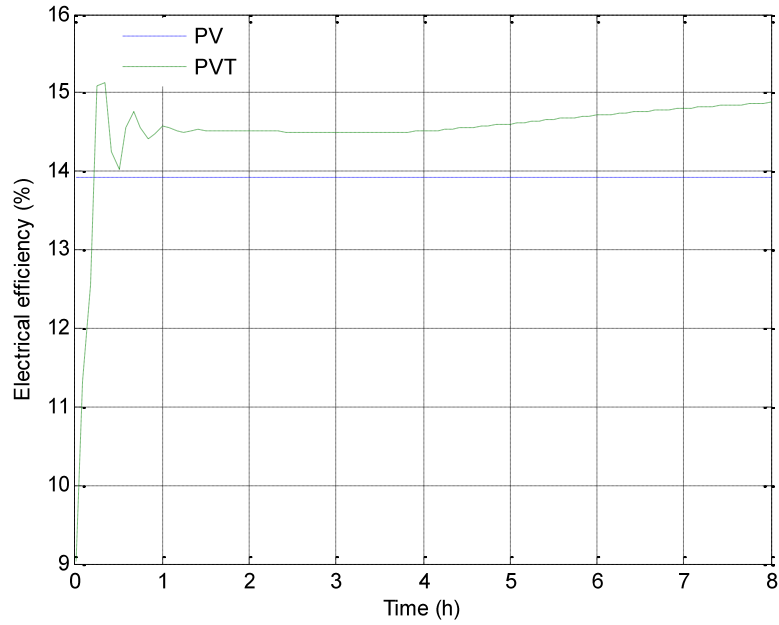


Figure 6.9: Electrical efficiency behaviors for the variation of wind velocity for PV module and PVT module at 1000w/m^2 insolation and 25°C ambient temperature

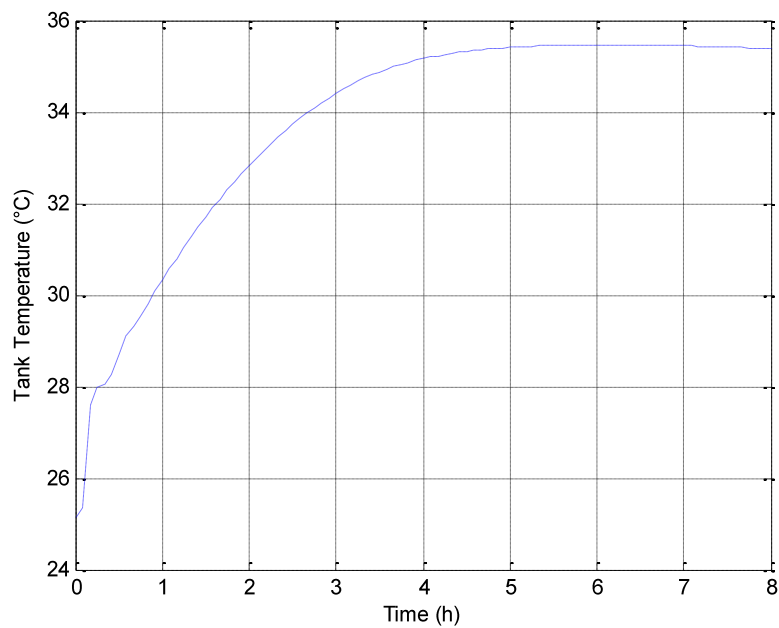


Figure 6.10: Water tank temperature for the variation of wind velocity for PVT module at 1000W/m^2 insolation and 25°C ambient temperature

The electrical efficiency of the PV module remains constant to the value of 13.92% as the PV module temperature is constant, while the PVT module temperature increases from 9% to 14.57% following the oscillation behaviours of the temperature for the first hour, then remains constant between 15.51% and 14.57% for the next three hours then increases to 14.88% as seen in Figure 6.9.

The water tank temperature increases logarithmically with wind velocity from 25.13°C to 38.56°C as seen at Figure 6.10. The maximum tank temperature reached was 35.8°C.

CHAPTER SEVEN

DESIGN OF THERMOSYPHON HYBRID GRID CONNECTED PHOTOVOLTAIC SYSTEM FOR DURBAN MODEST HOUSEHOLD

Electricity is used for a number of objectives ranging from everyday domestic needs for the using of electrical appliances to industrial purposes for production through to commercial use. Between 1994 and 1999, approximately 2.8 million of household in South Africa have been connected to the national electricity network. The acceleration of electrification of households anticipates an increase in electricity demand for residential use (51). It is estimated that around 2025, approximately 11.4 million of household in South Africa will be connected (52).

7.1 Load determination

Prediction of daily peak load demand is very important for decision making processes in the electricity sector (53). This is accomplished by selecting items that are often used to determine the average load for designing the PV system for modest household demand.

Based on electrical rating, hours used per day, and days used per month, the following household appliances have been considered from the Eskom residential tariff (see Appendix D):

- Computer
- Geyser
- Heater: two bars
- Hotplate: two plates
- Kettle
- Lighting: ten FLC
- Microwave oven
- M-net decoder/DVD player
- Refrigerator with freezer
- Television: 51cm colour
- Toaster

Items not enumerated will be used based on the energy management of home owner or user.

The electrical rating, hours used, days used and kWh used for those items are given in Table 7.1.

The total of energy hours used is $692.3kWh/month$ or $8307.6kWh/year$.

Table 7.1: Daily electrical use and kWh used per month for modest household

Electrical Appliances	Electrical Rating (Watts)	Hours Used Per Day	Days Used Per Month	kWh Used Per Month
Computer	480	2	15	14.4
Geyser	2000	5	30	300
Heater: 2 Bar	1000	5	15	75
Hotplate: 2 Plate	1500	3	30	135
Kettle	2000	0.5	30	30
Lighting: Single 100 W	100	5	30	15
Microwave Oven	1000	1	20	20
M-Net Decoder / DVD Player	25	6	30	4.5
Refrigerator (With Freezer)	400	6.5	30	78
Television: 51cm Colour	80	6	30	14.4
Toaster	800	0.5	15	6

7.2 Grid connected photovoltaic array sizing

7.2.1 PV generator

The design is based on the Q-PEAK 250 monocrystalline solar module with characteristics given in Appendix E.

A First Pass:

The design of the PV generator is based on the roof top non-tracking fixed orientation array. The maximum averaged irradiation for a year is obtained at the tilt angle 29° , as explained in Chapter

One. The average irradiance on the horizontal surface is 5.18kWh/m²/day at tilt angle 29° obtained from NASA surface meteorological Data (see Appendix F).

Using the peak hour approach:

$$Energy \left(\frac{kWh}{year} \right) = E_{ac}(kW) \left(\frac{h}{day} @ 1sun \right) * \frac{365days}{year} \quad (7.1)$$

or

$$E_{ac}(kW) = \frac{Energy \left(\frac{kWh}{year} \right)}{\frac{h}{day} @ 1sun * \frac{365days}{year}} = \frac{8307.6}{5.18 * 365} = 4.3939kW \quad (7.2)$$

The impacts of temperature, inverter efficiency, module mismatch and dirt is considered to be 25% lost for an efficiency of 75%.

$$E_{dc,STC} = \frac{E_{ac}}{Conversionefficiency} = \frac{4.3939}{0.75} = 5.8585kW \quad (7.3)$$

Using Q PEAK BLK 250 PV module to reduce area,

$$E_{dc,STC} = \frac{1kW}{m^2} * Insolation * A(m^2) * \eta_r \quad (7.4)$$

And the collector area is:

$$A(m^2) = \frac{E_{dc,STC}}{1 \frac{kW}{m^2} * \eta_r} = \frac{5.8585}{1 * 0.15} = 39.0567m^2 \quad (7.5)$$

The number of modules required is given by:

$$Numberofmodules = \frac{E_{dc,STC}}{E_{dc,STC}/module} = \frac{5858.5}{250} = 23.43 \approx 24modules \quad (7.6)$$

Arrangement into an array

The architecture of modules into array is led by the choice of the converter and the size of the grid. For large grid connected systems, each string of modules can be connected to its own inverter in the same way as for the single module-inverter topology as presented in Figure 7.1. This makes the system modularised, so that maintenance can be done on certain parts of the system without disconnecting the whole system. In addition, installation costs are lower because of using many small inverters instead of one large central inverter (42).

To connect 24 PV panels in a string, there are seven possible combinations SMA Solar is the biggest solar inverter manufacturer in the solar inverter market with a 40% share of the global market. For SMA Solar inverter, the best option is to use two Sunny Boy 3000TL inverters instead of one mini central 6000TL inverter for 5858.5W, as explained above. Technical data for the Boy 3000TL inverter is given in Appendix F.

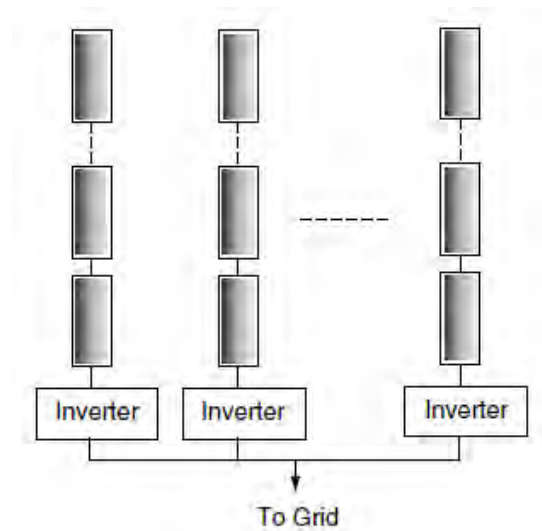


Figure 7.1: Large grid-connected system using an individual inverter for each string

Based on the array output energy and MPP voltage range, four strings of six modules each arranged into an array are obtained. With six modules per string, the STC rated voltage would be:

$$6 * 30.01V = 180.06V \quad (7.7)$$

The Sunny Boy 3000TL inverter has one MPP tracker with two string plugs so that for the maximum input current of 17A, an MPP voltage range of 188V-440V, and a maximum current per string of 17A.

The STC rated voltage for two strings for one MPP tracker is 180.06V. This is in the range of 180-280V and the maximum input current of 16.82A which is less than 17A.

It is important to limit the maximum open-circuit voltage of the strings for the inverter to operate safely. That voltage must be less than the highest DC voltage that can be supported by the inverter. With two strings of six modules in parallel at each input of the inverter, the total voltage is about 180.06V and is much less than the limit of 550V of the inverter.

But V_{oc} increases when the temperature of solar cells is less than the temperature of solar cells at Standard Test Condition of 25°C. It can be imagined that on a cold morning, with a strong and cold wind, and poor insolation, cell temperature can be close to ambient temperature and can be less than 25°C with a temperature coefficient for the open-circuit voltage of -0.32% and the lowest recorded temperature of 6°C (54).

Assuming that cell temperature and ambient temperature are the same, the open-circuit voltage $V_{oc,m}$ at one MPP tracker would now be:

$$V_{oc,m} = V_{oc,String} [1 + \beta_V (T_c - T_r)] \quad (7.8)$$

where:

$V_{oc,Strings}$	Open-circuit voltage of the photovoltaic string at NOCT (V)
β_V	Voltage temperature coefficient (1/K)
T_c	Cell temperature (°C)
T_r	Reference temperature (°C)

or

$$V_{oc,m} = 180.04 * [1 - 0.0032 * (6 - 25)] = 190.9864V \quad (7.9)$$

This is still below the 550V limit of this inverter.

The other motive to verify the open-circuit voltage of a grid-connected array under strongest cold ambient conditions on the site is to limit the open-circuit voltage to a value less than 600V as specified by the National Electrical Code for one or two households (42). The array designed satisfied this constraint, and 24 modules arranged in 4 strings, with each string constituted of modules is suitable to be used for this purpose.

Second Pass:

The roof area required for the 24 modules Durban system with the fixed orientation collector, and the estimate of the annual energy produced:

By considering module dimensions given in Appendix E, for 24 modules, the collector area is:

$$A = 24 \text{ modules} * 1.16 * 1.53 = 42.5952m^2 \quad (7.10)$$

The DC STC rated power of the array will be:

$$E_{dc,STC} = \frac{250W}{\text{module}} * 24 = 6000W \quad (7.11)$$

Assuming a 25% de-rating for AC and using the 5.18 kWh/m²day average solar radiation for Durban, it implies that the system is predicted to produce:

$$E = 6(kW) * 0.75 * \frac{5.18h}{\text{day}} * \frac{365\text{days}}{\text{year}} = 8508.15kWh/year \quad (7.12)$$

From the above calculations it can be seen that the system can produce 8508.15kWh/year. From Table 7.1 above it is evident that the electrical power required by a modest Durban house is 8307.6 kWh/year. Therefore, the PV system can easily meet the requirements.

The designed results for the PV generator are given in the Table 7.2:

Table 7.2: Array description

Array Description	
Module Type	Q-PEAQK 250 Monocrystalline Silicon
Array Size	42.60 m ²
Number of Strings	24
Number of Modules per String	6
Electrical Data	
Maximum Voltage at MPP (V_{PM})	180.06V
Open Circuit Voltage (V_{OC})	222.90V
Maximum Current at MPP (I_{PM})	33.64A
Short Circuit Current (I_{SC})	36.28 A

7.2.2 Cable sizing and over-current protection

The procedure based on NEC requirements of Section 690-9, 690-8, 210-22(C), 220-3(a), 220-10(b), 215-3, and 240-3(b) have been used for cable sizing and over-current protections of cables.

(a) From array to inverter:

Circuit Current:

For circuits carrying currents from the PV array, multiplying the short-circuit current by 125% and using this value for all further calculations. The circuit current obtained is:

$$1.25 * 2 * (9.07A) = 22.68A$$

(7.13)

Over-current Device Rating:

The over-current device must be rated at 125% of the circuit current determined in Step 1. This is to prevent over-current devices from being operated at more than 80% of rating.

The required fuse (with 75°C terminals) is:

$$1.25 * 22.68A = 28.35A \quad (7.14)$$

From NEC 240.6 (A) in appendix H, the next standard fuse size is 30A.

Cable Sizing:

To assure a good operation of connected over-current devices, cables must have an ampacity of 125% of circuit-current at 30°C. No additional deratings are applied with this calculation. Same procedure as Step 2, the cable ampacity without deratings must be 28.35A.

Cable Derating:

The cable size and estimated temperature of insulation (60, 75 or 90°C) are selected from NEC ampacity Tables using results from Step 3 and the specific location of the cable (raceway or free-air). For a roof-mounted PV array, free-air cables are used and for 28.35A cable ampacity without deratings, cable size and insulation temperature are selected from NEC Ampacity Table 310-17 in Appendix I. In this table, the 75°C cable ampacities are used to get the size, and then the ampacities from the 90°C column are used in case the deratings are to be determined. The cable is then derated for the temperature. The derated ampacity obtained must be greater than the circuit current. If this condition is not satisfied, a larger cable size or higher insulation temperature is to be chosen.

From Table 310-17 in Appendix I, for cables with 75°C insulation, a No. 14 AWG conductor at 30Amps is needed. This meets Step 3 requirements. This leads to the installation of a No. 14 AWG Copper cable with 90°C insulation and 30°C ampacity of 35 A. The cable temperature derated correction factor is 1.04 for 21° to 25°C. The temperature range is chosen based on meteorological data annual range of 14°C and 27°C (see Appendix G).

The derated ampacity is:

$$35 * 1.04 = 36.4A \quad (7.15)$$

This is greater than the required 22.68A circuit current and meets the requirement.

Ampacity versus Over-current Device:

The over-current device rating calculated in Step 2 must be less or equal to the derated ampacity of the cable selected ampacity of the cable selected in Step 4. If not, then a larger cable is to be chosen. In case the derated cable ampacity is between the standard over-current device sizes obtained in NEC section 240-6, the next larger standard size over-current device is used.

$$36.4A > 30A \quad (7.16)$$

The above obtained current meets requirements.

Device Terminal Compatibility:

As long as most of over-current devices have terminals to be used at 75°C (or 60°C) cables, compatibility is checked. A 90°C insulated cable is chosen in the above process, the circuit-current obtained in Step 1 must be greater than the 30°C ampacity of the same size cable with 75°C (60°C) insulation.

36A exceeds the 30A requirement. Verifying the cable with a 75°C insulation, the fuse end has an ampacity of 30A which is greater than 22.68A required. This cable can be protected by a 30A fuse or by a circuit breaker (125% of 2x9.07A is 22.68A).

The fuse has 75°C terminals, so the allowable ampacity for a No 14 AWG cable with 75°C insulation is 30A and is higher than the 22.68A circuit-current obtained in Step 1. To be sure that this check is passed, the 75°C column in Table 310-17 in Appendix I is used to begin Step 4.

The derated ampacity is:

$$30 * 1.05 = 31.5A > 22.68A \quad (7.17)$$

(b) From inverters to inverters junction, the strings are in parallel so that the maximum current flowing in the conductor is the sum of the two string currents:

$$9.07 * 2 = 18.14A \quad (7.18)$$

The same calculations as above are performed for:

Circuit current is:

$$1.25 * 18.14A = 22.68A \quad (7.19)$$

Over-current device rating:

Applying the NEC 1.25 current multiplier to the 3000TL 240V inverter, its fuse must be rated to handle a current greater than:

$$1.25 * \frac{3000}{240} = 12.5A \quad (7.20)$$

From table NEC 240.6(A) in Appendix H, the next standard fuse size is 15A. The 15A standard fuse has been chosen for strings so that for the inverters, the 20A standard fuses are used.

Notice that only a single 1.25 multiplier is used for the inverter since the PV temperature and insolation adjustments are inapplicable to the AC portions of the system (42).

Cable sizing:

The cable ampacity without deratings must be 28.34A.

Cable derating:

From Table 310-17 in Appendix I for cable with 75°C insulation, the No. 14 AWG conductor at 35A is needed. The derated ampacity is:

$$35 * 1.04 = 36.4A \quad (7.21)$$

This is greater than the required 22.68A circuit current in the cables.

Ampacity versus over-current device:

$$36.4A > 30A \quad (7.22)$$

This meets the requirements.

Device terminal compatibility:

The ampacity of a No. 14 AWG cable with 75°C insulation is 35A.

$$35A > 22.68A \quad (7.23)$$

(c) From inverters junction to load and utility grid, inverters are in parallel so that the maximum current flowing in conductor is the sum of the four string currents:

$$9.07 * 4 = 36.28A \quad (7.24)$$

The same calculations as above will be performed:

Circuit current is:

$$1.25 * 36.28A = 45.35A \quad (7.25)$$

Over-current device rating:

$$1.25 * 45.35A = 56.69A \quad (7.26)$$

From Table NEC 240.6(A) in appendix H, the next standard fuse size is 60A.

Cable sizing:

The cable ampacity without deratings must be 56.69A.

Cable derating:

From Table 310-17 in Appendix I for cable with 75°C insulation, the No. 8 AWG conductor at 70A is needed. The derated ampacity is:

$$80 * 1.04 = 83.2A \quad (7.27)$$

This is greater than the required 45.35A circuit current in the cables.

Ampacity versus over-current device:

$$83.2A > 60A \quad (7.28)$$

This meets requirements.

Device terminal compatibility:

The ampacity of a No. 8 AWG cable with 75°C insulation is 70A.

$$70A > 56.69A \quad (7.29)$$

The same No. 8 AWG cable is selected for all other system wiring, because it has the necessary ampacity for each circuit. The No. 14 AWG is the minimum wire size and may need to be enlarged to 8 AWG to reduce voltage drop.

Finally, the results are tabulated in the Table 7.3 below:

Table 7. 3: Wire sizing specification

Wire Runs	System Voltage (V)	Maximum Current (A)	AWG Number	Wire Type
Array to inverter	180	16.82	8 or 14	THHN
Inverter to inverters junction	240	16.82	8 or 14	THHN
Inverters junction to load	240	33.64	8	NM

For switches and protection components, we have:

Array to inverter:

Should a ground fault occur in the module while the inverter is engaged, the fuse is provided to protect strings and the conductors from high current. For this purpose, we will use a 15A 180V fuse.

Inverter to inverters junction:

A 30A utility disconnect switch or breaker is also installed to provide the capacity to manually insulate each array separately to the load in case of fault or maintenance.

Inverters junction to load:

In the load circuits, a fuse or circuit breaker is installed for each significant load as seen in Figure 7.2. For this purpose, a 60A circuit breaker is used in the lead circuit to provide the capacity to manually interrupt power to the house load in case of emergency or maintenance.

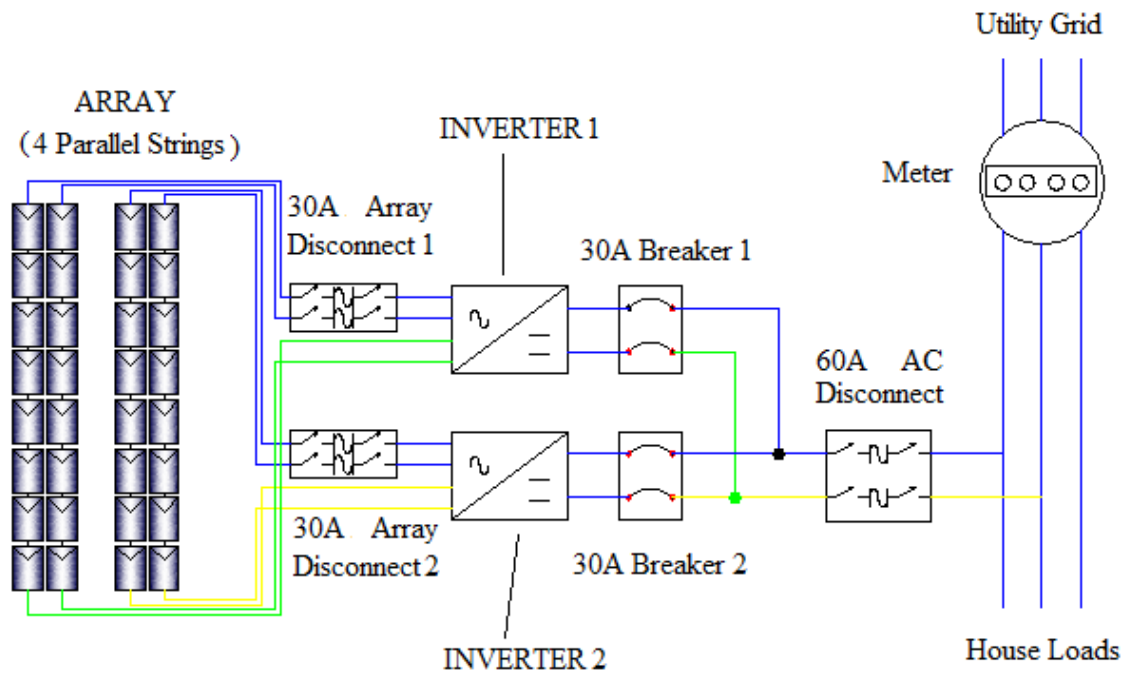


Figure 7.2: Electrical drawing of the system design for the Durban modest household demand

Table 7.4 shows switches and protection components for a grid connected PVT system:

Table 7.4: Switches and protection components for grid connected a PVT system for Durban modest household demand

Switches and Protection Components							
Circuit	Protection Device				Rated current (A)	Rated voltage (V)	Description
	Switch	Diode	Fuse	Surge			
String output			X		15	180	DC fused disconnect switch
Inverter to inverters junction	X				30	240	Circuit breaker in a lead circuit
Inverters junction to load	X				60	240	Circuit breaker in a lead circuit
Inverters junction to load	X						Circuit breaker in a lead circuit

7.3 Thermal collector and water tank

7.3.1 The design of thermal absorber

The design of thermal collector is based on Chow's research results (55), (56). An air-gap is left between the front glazing and solar cells to increase the thermal efficiency of the system by recovery of the energy lost from the top of solar cells. The thermal absorber length and width are approximately equal to 1670mm and 1000mm respectively, and key dimensions of Q-PEAK 250 PV module are given in Appendix E. Each thermal absorber is attached to individual PV modules to make a unity and has 42 rectangular channels with channel width equal to two times the height of the channel.

The thermal collector channel width a is:

$$a = \frac{PV \text{ module width}}{\text{number of channels}} = \frac{1000}{42} = 24mm \quad (7.30)$$

By substituting the value of a in the equation below, the thermal collector channel height b is obtained as:

$$b = \frac{a}{2} = \frac{24}{2} = 12mm \quad (7.31)$$

Results are obtained for the module packing factor (PF) of 0.9 and Q cells dimensions of 156mm x 156mm, dimensions obtained from Q cells data sheets in Appendix E.

7.3.2 Design of water tank

The average South African rural household potable water consumption per person is less than 20 litres per day with half of this quantity used for hygiene purpose like bathing and washing of dishes (57). This has been confirmed by Taylor's investigation of rural households in the Pretoria area (58). Zingano (59) concluded that a temperature of about 40 to 41°C is preferred for bath water in South Africa (57). Solar water heating should have the capacity to meet all household heated water requirements (60). Tank size depends on daily hot water need. The size of the system should be based on the number of people in the house. Eskom have produced the following sizing for an urban household (61):

- 50 litres per person of daily hot water is required;
- 5 litres per person per day for hand basins;
- 3 litres per meal, assume 2 meals at home daily for dishwashing; and
- 20% of total above is added for compensation for heat loss due to cold water mixing.

Those values are established with no washing machine added.

For a house of four people the tank size is;

$$4 * (50 + 5 + 3 * 2) + \frac{4 * 20}{100} (50 + 5 + 3 * 2) = 292.8 \text{ litres per day} \quad (7.32)$$

The standard tank size is 300 litres.

Thermal collectors are connected through pipes to make an array. The array and storage tank are in close vicinity to the backup and house distribution systems. This is to avoid extreme pipe losses therefore the pipes need to be well insulated.

7.4 The Design summary

Components of the grid connected photovoltaic thermal system for a modest Durban household without indicating the electricity distribution inside the house are listed in Table 7.5.

Table 7.5: Hybrid Grid Connected PVT System Components

Compound	Make/Model	Quantity
Solar module	Q-PEAK 250	24
Thermal absorber	Flat plat	24
Water tank	Vertical	300 l
Inverter	Sunny Boy 3000TL	2
DC fused disconnect switch	15A/180V	4
Circuit breaker	30A/240V	2
Circuit breaker	60A/240V	1
Wire	AWG #6	

Physical and electrical properties of the components are given in Appendices E and F.

CHAPTER EIGHT

GRID CONNECTED PVT SYSTEM SIMULATIONS

For this study, the grid connected PVT system was designed to provide electricity and hot water for modest Durban household demand. It is simulated to predict its performance before economic analysis and implementation.

The simulation of the system at different environmental parameters allows understanding of the system behaviors in outdoor conditions. Developed mathematical models of different components are connected in the way that components interact in order to produce the behaviors of the entire system through simulations. Based on the mathematical models developed in previous chapters, grid connected PV and PVT arrays will be simulated. The results from simulations are compared to those found in the literature and also to the experimental results obtained by Chow (62).

A comparison between the two systems for different days in terms of energy and efficiency is presented and the results discussed.

8.1 Description of dynamical simulation tool program

Several hybrid system simulation packages including TRNSYS, INSEL, HYBRID2 and so on have been developed by different research teams and agencies during the last twenty years (63).

In this work, Matlab codes based on Matlab version 7.8 were written. Matlab (matrix laboratory) is a numerical computing environment and fourth-generation programming language.

Two types of input data are used. The first type groups the technical characteristics and physical properties of components; this type has been defined for developing mathematical models. The second type of input data consists of environmental parameters; this is constituted of solar insolation, ambient temperature and wind speed and is used for proper simulation of design systems. Daily and average monthly environmental data are obtained from excel worksheets through an m-file in Matlab codes for simulations.

The system and its components' performances are provided by the developed simulation models. Results from simulations are displayed as Tables and Graphs. Selected results from simulations are given in Appendix J.

8.2 Simulation results

An array of 24 Q PEAK 250 PV modules for PV system and an array of 24 Q PEAK 250 PV modules attached on top of thermal absorbers connected to a 300 l water tank have been used for simulation for the Durban area. The two systems were tilted at 29.867° and weather data for two particular days were used. The environmental parameters were obtained from the Greater Durban Radiometric network (GRADRAD) for solar irradiance, and Weather Analytics for ambient temperature and wind velocity.

For summer period:

Environmental data and simulation results for the day of 04/12/2010 are represented in Figures 8.1 to 8.5.

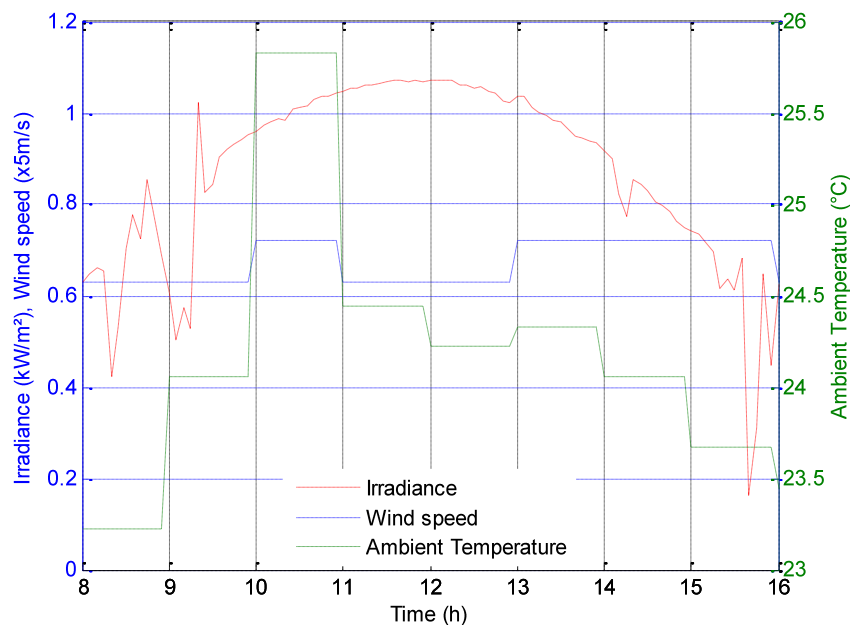


Figure 8.1: Environmental parameters for summer day of 04/12/2010

Environmental parameters for summer day of 04/12/2010 are presented in Figure 8.1. Before the solar insolation reaches the arrays, the temperature of the water in the storage tank is assumed to be equal to the ambient temperature. From 8h00, the solar insolation, the ambient temperature and the wind speed are increasing to the ambient temperature of 25.83°C and the wind speed of 3.6m/s for the insolation of 1043W/m². The temperature decreases to 24.44°C and the wind speed decreases to 3.15m/s at 11h15 while the insolation continues to increase to the maximum of 1072W/m² at 12h00.

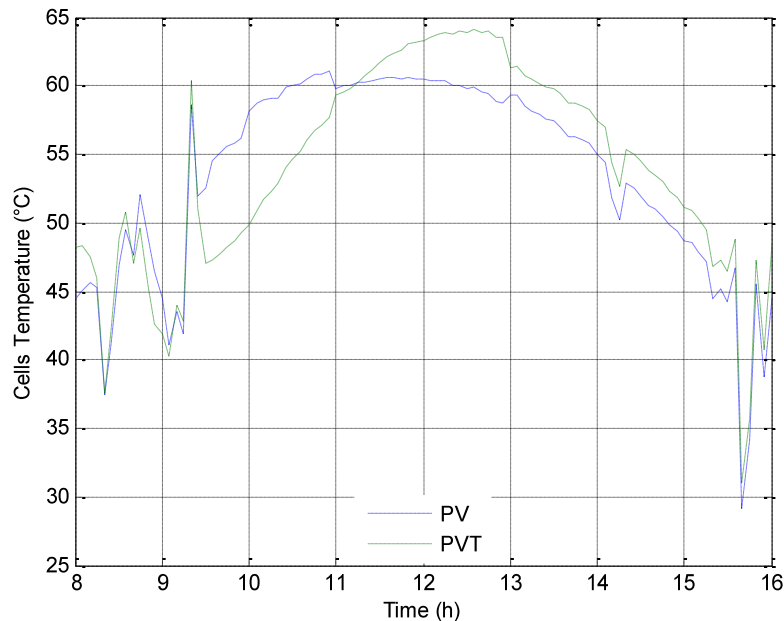


Figure 8.2: PV and PVT solar cell temperatures for summer day of 04/12/2010

As can be seen from Figure 8.2, the PV array temperature is higher than the PVT array temperature as, which justifies the high electrical efficiency of the PVT array compared to the PV array as shown in Figure 8.3. At 11h15, the temperature of PV array is 60.23°C and is equal to the temperature of the PVT array (Figure 8.2). The temperature of the storage tank is 56.67°C as shown in Figure 8.4 and is higher than the ambient temperature of 24.44°C.

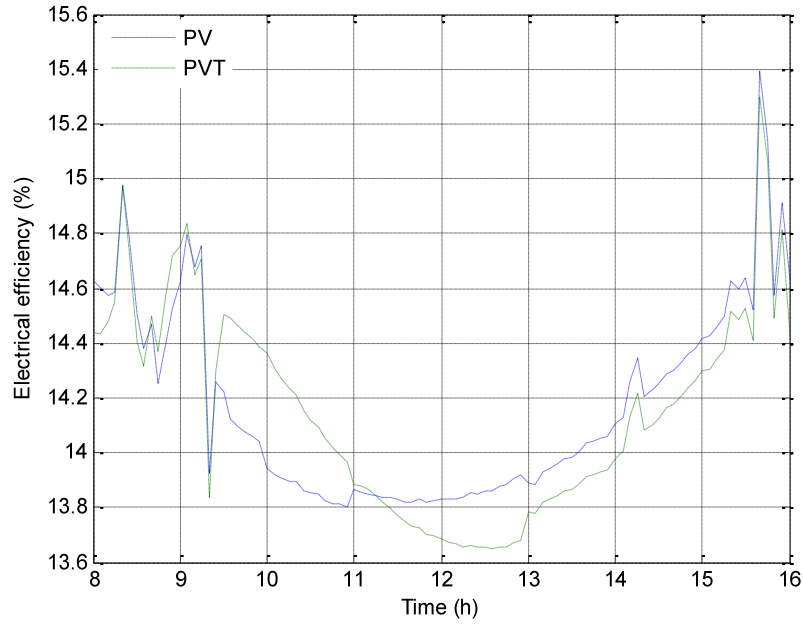


Figure 8.3: PV and PVT arrays electrical efficiencies for summer day of 04/12/2010

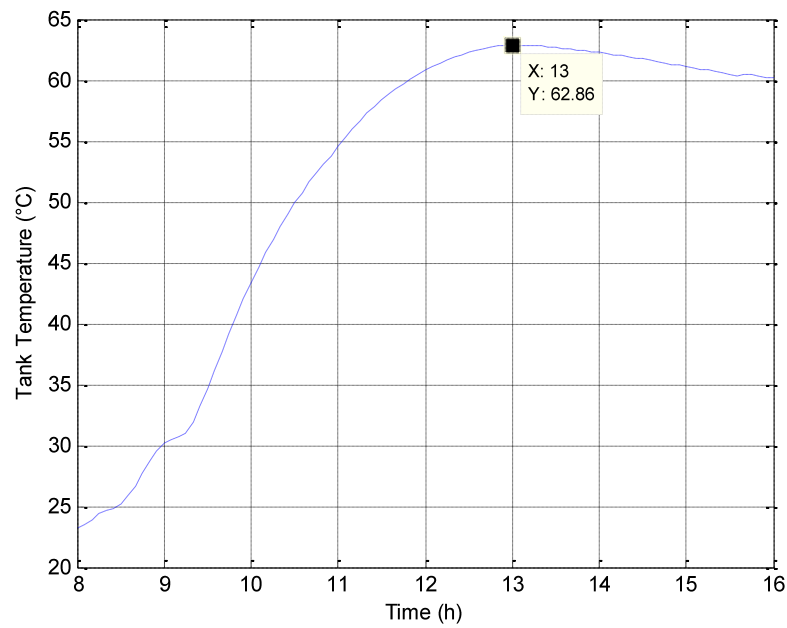


Figure 8.4: Storage tank temperature for summer day of 04/12/2010

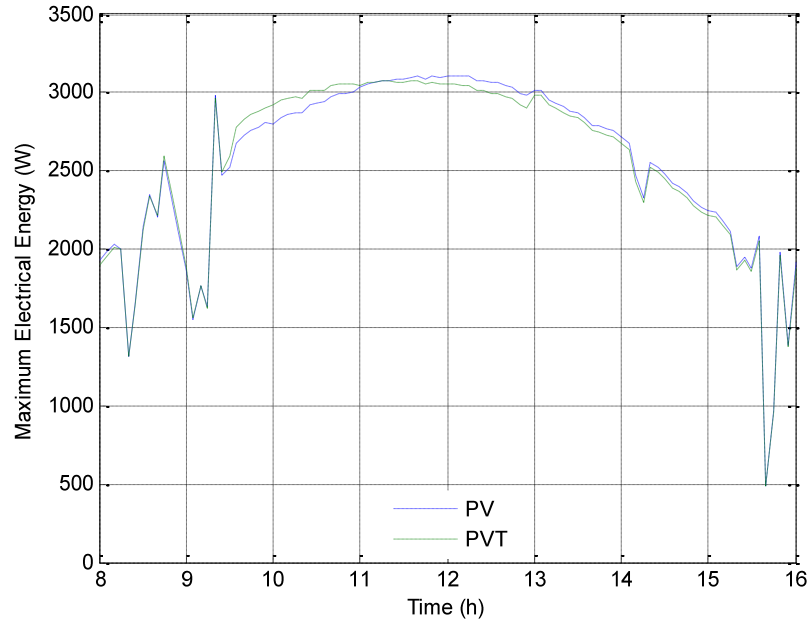


Figure 8.5: PV and PVT arrays MPP for summer day of 04/12/2010

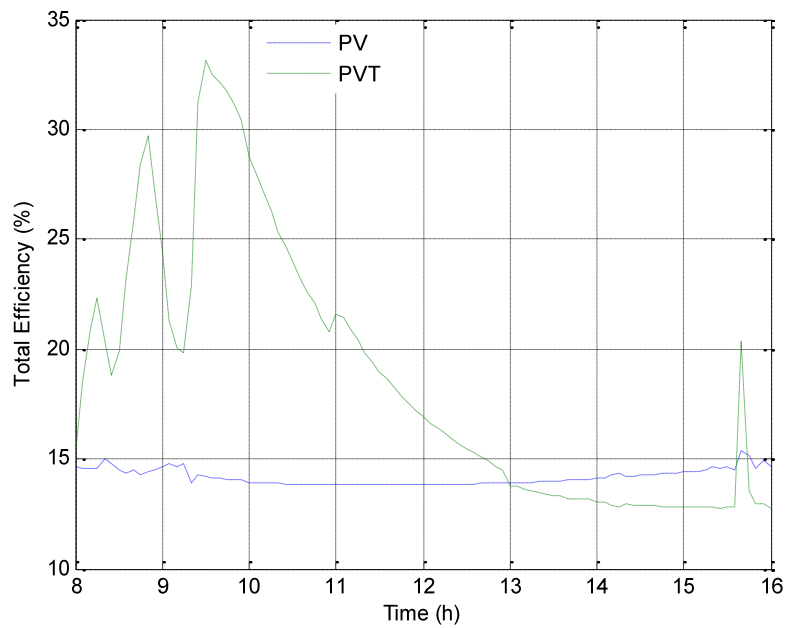


Figure 8.6: PV and PVT arrays total efficiency for summer day of 04/12/2010

At this stage, the PVT array is no longer cooled by the water from the storage tank, the thermal absorber constitutes a thermal resistance between solar cells and ambient from the back side of the PVT array. There is more heat transferred from the solar cells of the PV array to the ambient than from the solar cells of the PVT array to the ambient. The temperature of the PVT array increases, reaching a maximum of 64.13°C at 12h35 then decreases (Figure 8.2) with the consequence that the efficiency of the PV system is improved more than the electrical efficiency of the PVT array (Figure 8.3). The PV array delivers more electrical power than the PVT array as shown in Figure 8.5.

The solar insolation reaches the maximum of 1073W/m² at 12h00 while the maximum temperature of 62.86°C of the storage tank is obtained at 12h55. Due to hot water produced by the PVT array, this total efficiency is higher than the efficiency of PV array which is used only for electricity purposes as shown in Figure 8.6.

It can be seen that at 13h00, the total energy of the PV array is higher than the total energy of the PVT system. The contribution of thermal energy to increase the total efficiency of the PVT system is considerable. At 13h00, the storage tank has reached its maximum temperature. No more heat transfer from array to storage tank, only the electrical efficiency is considered for the system. Results for others days are given in Appendices J and K.

Table 8.1 presents a summary of the results from simulation for a conventional photovoltaic array and a hybrid photovoltaic array for Durban for four particular days in winter and summer weather conditions.

It can be seen from the above that the PVT array system performs well on summer days with high solar insolation and much better for regular solar insolation with a total efficiency of 87% against 15% for the PV array system for the summer day of 29/12/2010. The maximum storage tank temperature is about 68°C. This is in agreement with the findings of Chow's experiments at Hefei in which the storage tank temperature reached 60°C (55) (64).

Table 8.1: Summary of the results from simulation for PV and PVT systems

Measured Parameters		Summer				Winter			
		04/12/2010		29/12/2010		14/06/2011		28/06/2011	
		PV	PVT	PV	PVT	PV	PVT	PV	PVT
Cell temperature (°C)	Average	53.6	54	59	59	35.2	38.5	33.5	37.5
	Minimum	29.1	31	35	36	22.8	23.3	18.3	19.9
	Maximum	61.0	64.1	78	76	41.6	43.2	40.8	49.6
Maximum electrical power (W)	Average	2568.7	2564.4	2308	2316	1242.6	1222.8	1273.3	1244.5
	Minimum	488.5	483.4	611	608	387.2	386.2	407.2	405
	Maximum	3106.8	3075.7	3495	3590	1693.4	1682.1	1741.8	1721.3
Electrical efficiency (%)	Average	14.2	14.2	14	14	15.1	14.9	15.2	15
	Minimum	13.8	13.6	13	13	14.8	14.7	14.8	14.4
	Maximum	15.4	15.3	15	15	15.7	15.7	15.9	15.9
Tank water temperature (°C)	Average	0	51.9	0	62	0	29.2	0	32
	Minimum	0	23.3	0	30	0	18.1	0	13.7
	Maximum	0	62.9	0	68	0	36.2	0	47.4
Total efficiency (%)	Average	14.2	18.6	14	19	15.1	19.2	15.2	21.9
	Minimum	13.8	12.8	13	12	14.8	14.3	14.8	13.1
	Maximum	15.4	33.1	15	87	15.7	27	15.9	37.2

CHAPTER NINE

GRID-CONNECTED PV AND PVT SYSTEMS ECONOMICS

To complete the design, an economic analysis was performed. Economic analysis was considered necessary to perform based on two major inputs which are common to any economic analysis of a PV system to have a complete design. These are: initial cost of the system and the amount of energy it will deliver each year. The economic viability of the system ultimately depends on the price of the energy generated by the system which includes the possibility of tax credits, economic advantages and the mode in which system is paid for (42).

9.1. Cost of PV and PVT systems and energy delivery

The cost of the system is obtained using the SUNSIM simulation results published by Bekker (12). and the experimental results from Chow (56). Electricity yield is consumed directly without battery storage. A major cost advantage is that the equipment is maintenance free apart from material degradation since there are no moving parts in the integrated PV and thermosyphon systems (56). Table 9.1 gives cost for the components of both the PV and the PVT systems.

Table 9.1: PV and PVT Components Cost

SYSTEM DESCRIPTION	PV Component Cost (Rand)	PVT Component Cost (Rand)
Water tank		1,410
Collector frame and support	21,090.85	21,090.85
Thermal absorber		27,037.72
PV module	210,908.52	210,908.52
Inverter	46,868.56	46,868.56
Piping, wiring and accessories	5,858.57	9,783.81
Transport and installation	23,434.28	35,151.42
Total cost	308,160.78	352,250.88

Design results show that to attend to the required household electricity demand, a 4500W AC PV system should be used. The system must deliver 8508.15kWh per year to a house that currently pays R0.94 per kWh, which is the Eskom energy cost without VAT (2012 residential tariffs).

Solar power is considered one of the most reliable sources of renewable energy available today. By engaging it in water heating, which is one of the most intensive household activities (65), we have achieved a major milestone in maximum power saving.

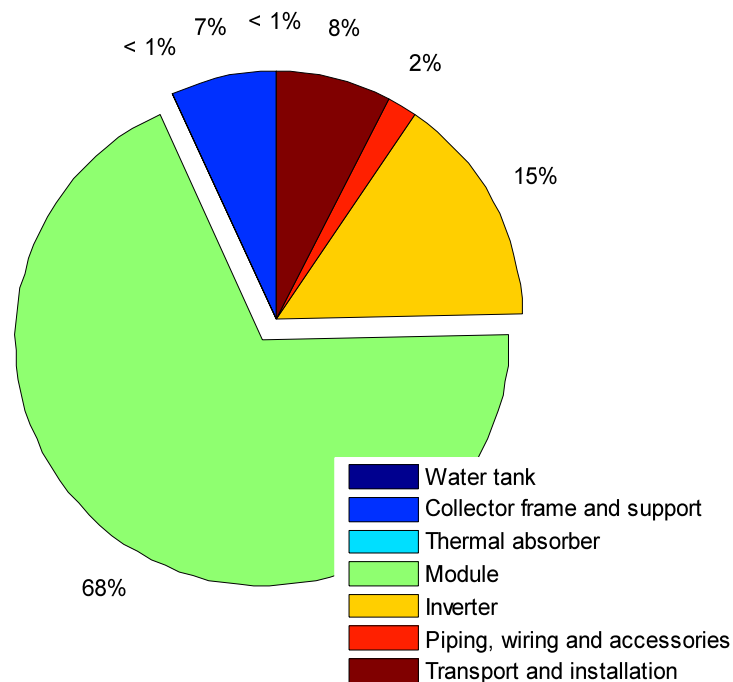


Figure 9.1: Average cost of residential PV systems for Durban modest household demand

Eskom is currently stimulating the demand for efficient water heating systems to counter the high consumption of electric geysers which account for 30-50% of the electricity consumed by an average household. The programmes are arranged in rebate schemes whereby rebates are paid directly to consumers such that the products, suppliers and installers are registered into the programme. Presently, two programmes exist in the market, the solar water heating rebate programme and the residential heat pump rebate programme (66).

The cost of electricity generator remains the same for both the PVT system and the PV system, but the PVT system is able to produce more useful energy. From the design in Chapter Six, we can see that the PV system is predicted to deliver $8508.15kWh/year$ with $3600kWh$ allocated to hot water corresponding to 42% of energy produced. If we take into consideration the thermal energy produced by the thermal absorber and the increase of electrical efficiency due to cooling of the PV array, and convert this total amount of energy into electricity (i.e. add the amount that would have been used to heat water separately to the kW produced by a more efficient PV array) the predicted energy for the PVT system is $12108.15kWh/year$.

As can be seen from Figure 9.1 and Figure 9.2, more than 70% of investment is allocated to the electricity generator, with 68% for PV modules and 15% for inverters for PV systems and 60% for PV modules and 13% for inverters for PVT systems, with at least 85% to PV modules for both systems. The PVT system cost is higher than the PV system due to addition of the thermal absorber, but is less costly in the medium to long term as explained below.

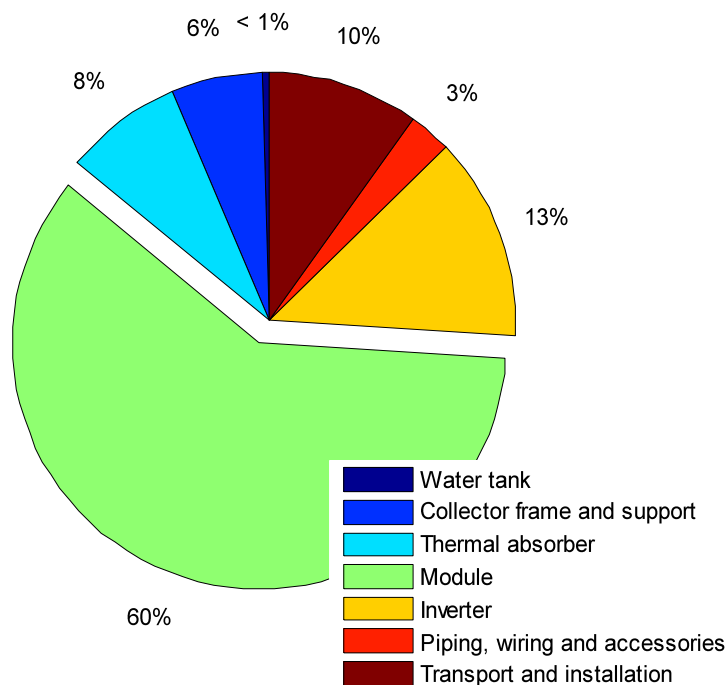


Figure 9.2: Average cost of residential PVT systems for Durban modest household demand

9.2 Loan terms and income tax

The following is assumed for the calculations below: the taxpayer earns R300,000 per year and so is in the 22.23% tax bracket (see Table 9.2); the bank loan will be for a term of 20 years at an interest rate of 8.5% (67); both systems are eligible for a rebate of R50 per WAC.

Table 9.2: The tax rates applicable to individuals for the tax year 2012/2013 (67)

Taxable Income	Tax Rate
R0.00 - R160,000.00	18% of taxable income
R160,001.00 - R250,000.00	R 28,800 + 25% of taxable income
R250,001.00 - R346,000.00	R 51,300 + 30% of taxable income
R346,001.00 - R484,000.00	R 80,100 + 35% of taxable income
R484,001.00 - R617,000.00	R 128,400 + 38% of taxable income
R617,001.00	R 178,940 + 40% of taxable income

9.3 Systems finance

Systems finance is based on the determination of the net economic benefit of both PV and PVT systems.

The net cost of the system, the annual load payment, annual cost and saving for both systems are calculated and compared over 20 years. The energy cost is also determined and compared to Eskom cost.

Net Cost of the System:

The net cost of the system, *NCS* is given by:

$$NCS = SC - ER * SNP \quad (9.1)$$

where *SC* is the system cost, *ER* is the energy rebate and *SNP* is the system nominal power.

Annual Loan Payment:

The annual loan payment is given by:

$$Loan = CRF(i, n) * NCS \quad (9.2)$$

where $CRF(i, n)$ is the capital recovery factor for an interest i over n years and is obtained from equation (7.2) below:

$$CRF(i, n) = \frac{i(1+i)^n}{(1+i)^n - 1} \quad (9.3)$$

Tax Savings:

The reduction in income taxes or tax savings TS is obtained using equation (9.4):

$$TS = i * NCS * MTB \quad (9.4)$$

where MTB is the marginal tax bracket

Cost of Electricity:

The cost of electricity CE from the system is obtained from equation (9.5):

$$CE = \frac{Loan - TS}{SEP} \quad (9.5)$$

where SEP is the system energy predicted

Net Economic Benefit:

The net economic benefit NEB is given by:

$$NEB = SEP * (PER - CE) \quad (9.6)$$

where PER is the public electricity rate which is the Eskom rate for South Africa.

By using data from Sections 9.1 and 9.2, we obtain the cost of PV and PVT electricity and the net economic benefit in the first year is given in Table 9.3.

Table 9.3: System electricity cost and net economic benefit in the first year

Parameter	PV	PVT
System power (kW)	4500.00	4500.00
System power predicted (kWh/yr)	8508.15	12108.15
Total cost (R)	308160.78	352250.88
PV rebate (R/W)	50.00	50.00
Loan interest (i)	0.09	0.09
Number of years (n)	20.00	20.00
Tax rate (MTB)	0.22	0.22
Eskom electricity tariff (R/kWh)	0.94	0.94
Net cost (R)	83160.78	127250.88
CRF (i,n)	0.11	0.11
Loan (R)	8787.68	13446.72
Tax saving (R)	1571.36	2404.47
System electricity cost (R/kWh)	0.85	0.91
System Net economic benefit (R)	756.67	304.29

Figure 9.3 represents the variation of loan balance and loan interest for both systems over 20 year for utility electricity cost increasing of 5% each year. The loan balance of the PVT system is higher due to the cost of the system. It can be seen that after twenty years, the balance is zero due to the saving realized over twenty years.

While the utility electricity cost increases from R0.94/kWh by 5% each year over 20 years to R2.49/kWh, the PV system and PVT system increase from R0.94/kWh to R1.01/kWh and from R0.91/kWh to R1.09/kWh respectively for 19 years then drop to R0/kWh at the twentieth year as shown in Figure 9.4 above, which means free electricity at the twentieth year.

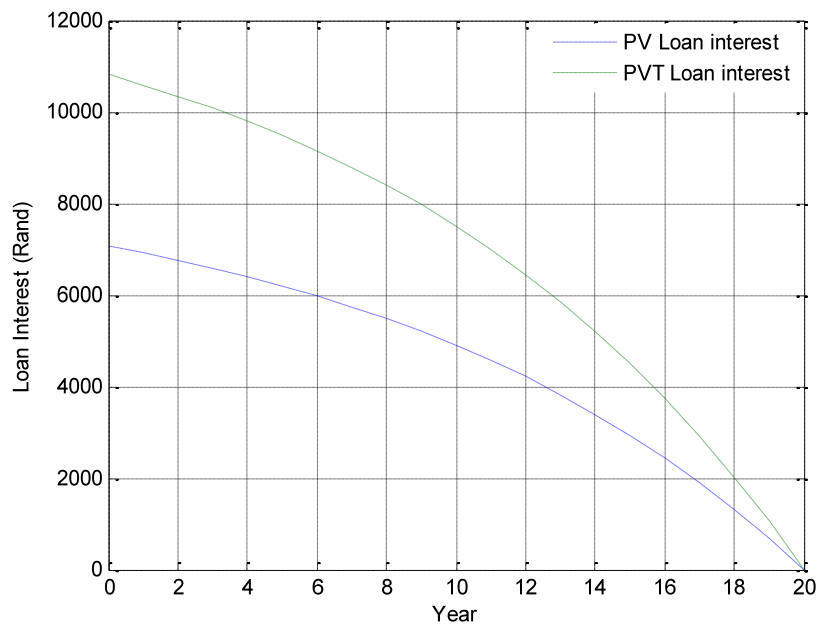


Figure 9.3: PV system and PVT system loan balance and loan interest over 20 years

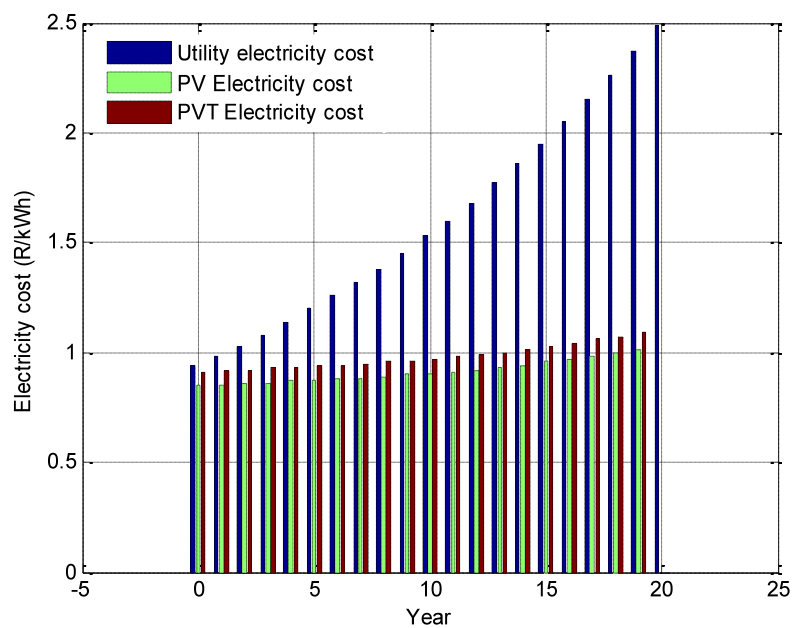


Figure 9.4: PV system and PVT system variation of electricity cost over 20 years

The savings for the PV system and the PVT system increase linearly over 19 years from R756.70 to R11,512.70 and from R304.30 to R15,460.06 per year respectively. At the twentieth year, the loan balance is zero for both systems, which justifies the brusque increase of savings to R21,154.71 per year for the PV system and R30,106.64 per year for the PVT system, in that year.

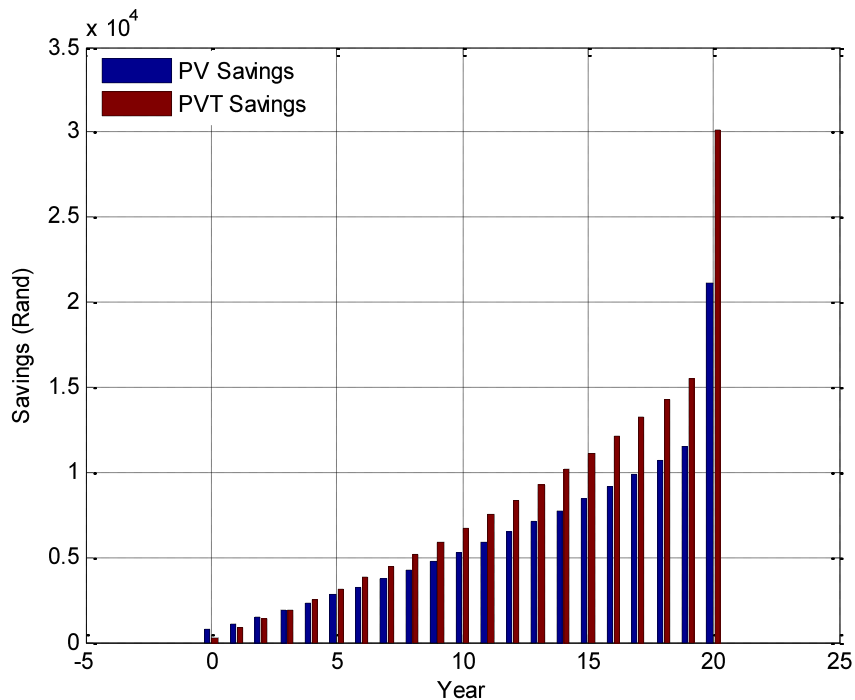


Figure 9.5: PV system and PVT system tax savings over 20 years

After 20 years of using a grid connected hybrid PVT system, R167,856.80 would be saved which is 29.5% more than the saving of R129,618.9 realized with the use of a grid connected PV system.

If the same calculations are made with the 15% increase in Eskom tariffs due to start from 2014; the savings would be R792,101.36 for the PV system and R1,110,678.54 for the PVT system which is very huge particularly for the PVT system.

More details of annual cash flow for each system are given in Appendix L.

CHAPTER TEN

CONCLUSION AND RECOMMENDATIONS

The overall goal of this study was to design a Thermosyphon Hybrid Photovoltaic Thermal System or PVT system for a moderate demand Durban household and evaluate the economic impact. The main conclusions and recommendations drawn from this are summarized below.

10.1 Conclusion

A comparison was made between the conventional grid connected photovoltaic system to grid connected hybrid photovoltaic thermal system for four particular Durban weather days (winter and summer). To achieve our goal, based on certain assumptions (as laid out in Chapter One and Chapter Four), a complete model of cell temperature for a PVT system using Fourier's series and a temperature model of water in a storage tank using finite difference method was developed and implemented using Matlab codes. This model was employed to predict the PVT system's operational performance through numerical simulation. Electrical and heat transfer relations were the basis for these models. However, a number of other empirical relationships for some coefficients were also used. The modeling, identification and validation of the system show that the agreement between simulation, literature and the Chow experiments is quite congruent (55) (64).

The answers to the key research questions of this study have been addressed as follows:

- 1) Referring to Eskom residential tariff 2012 and Eskom tank sizing, South Africa household energy demand was estimated for a household of four people.
- 2) Utilization of maximum power of a PV array is essential to the energy efficiency and cost effectiveness of the system. In most such systems made to date, voltage-conversion devices have commonly been used between the PV array and the house loads to maximize the energy transfer. The optimal performance and lowest unit power costs of these systems have been obtained by operating the systems at the maximum power point at low temperature. Clearly if cooling the PV system by water can be achieved without

the use of any intervening equipment such as a pump, the economic attractiveness of PVT systems compared to alternatives will be enhanced, since the costs of pumps and maintenance are avoided.

- 3) A PV module converts more than 60% of insolation to heat. The high electrical energy of a PV module is obtained at high solar insolation. But at high insolation, the efficiency of the module drops due to the increase of the temperature. By cooling the PV module with water using rectangular channels, a large surface for heat exchange between the PV module and the thermal absorber is provided and the maximum power point of the PVT module is shifted to the left of the conventional PV module. Both electrical and thermal energy are generated through the same hybrid PVT module.
- 4) The used of a grid connected PVT system for household energy demand is more beneficial in terms of energy output with 42% more than a conventional grid connected PV system due to the production of thermal energy for production of hot water. The grid connected PVT system is also economically more beneficial for the household. With this system, 30.26% greater savings than a conventional grid connected PV system can be realized over 20 years.

10.2 Recommendations

The maximum power point (MPP) of the PVT is at the right of the MPP curve of PV array at low irradiance. This then shifts to the left of the PV array curve for regular insolation and constant ambient temperature and wind speed. It is possible in principle to improve the maximum power point curve of the PVT array at low insolation by increasing the water rate in absorber channels and improving the insulation at the storage tank, causing the array temperature to drop and shift the maximum power point curve further to the left by combining thermosyphon and force convection. This can be achieved by connecting two storage tanks in series through a control valve and a pump at the inlet of the thermal absorber to control the rate of heat removal by the water flowing in the thermal absorber channels. In a design such as this, heat from the thermal collector is removed to the first tank. At a specified temperature the control valve will transfer hot water from the first tank to a second tank for storage. The transfer is stopped when the water in the first tank reaches a specified minimum level. At this point a pump will start

automatically to fill the first tank and stop when the maximum level required for the thermosyphon phenomena to occur in the circuit branch between the first and thermal absorber is reached. Thus, cooler water will once again circulate through the thermal absorber to cool the PV array and accumulate hot water in the first tank. Hot water from the second tank will be available for household use. A design like this will no doubt cause an increase in the capital cost of the system, but the overall efficiency improvement will more than compensate for those costs.

In this study a life cycle assessment has been carried out to estimate the cost of systems and economic recovery/savings. This assessment revealed that the PVT is more economical in the long term than the conventional PV system and the increase in the capital costs of the system to improve efficiency can easily be recovered. A separate analysis of unit lifecycle costs to confirm the economically-optimal combination of PVT components is recommended.

REFERENCES

1. Niez A. Comparative study on rural electrification policies in emerging economies: Keys to successful policies. Information Paper, International Energy Agency (IEA): Paris-France; 2010.
2. Pereira MG, Sena JA, Freitas MAV, Silva NFD. Evaluation of the impact of access to electricity: A comparative analysis of South Africa, China, India and Brazil. *Renewable and Sustainable Energy Reviews* 2011; 15(3):1427-1441.
3. Cristóbal J, Guillén-Gosálbez G, Jiménez L, Irabien A. Optimization of global and local pollution control in electricity production from coal burning. *Applied Energy* 2012; 92:369-378.
4. Hamed A, Kafayat A, Ramos M. Aggregate demand for electricity in South Africa: An analysis using the bounds testing approach to cointegration. *Energy Policy* 2009; 37(10):4167-4175.
5. Schmidt S. Coal deposits of South Africa - the future of coal mining in South Africa. Institute for Geology: Freiberg. Available from: http://www.geo.tu-freiberg.de/oberseminar/os07_08/stephan_Schmidt.pdf; n.d.
6. Inglesi R. Aggregate electricity demand in South Africa: Conditional forecasts to 2030. *Applied Energy* 2010; 87(1):197-204.
7. Inglesi-Lotz R. The evolution of price elasticity of electricity demand in South Africa: A Kalman filter application. *Energy Policy* 2011; 39(6):3690-3696.
8. Rafey W, Sovacool BK. Competing discourses of energy development: The implications of the Medupi coal-fired power plant in South Africa. *Global Environmental Change* 2011; 21(3):1141-1151.
9. Czarnowska L, Frangopoulos CA. Dispersion of pollutants, environmental externalities due to a pulverized coal power plant and their effect on the cost of electricity. *Energy* 2012; 41(1):212-219.
10. Bellingham C, Davies G, Human A. Greening Durban 2010. eThekweni Municipality; October 2009.
11. Suri M, Cebecauer T, Skoczek A. Solar electricity production from fixed-inclined and sun-tracking c-Si photovoltaic modules in South Africa. 1st Southern African Solar Energy Conference (SASEC); Stellenbosch 2012.

12. Bekker B. Irradiation and PV array energy output, cost, and optimal positioning estimation for South Africa. *Journal of Energy in South Africa*, 2007; 18(2):16-25.
13. Zawilska E, Brooks MJ. Solar energy measurement on the Southern Africa east coast. *World Renewable Energy Congress*, Linköping, Sweden; 2011.
14. Chow T-T. A review on photovoltaic/thermal hybrid solar technology. *Applied Energy* 2010; 87(2):365-379.
15. California Solar Center. Photovoltaics [Internet]. http://www.californiasolarcenter.org/history_pv.html; 2005.
16. Energy Efficiency and Renewable Energy: The History of Solar. U.S. Department of Energy; n.d.
17. Wolf M. Performance analyses of combined heating and photovoltaic power systems for residences. *Energy Conversion* 1976; 16:79-90.
18. Florschuetz LW. Extension of the Hottel-Whillier model to the analysis of combined photovoltaic/thermal flat plate collectors. *Solar Energy* 1979; 22(4):361-366.
19. Raghuraman P. Analytical predictions of liquid and air photovoltaic/thermal, flat-plate collector performance. *Journal of Solar Energy Engineering* 1981; 103:291–298.
20. Cox CH, Raghuraman P. Design considerations for flat-plate-photovoltaic/thermal collectors. *Solar Energy* 1985; 35(3):227-241.
21. Agarwal RK, Garg HP. Study of a photovoltaic-thermal system-Thermosyphonic solar water heater combined with solar cells. *Energy Conversion and Management*. 1994; 35(7):605-620.
22. Garg HP, Agarwal RK, Joshi JC. Experimental study on a hybrid photovoltaic-thermal solar water heater and its performance predictions. *Energy Conversion and Management* 1994; 35(7):621-633.
23. Garg HP, Agarwal RK. Some aspects of a PVT collector/forced circulation flat plate solar water heater with solar cells. *Energy Conversion and Management* 1995; 36(2):87-99.
24. Bergene T, Løvvik OM. Model calculations on a flat-plate solar heat collector with integrated solar cells. *Solar Energy* 1995; 55(6):453-462.
25. Huang BJ, Lin TH, Hung WC, Sun FS. Performance evaluation of solar photovoltaic/thermal systems. *Solar Energy* 2001; 70:443-448.
26. Sandnes B, Rekstad J. A photovoltaic/thermal (PV/T) collector with a polymer absorber plate. Experimental study and analytical model. *Solar Energy* 2002; 72(1):63-73.

27. Zondag HA, Vries DWD, Helden WGJV, Zolingen RJC, Steenhoven AAV. The thermal and electrical yield of a PV thermal collector. *Solar Energy* 2002; 72:113-128.
28. Zondag HA, Vries DWD, Helden WGJV, Zolingen RJC, Steenhoven AAV. The yield of different combined PV-thermal collector designs. *Solar Energy* 2003; 74(3):253-269.
29. Chow T-T. Performance analysis of photovoltaic-thermal collector by explicit dynamic model. *Solar Energy* 2003; 75(2):143-152.
30. Coventry J.S, Lovegrove K. Development of an approach to compare the „value“ of electrical and thermal output from a domestic PV/thermal system. *Solar Energy* 2003; 75(1):63-72.
31. Kauko H. A MATLAB program for PV module performance analysis based on real outdoor data stored in a Postgre SQL database [Master's Dissertation]: University of Jyväskylä; 2008.
32. Standard F. Procedures for Photovoltaic System Design Review and Approval. A Research Institute of the University of Central Florida; 2005.
33. Foster R, Ghassemi M, Cota A. *ENERGY: Renewable Energy and the Environment*. CRC Press; 2010.
34. Kalogirou SA. *Solar energy engineering: Processes and systems*. Elsevier; 2009.
35. Wenham AR, Green MA, Watt ME, Corkish R. *Applied photovoltaics*. 2nd ed. TJ International Ltd; 2007.
36. Potter MC, Wiggert DC. *Fluid mechanics*. SsO Series, McGraw-Hill; 2008.
37. White FM. *Fluid mechanics*. 4th ed. McGraw-Hill; 2003.
38. Wrede R, Spiegel MR. *Theory and problems of advanced calculus*. 2nd ed. McGraw-Hill; 2002.
39. Asmar NH. *Partial differential equations with Fourier series and boundary value problems*. 2nd ed. Pearson Prentice Hall; 2000.
40. Cengel YA. *Heat and mass transfer: A practical approach*. 3rd ed. McGraw-Hill; 2006.
41. Oi A. Design and simulation of photovoltaic water pumping system. California Polytechnic State University; September 2005.
42. Masters GM. *Renewable and efficient electric power systems*. John Wiley and Sons Inc Publication; 2004.
43. Hansen AD. *Models for a stand-alone PV System*. Roskilde: Riso National Laboratory; 2000.

44. Luque A, Hegedus S. Handbook of photovoltaic science and engineering. John Wiley & Sons Ltd; 2003.
45. Walker GR. Evaluating MPPT converter topologies using a MATLAB PV model. Australasian Universities Power Engineering Conference (AUPEC), Brisbane; 2000.
46. Mattei M, Notton G, Cristofari C, Muselli M, Poggi P. Calculation of the polycrystalline PV module temperature using a simple method of energy balance. *Renewable Energy* 2006; 31(4):553-567.
47. Evans DL, Florschuetz LW. Cost studies on terrestrial photovoltaic power systems with sunlight concentration. *Solar Energy* 1977; 19(3):255-262.
48. Skoplaki E, Palyvos JA. On the temperature dependence of photovoltaic module electrical performance: A review of efficiency/power correlations. *Solar Energy* 2009;83(5):614-624.
49. Janna WS. Engineering heat transfer. 2nd ed. Press C, Boca Raton: Library of Congress; 2000.
50. Graebel WP. Advanced fluid mechanics. Press A, Elsevier; 2007.
51. Ziramba E. The demand for residential electricity in South Africa. *Energy Policy* 2008; 36(9):3460-3466.
52. Davidson O, Tyani L, Afrane-Okesse Y. Climate change, sustainable development and energy: Future perspectives for South Africa. OECD; 2002.
53. Sigauke C, Chikobvu D. Prediction of daily peak electricity demand in South Africa using volatility forecasting models. *Energy Economics* 2011; 33(5):882-888.
54. Post W. Longterm historical data Durban South Africa: Washington Post; 2012/07/16. 01:53 pm [cited 2012 2012/07/16]. Available from: http://www.washingtonpost.com/wp-srv/weather/longterm/historical/data/Durban_South_Africa.htm
55. Chow T-T, He W, Ji J. Hybrid photovoltaic-thermosyphon water heating system for residential application. *Solar Energy* 2006; 80(3):298-306.
56. Chow T-T, He W, Ji J, Chan ALS. Performance evaluation of photovoltaic-thermosyphon system for subtropical climate application. *Solar Energy* 2007; 81(1):123-130.
57. Nieuwoudt MN, Mathews EH. A mobile solar water heater for rural housing in Southern Africa. *Building and Environment* 2005; 40(9):1217-1234.

58. Taylor PB. Energy and thermal performance in the residential sector: Developing a new low cost solar water heater [PhD dissertation]. Potchefstroom, University of Potchefstroom; 2001.
59. Zingano BW. A discussion on thermal comfort with reference to bath water temperature to deduce a midpoint of the thermal comfort temperature zone. *Renewable Energy* 2001; 23(1):41-47.
60. Eskom. Choose the right solar water heater for your home. Eskom; 2011, p2.
61. Africa ESS. Sizing your solar geyser requirement [cited 2012 17/07/2012; 11:04]. Available from: <http://www.ecoenergysa.com/installation-options.html>.
62. He W, Chow T-T, Ji J, Lu J, Pei G, Chan L-S. Hybrid photovoltaic and thermal solar-collector designed for natural circulation of water. *Applied Energy* 2006; 83(3):199-210.
63. El-Aal AE-M. MAA. Modelling and simulation of photovoltaic fuel cell hybrid system [PhD], University of Kassel; 2005.
64. Ji J, Chow T-T, He W. Dynamic performance of hybrid photovoltaic/thermal collector wall in Hong Kong. *Building and Environment* 2003; 11//; 38(11):1327-1334.
65. Eskom. Solar water heating programme [Internet]. [2012/12/08 08:10]. Available from: <http://www.eskom.co.za/c/56/eskom-solar-water-heating-programme/>; 2012
66. Eskom. Eskom demand funding options [Internet]. [cited 2012 2012/12/08]. Available from: <http://www.eskomidm.co.za/funding-options>; 2010
67. Loans SA. SA Home Loans Economic Update; February 2012.

APPENDICES

Appendix A: The Newton Raphson's method

The Newton's method is described as:

$$x_{n+1} = x_n - \frac{f(x_n)}{f'(x_n)} \quad (\text{A-1})$$

Where: $f'(x)$ is the derivative of the function, $f(x)=0$, x_n is a present value, and x_{n+1} is a next value.

Rewriting the equation (3.17) gives the following function:

$$f(I) = I_{sc} - I - I_o \left[e^{q\left(\frac{V+I.R_s}{AkT}\right)} - 1 \right] = 0 \quad (\text{A-2})$$

Plugging this into the equation (A-1) gives a following recursive equation, and the output current (I) is computed iteratively.

$$I_{n+1} = I_n - \frac{I_{sc} - I_n - I_o \left[e^{q\left(\frac{V+I.R_s}{AkT}\right)} - 1 \right]}{-1 - I_o \left(\frac{q.R_s}{AkT}\right) e^{q\left(\frac{V+I.R_s}{AkT}\right)}} \quad (\text{A-3})$$

Where:

I_{n+1} Module current at step $n+1$ (A)

I_n Module current at step n (A)

Appendix B: Heat transfer coefficients

Fluid heat transfer coefficients calculation

- Convective heat transfer coefficient for wind h_w (W/m²K):

$$h_w = 2.8 + 3V_w \quad (\text{B.1})$$

- Convective heat transfer coefficient for the air gap (W/m²K):

$$h_{ag} = Nu_{ag} \frac{k_{ag}}{\delta_{ag}} \quad (\text{B.2})$$

Where:

Nu_{ag} is the Nusselt number for the air gap and is given by:

$$Nu_{ag} = 1 + 1.44 \left(\frac{1 - 1708}{Ra_{ag} \cos \theta} \right) \left(1 - 1708 \frac{\sin(1.8\theta)^{1.6}}{Ra_{ag} \cos \theta} \right) + \left[\left(\frac{Ra_{ag} \cos \theta}{5830} \right)^{1/2} - 1 \right] \quad (\text{B.3})$$

Ra_{ag} is the Rayleigh number for the air gap. It is obtained by using equation below:

$$Ra_{ag} = g\beta_{ag}(T_c - T_g) \frac{\delta_{ag}^3 Pr_{ag}}{\alpha_{ag} \nu_{ag}} \quad (\text{B.4})$$

β_{ag} Volume expansion coefficient of the air gap (1/K)

Pr_{ag} Prandtl number for the air gap

α_{ag} Thermal diffusivity (m²/s)

ν_{ag} Kinematic viscosity of the air gap (m²/s)

The values of β_{ag} , Pr_{ag} , α_{ag} and ν_{ag} are obtained from Thermodynamic Tables.

- Convective heat transfer coefficient for the water in channel h_f (W/m²K)

The convective heat transfer coefficient for the water flowing in the channel is given by:

$$h_f = Nu_f \frac{k_f}{D_f} \quad (\text{B.5})$$

Where:

Nu_f is the Nusselt number for water flowing in rectangular channel with length side equal two times width side and is:

$$Nu_f = 4.11 \quad (\text{B.6})$$

K_f is the conductive heat transfer for the water. This coefficient depends on the temperature of the water and is given Thermodynamic tables.

D_h is the hydraulic perimeter of the channel and is obtained from equation below:

$$D_h = 4 \frac{A_z}{p_z} \quad (\text{B.7})$$

Where:

A_z Cross section of the channel (m²)

p_z Perimeter of the cross section of the channel (m)

Overall heat transfer coefficients:

- The overall heat transfer between solar cells and ambient temperature from the top U_{c-a} (W/m²K) is given by:

$$U_{c-a} = \frac{1}{\frac{1}{h_{ag}} + \frac{\delta_g}{k_g} + \frac{1}{h_w}} \quad (\text{B.8})$$

- The overall heat transfer between solar cells and upper channel wall U_{c-ucw} is given by:

$$U_{c-ucw} = \frac{k_{ucw}}{\delta_{ucw}} \quad (\text{B.9})$$

- The overall heat transfer coefficient between fluid in the channel and the ambient by the backside U_{f-a} (W/m²K) is given by:

$$U_{f-a} = \frac{1}{\frac{1}{h_f} + \frac{\delta_{lcw}}{k_{lcw}} + \frac{\delta_{ins}}{k_{ins}} + \frac{1}{h_w}} \quad (\text{B.10})$$

- The overall heat transfer coefficient between water in the tank and ambient U_{a-t} (W/m²K) is given by:

$$U_{a-t} = \frac{1}{\frac{1}{h_w} + \frac{\delta_{ins}}{k_{ins}} + \frac{\delta_t}{k_t} + \frac{1}{h_t}} \quad (\text{B.11})$$

Appendix C: Dimensionless coefficients

The dimensionless coefficients are used to simplify the model. Those coefficients are obtained by combining or grouping different heat transfer coefficients in one equation and are given below:

- Coefficient τ_{eff} :

$$\tau_{eff} = \tau_g [PF\alpha_c(1 - \eta_r) + \alpha_T(1 - PF)] \quad (C.1)$$

- Coefficient ξ_{cu} :

$$\xi_{cu} = \frac{U_{c-ucw}}{U_{c-a} + U_{c-ucw} + U_{c-r}} \quad (C.2)$$

Where:

$$U_{c-r} = \Gamma PF \tau_g \alpha_c G \quad (C.3)$$

and

$$\Gamma = \frac{\eta_r}{\beta_c} \quad (C.4)$$

- Coefficient ξ_{fu} :

$$\xi_u = \frac{h_f}{h_f + U_{c-ucw}(1 - \xi_{cu})} \quad (C.5)$$

Appendix D: Eskom Residential Tariff

The following Table shows the typical costs of running appliances on the residential tariffs¹.

Electrical Appliances	Electrical Rating In Watts	Hours Used Per Day	Days Used Per Month	Kwh Used Per Month	Monthly Cost At 106.83 Cents/kWh Incl.VAT
Air Conditioner	1500	12	20	360	R 384.59
Cellphone Charger	28	5	7	0.98	R 1.05
Clothes Iron	1500	4	6	36	R 38.46
Computer	480	2	15	14.4	R 15.38
Dishwasher	2500	2	25	125	R 133.54
Freezer (Chest)	250	6.5	30	48.75	R 52.08
Geyser	2000	5	30	300	R 320.49
Heater: 2 Bar	1000	5	15	75	R 80.12
Hotplate: 2 Plate	1500	3	30	135	R 144.22
Kettle	2000	0.5	30	30	R 32.05
Lighting: Simple 100W	100	5	30	15	R 16.02
Microwave Oven	1000	1	20	20	R 21.37
M-Net Decoder/DVD Player	25	6	30	4.5	R 4.81
Oven: Bake Element	1500	0.5	20	15	R 16.02
Oven: Grill Element	1500	0.5	15	11.25	R 12.02
Oven: Warmer Drawer	400	0.8	25	8	R 8.55
Pool Pump	750	8	30	180	R 192.29
Refrigerator (With Freezer)	400	6.5	30	78	R 83.33
Stove: Back Large Plate	1500	1.5	30	67.5	R 72.11
Stove: Back Small Plate	1000	1	25	25	R 26.71
Stove: Front Large Plate	1500	2	30	90	R 96.15
Stove: Front Small Plate	1000	1	15	15	R 16.02
Total Stove				197.5	R 210.99
Television: 51cm Colour	80	6	30	14.4	R 15.38
Toaster	800	0.5	15	6	R 6.41
Vacuum Cleaner	1400	3	4	16.8	R 17.95
Washing Machine	2300	4	6	55.2	R 58.97

¹Ethekewini Electricity: Tariff 2011/2012, 2010: Durban

Appendix E: Q cells and Q PEAK Module characteristics



With efficiencies of up to 17.4 %, the **Q6LMX3** is one of the most powerful monocrystalline solar cells on the market. The **Q6LMX3** enables the production of modules with a homogeneous black appearance. Therefore, it is ideally suited for applications where aesthetics are especially important.

HIGHLY RELIABLE ENERGY OUTPUT ON MODULE LEVEL

- 3 % performance increase because of full-square format*
- Maximum yield and longevity due to 100 % hotspot prevention
- Excellent performance due to outstanding low-light behavior
- Prevention of power loss on module level through precise cell efficiency sorting (± 0.2 % absolute)
- Excellent electrical long-term stability through use of best raw materials and strict quality inspection procedures
- Breakage decrease and performance increase on module level with 3-busbar layout

ATTRACTIVE AND SOPHISTICATED VISUAL APPEARANCE

- Homogeneous, true black surface for highly aesthetical modules

PROFICIENT AND APPLICATION-ORIENTED SERVICE

- Application-oriented advice regarding further processing
- Professional on-site service
- Comprehensive support for module certifications

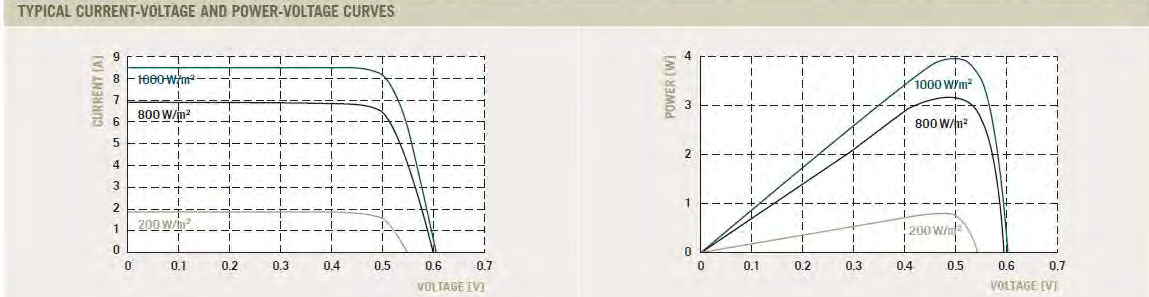


* COMPARED TO A STANDARD MONOCRYSTALLINE SOLAR CELL WITH A 105 MM DIAGONAL AT THE SAME LEVEL OF EFFICIENCY

Q.CELLS

MECHANICAL SPECIFICATION		TECHNICAL DRAWING
Product	Monocrystalline solar cell	
Format	156 mm × 156 mm ±0.5 mm Diameter: 220 ±0.5 mm	
Average thickness (Si)	200 μm ±30 μm	
Front contacts (-)	Three 1.5 mm wide bus bars (silver) Alkaline texturized surface Dark blue anti-reflecting coating (silicon nitride)	
Back contacts (+)	Three 3 mm wide bus bars (silver/aluminum) Aluminum backside metallization	

ELECTRICAL CHARACTERISTICS										
PERFORMANCE AT STANDARD TEST CONDITIONS, STC: 1000 W/m ² , 25 °C, AM 1.5 G (IEC 60904-3 ED.1), P _{MPP} ± 1.5 % REL., EFFICIENCY: ± 0.2 % ABS.										
POWER CLASS			3.89	3.94	3.99	4.04	4.09	4.14	4.19	4.23
Efficiency	η	[%]	16.0	16.2	16.4	16.6	16.8	17.0	17.2	17.4
Nominal Power	P _{max}	[W]	3.89	3.94	3.99	4.04	4.09	4.14	4.19	4.23
Short Circuit Current	I _{sc}	[A]	8.51	8.52	8.54	8.57	8.60	8.63	8.66	8.69
Open Circuit Voltage	U _{oc}	[mV]	599	601	603	605	608	610	612	614
Current at 0.5 V	I	[A]	≥ 7.90	≥ 8.02	≥ 8.12	≥ 8.21	≥ 8.29	≥ 8.37	≥ 8.47	≥ 8.57



SPECTRAL RESPONSE	INTENSITY DEPENDENCE	TEMPERATURE COEFFICIENTS
	INTENSITY W/m ²	U _{MPP} * I _{MPP} *
	1000	1.000 1.0
	800	0.999 0.8
	500	0.994 0.5
	400	0.986 0.4
	300	0.970 0.3
200	0.936 0.2	
100	0.862 0.1	
	* Ratio of U _{MPP} (I _{MPP}) at reduced intensity to U _{MPP} (I _{MPP}) at 1000 W/m ²	Power -0.47 %/K Current +0.05 %/K Voltage -0.37 %/K
		PROCESSING RECOMMENDATION Solder joint Copper ribbons coated with 10 – 15 μm; 62 % Sn / 36 % Pb / 2 % Ag Cells per bypass diode Maximum 24* per bypass diode Light induced degradation** 2.5 % (rel. P _{MAX}) considered in the electrical classification
		<small>* An electro luminescence based outgoing inspection as well as a visual inspection of the cell distances after module assembly is recommended. ** one-time power reduction after 24 hours sunlight exposure</small>

QUALIFICATIONS AND CERTIFICATES	PARTNER
<p>The Q-Cells SE quality and environmental management system is certified according to: DIN EN ISO 9001:2008 DIN EN ISO 14001:2004 Certificate: 01 150 055125</p>	

Q-CELLS SE
OT Thalheim, Sonnenallee 17–21
06766 Bitterfeld-Wolfen, Germany

TEL +49 (0)3494 66 99-0
FAX +49 (0)3494 66 99-199

EMAIL service@q-cells.com
WEB www.q-cells.com

Q.CELLS

Specifications subject to technical changes © Q-Cells SE 0661.MX3_English_09/2010_02



Q.CELLS
YIELD SECURITY

- ✓ ANTI-PID TECHNOLOGY (APT)
- ✓ HOT-SPOT PROTECT (HSP)
- ✓ TRACEABLE QUALITY (TRA.Q™)

PLUS X AWARD
honored as:
BEST PRODUCT OF THE YEAR 2011

EUPD RESEARCH
TOP BRAND PV
MODULES
GERMANY
2012

MONOCRYSTALLINE SOLAR MODULE

Q.PEAK 245-265

Maximum power and reliability

The monocrystalline **Q.PEAK** solar module with power classes up to 265 W is one of the most powerful 60 cell standard modules on the market globally. But be careful: Not all solar modules are the same. Only Q.CELLS offers German engineering quality with our unique triple Yield Security.

YOUR EXCLUSIVE TRIPLE YIELD SECURITY

- **Anti PID Technology (APT)** reliably prevents power loss resulting from unwanted leakage currents (potential-induced degradation)¹.
- **Hot-Spot Protect (HSP)** prevents yield losses and reliably protects against module fire.
- **Traceable Quality (Tra.Q™)** is the „Finger Print“ of a solar cell. Tra.Q™ ensures continuous quality control throughout the entire production process from cells to modules while making Q.CELLS solar modules forgery proof.

ONE MORE ADVANTAGE FOR YOU

- **Improved energy yield:** The actual output of all Q.CELLS solar modules is up to 5 Wp higher than the nominal power thanks to positive sorting.
- **Controlled quality:** Q.CELLS tests its solar modules in the world's largest module testing center at head office in Thalheim, Germany, longer and more stringently than prescribed in the standards.
- **Guaranteed performance:** Q.CELLS offers the best warranties on the market. A 10-year product warranty plus a 25-year linear performance warranty².

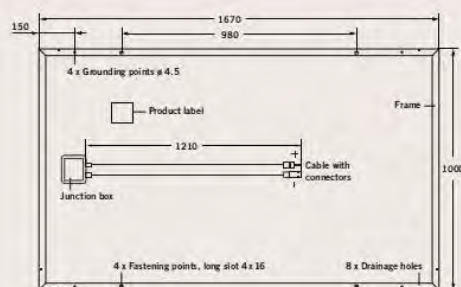


APT test conditions: Cells at 1000 V against ground, with conductive metal foil covered module surface, 25 °C, 168 h (TDV test conditions)
See data sheet on rear for further information.

Q.CELLS

MECHANICAL SPECIFICATION

Format	1670 mm x 1000 mm x 50 mm (including frame)
Weight	19.8 kg
Front Cover	3.2 mm thermally pre-stressed solar glass
Back Cover	Composite film
Frame	Anodized aluminum
Cell	6 x 10 monocrystalline solar cells
Junction box	116 mm x 153 mm x 20 mm Protection class IP 68, with bypass diodes
Cable	4 mm ² Solar cable; (+) 1210 mm, (-) 1210 mm
Connector	Yamaichi Y-SOL4, IP 68



ELECTRICAL CHARACTERISTICS

PERFORMANCE AT STANDARD TEST CONDITIONS (STC: 1000 W/m², 25 °C, AM 1.5 G SPECTRUM)¹

NOMINAL POWER (+5 / -0 W)		[W]	245	250	255	260	265
Average Power	P_{MPP}	[W]	247.5	252.5	257.5	262.5	267.5
Short Circuit Current	I_{SC}	[A]	9.01	9.07	9.12	9.17	9.23
Open Circuit Voltage	V_{OC}	[V]	36.76	37.15	37.54	37.92	38.30
Current at P_{MPP}	I_{MPP}	[A]	8.33	8.41	8.50	8.58	8.66
Voltage at P_{MPP}	V_{MPP}	[V]	29.71	30.01	30.31	30.60	30.88
Efficiency (Nominal Power)	η	[%]	≥ 14.7	≥ 15.0	≥ 15.3	≥ 15.6	≥ 15.9

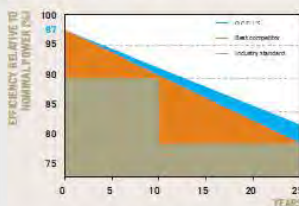
PERFORMANCE AT NORMAL OPERATING CELL TEMPERATURE (NOCT: 800 W/m², 47 ± 3 °C, AM 1.5 G SPECTRUM)²

NOMINAL POWER (+5 / -0 W)		[W]	245	250	255	260	265
Average Power	P_{MPP}	[W]	187.6	191.4	195.1	198.8	202.6
Short Circuit Current	I_{SC}	[A]	7.17	7.22	7.26	7.30	7.35
Open Circuit Voltage	V_{OC}	[V]	34.53	34.91	35.29	35.65	36.01
Current at P_{MPP}	I_{MPP}	[A]	6.66	6.72	6.79	6.85	6.92
Voltage at P_{MPP}	V_{MPP}	[V]	28.17	28.46	28.74	29.01	29.29

¹ Measurement tolerances STC: ± 3 % (P_{MPP}); ± 10 % (I_{SC} , V_{OC} , I_{MPP} , V_{MPP})

² Measurement tolerances NOCT: ± 5 % (P_{MPP}); ± 10 % (I_{SC} , V_{OC} , I_{MPP} , V_{MPP})

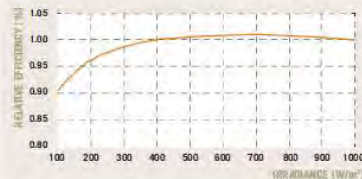
Q-CELLS PERFORMANCE WARRANTY



At least 97% of nominal power during first year. Thereafter max. 0.6% degradation per year.
At least 92% of nominal power after 10 years.
At least 83% of nominal power after 25 years.

All data with measurement tolerances.
Full product and performance warranties in accordance with the Q-CELLS warranties applicable in your country.

PERFORMANCE AT LOW IRRADIANCE



The typical change in module efficiency at an irradiance of 200 W/m² in relation to 1000 W/m² (both at 25 °C and AM 1.5 G spectrum) is -4 % (relative).

TEMPERATURE COEFFICIENTS (AT 1000 W/m², 25 °C, AM 1.5 G SPECTRUM)

Temperature Coefficient of I_{SC}	α	[%/K]	+0.04	Temperature Coefficient of V_{OC}	β	[%/K]	-0.32
Temperature Coefficient of P_{MPP}	γ	[%/K]	-0.46				

PROPERTIES FOR SYSTEM DESIGN

Maximum System Voltage V_{SYS}	[V]	1000	Safety Class	II
Maximum Reverse Current I_R	[A]	20	Fire Rating	C
Wind/Snow Load (in accordance with IEC 61215)	[Pa]	5400	Permitted module temperature on continuous duty	-40 °C up to +85 °C

QUALIFICATIONS AND CERTIFICATES

VDE Quality Tested, IEC 61215 (Ed.2); IEC 61730 (Ed.1), Application class A
This data sheet complies with DIN EN 50380.



PARTNER

NOTE: Installation instructions must be followed. See the installation and operating manual or contact the technical service for further information on approved installation and use of this product.

Q-CELLS SE

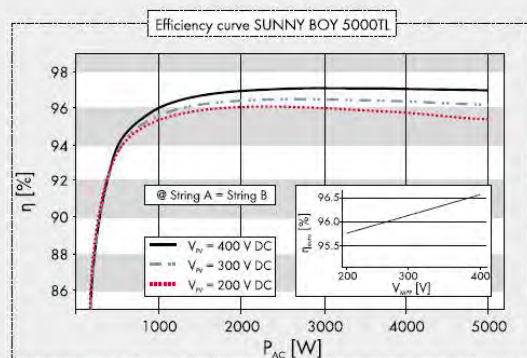
OT Thalheim, Sonnenallee 17–21
06766 Bitterfeld-Wolfen, Germany

TEL +49 (0)3494 66 99-23444
FAX +49 (0)3494 66 99-23000

EMAIL sales@q-cells.com
WEB www.q-cells.com



Technical data	Sunny Boy 3000TL	Sunny Boy 4000TL	Sunny Boy 4000TL/V	Sunny Boy 5000TL
Input (DC)				
Max. DC power (@ $\cos \phi = 1$)	3200 W	4200 W	4200 W	5300 W
Max. DC voltage	550 V	550 V	550 V	550 V
MPP voltage range	188 V - 440 V	175 V - 440 V	175 V - 440 V	175 V - 440 V
DC nominal voltage	400 V	400 V	400 V	400 V
Min. DC voltage / start voltage	125 V / 150 V	125 V / 150 V	125 V / 150 V	125 V / 150 V
Max. input current / per string	17 A / 17 A	2 x 15 A / 15 A	2 x 15 A / 15 A	2 x 15 A / 15 A
Number of MPP trackers / strings per MPP tracker	1 / 2	2 / A: 2, B: 2	2 / A: 2, B: 2	2 / A: 2, B: 2
Output (AC)				
AC nominal power (@ 230 V, 50 Hz)	3000 W	4000 W	3680 W	4600 W
Max. AC apparent power	3000 VA	4000 VA	4000 VA	5000 VA
Nominal AC voltage; range	220, 230, 240 V; 180 - 280 V	220, 230, 240 V; 180 - 280 V	220, 230, 240 V; 180 - 280 V	220, 230, 240 V; 180 - 280 V
AC grid frequency; range	50, 60 Hz; ± 5 Hz	50, 60 Hz; ± 5 Hz	50, 60 Hz; ± 5 Hz	50, 60 Hz; ± 5 Hz
Max. output current	16 A	22 A	22 A	22 A
Power factor ($\cos \phi$)	1	1	1	1
Phase conductors / connection phases	1 / 1	1 / 1	1 / 1	1 / 1
Efficiency				
Max. efficiency / Euro-eta	97.0 % / 96.3 %	97.0 % / 96.4 %	97.0 % / 96.4 %	97.0 % / 96.5 %
Protection devices				
DC reverse-polarity protection	●	●	●	●
ESS switch-disconnector	●	●	●	●
AC short circuit protection	●	●	●	●
Ground fault monitoring	●	●	●	●
Grid monitoring (SMA Grid Guard)	●	●	●	●
Galvanically isolated / all-pole sensitive fault current monitoring unit	-/●	-/●	-/●	-/●
Protection class / overvoltage category	I / III	I / III	I / III	I / III
General data				
Dimensions (W / H / D) in mm	470 / 445 / 180	470 / 445 / 180	470 / 445 / 180	470 / 445 / 180
Weight	22 kg	25 kg	25 kg	25 kg
Operating temperature range	-25 °C ... +60 °C	-25 °C ... +60 °C	-25 °C ... +60 °C	-25 °C ... +60 °C
Noise emission (typical)	≤ 25 dB(A)	≤ 29 dB(A)	≤ 29 dB(A)	≤ 29 dB(A)
Internal consumption (night)	< 0.5 W	< 0.5 W	< 0.5 W	< 0.5 W
Topology	transformerless	transformerless	transformerless	transformerless
Cooling concept	Convection	OptiCool	OptiCool	OptiCool
Electronics protection rating / connection area (as per IEC 60529)	IP65 / IP54	IP65 / IP54	IP65 / IP54	IP65 / IP54
Climatic category (per IEC 60721-3-4)	4K4H	4K4H	4K4H	4K4H
Features				
DC connection: SUNCLIX	●	●	●	●
AC connection: screw terminal / plug connector / spring-type terminal	-/●	-/●	-/●	-/●
Display: text line / graphic	-/●	-/●	-/●	-/●
Interfaces: RS485 / Bluetooth®	○/●	○/●	○/●	○/●
Warranty: 5 / 10 / 15 / 20 / 25 years	●/○/○/○/○	●/○/○/○/○	●/○/○/○/○	●/○/○/○/○
certificates and permits (more available on request)	CE, VDE 0126-1-1, DK 5940, RD 661, RD 1663, G83/1-1, PPC, AS4777, EN 50438*, C10/C11, PPDS, KEMCO (only SB 3000TL-20)			
* Does not apply to all national deviations of EN 50438				
● Standard features ○ Optional features - not available Data at nominal conditions				
Type designation	SB 3000TL-20	SB 4000TL-20	SB 4000TL-20/V 0159	SB 5000TL-20



Accessories



RS485 interface
DM-485CB-10

Appendix G: NASA insolation Data for Durban



ATMOSPHERIC
SCIENCE
DATA CENTER

NASA Surface meteorology and Solar Energy -
Available Tables



Latitude -29.867 / Longitude 30.967 was chosen.

Parameters for Sizing and Pointing of Solar Panels and for Solar Thermal Applications:

Monthly Averaged Insolation Incident On A Horizontal Surface (kWh/m ² /day)													
Lat -29.867	Jan	Feb	Mar	Apr	May	Jun	Jul	Aug	Sep	Oct	Nov	Dec	Annual Average
Lon 30.967													
22-year Average	5.67	5.51	5.03	4.40	3.81	3.40	3.65	4.25	4.84	4.93	5.30	5.69	4.70

Minimum And Maximum Difference From Monthly Averaged Insolation (%)													
Lat -29.867	Jan	Feb	Mar	Apr	May	Jun	Jul	Aug	Sep	Oct	Nov	Dec	
Lon 30.967													
Minimum	-11	-19	-14	-15	-12	-14	-19	-18	-20	-21	-23	-18	
Maximum	14	12	16	21	12	9	13	9	15	17	18	16	

Parameters for Tilted Solar Panels:

Monthly Averaged Radiation Incident On An Equator-Pointed Tilted Surface (kWh/m ² /day)													
Lat -29.867	Jan	Feb	Mar	Apr	May	Jun	Jul	Aug	Sep	Oct	Nov	Dec	Annual Average
Lon 30.967													
SSE HRZ	5.67	5.51	5.03	4.40	3.81	3.40	3.65	4.25	4.84	4.93	5.30	5.69	4.70
K	0.47	0.50	0.53	0.58	0.63	0.64	0.65	0.62	0.56	0.47	0.45	0.46	0.55
Diffuse	2.61	2.30	1.84	1.31	0.87	0.72	0.76	1.07	1.59	2.17	2.53	2.67	1.70
Direct	4.47	4.79	5.08	5.59	6.18	6.15	6.38	6.10	5.40	4.18	4.06	4.39	5.23
Tilt 0	5.64	5.48	4.95	4.36	3.71	3.34	3.57	4.22	4.78	4.82	5.27	5.66	4.65
Tilt 14	5.53	5.52	5.23	4.94	4.53	4.27	4.48	4.96	5.18	4.92	5.21	5.51	5.02
Tilt 29	5.17	5.30	5.27	5.31	5.16	5.02	5.21	5.49	5.35	4.81	4.91	5.12	5.18
Tilt 44	4.58	4.85	5.05	5.39	5.50	5.48	5.63	5.71	5.23	4.47	4.39	4.51	5.07
Tilt 90	2.13	2.43	2.97	3.89	4.55	4.83	4.84	4.42	3.34	2.38	2.12	2.07	3.34
OPT	5.64	5.53	5.28	5.39	5.55	5.61	5.73	5.72	5.35	4.92	5.28	5.66	5.47
OPT ANG	0.00	9.00	24.0	40.0	52.0	57.0	55.0	47.0	30.0	14.0	2.00	0.00	27.6

http://eosweb.larc.nasa.gov/cgi-bin/sse/grid.cgi?&num=211061&lat=-29.867&submit=Submit&hgt=100&veg=6&sitelev=&email=marcntumba@yahoo.fr&step=2&p=grid_id&p=swv_dwn&p=exp_dif&p=avg_dnr&p=daylight&p=DLYRANGE&p=wspd50m&p=ws50_0_2&p=wspd10arpt&lon=30.967

Meteorology (Temperature):

Monthly Averaged Air Temperature At 10 m Above The Surface Of The Earth (°C)													
Lat -29.867 Lon 30.967	Jan	Feb	Mar	Apr	May	Jun	Jul	Aug	Sep	Oct	Nov	Dec	Annual Average
22-year Average	21.1	21.2	20.6	18.8	16.8	14.4	14.4	16.4	18.2	18.5	19.5	20.5	18.3
Minimum	17.5	17.6	17.0	15.1	13.1	10.7	10.5	12.2	13.9	14.6	15.7	16.9	14.5
Maximum	25.1	25.3	24.8	23.3	21.7	19.3	19.2	21.0	22.6	22.4	23.3	24.4	22.7

Average Daily Temperature Range (°C)												
Lat -29.867 Lon 30.967	Jan	Feb	Mar	Apr	May	Jun	Jul	Aug	Sep	Oct	Nov	Dec
22-year Average	7.61	7.64 *	7.77	8.19	8.63	8.66	8.63	8.84	8.65	7.83	7.69	7.52

Average Minimum, Maximum and Amplitude Of The Daily Mean Earth Temperature (°C)													
Lat -29.867 Lon 30.967	Jan	Feb	Mar	Apr	May	Jun	Jul	Aug	Sep	Oct	Nov	Dec	Annual Amplitude
Minimum	17.6	17.7	17.0	14.7	12.2	9.75	9.68	11.5	13.7	14.7	15.9	17.0	
Maximum	29.2	29.4	28.7	27.1	25.4	22.9	23.4	26.4	28.8	28.2	28.4	28.5	
Amplitude	5.79	5.86	5.84	6.16	6.57	6.58	6.86	7.44	7.53	6.73	6.29	5.75	9.90

Meteorology (Wind):

Monthly Averaged Wind Speed At 50 m Above The Surface Of The Earth (m/s)													
Lat -29.867 Lon 30.967	Jan	Feb	Mar	Apr	May	Jun	Jul	Aug	Sep	Oct	Nov	Dec	Annual Average
10-year Average	4.73	4.41	4.43	4.55	4.63	5.23	5.25	5.48	5.77	5.47	5.07	4.70	4.98

Monthly Averaged Wind Speed At 10 m Above The Surface Of The Earth For Terrain Similar To Airports (m/s)													
Lat -29.867 Lon 30.967	Jan	Feb	Mar	Apr	May	Jun	Jul	Aug	Sep	Oct	Nov	Dec	Annual Average
10-year Average	3.74	3.48	3.50	3.60	3.66	4.13	4.15	4.33	4.55	4.32	4.01	3.71	3.93

http://eosweb.larc.nasa.gov/cgi-bin/sse/grid.cgi?&num=211061&lat=-29.867&submit=Submit&hgt=100&veg=6&sitelev=&email=marcntumba@yahoo.fr&step=2&p=grid_id&p=swv_dwn&p=exp_dif&p=avg_dnr&p=daylight&p=DLYRANGE&p=wspd50m&p=ws50_0_2&p=wspd10arpt&lon=30.967

Appendix H: Table 310.17 Allowable Ampacities of Single-Insulated Conductors Rated 0 Through 2000 Volts in Free Air, Based on Ambient Air Temperature of 30°C (86°F)

Size AWG or kcmil	Temperature Rating of Conductor [See Table 310.13(A).]						Size AWG or kcmil
	60°C (140°F)	75°C (167°F)	90°C (194°F)	60°C (140°F)	75°C (167°F)	90°C (194°F)	
	Types TW, UF	Types RHW, THHW, THW, THWN, XHHW, ZW	Types TBS, SA, SIS, FEP, FEPB, MI, RHH, RHW-2, THHN, THHW, THW-2, THWN-2, USE-2, XHH, XHHW, XHHW-2, ZW-2	Types TW, UF	Types RHW, THHW, THW, THWN, XHHW	Types TBS, SA, SIS, THHN, THHW, THW-2, THWN-2, RHH, RHW-2, USE-2, XHH, XHHW, XHHW-2, ZW-2	
COPPER			ALUMINUM OR COPPER-CLAD ALUMINUM				
18			18				
16			24				
14	25	30	35				
12	30	35	40	25	30	35	12
10	40	50	55	35	40	40	10
8	60	70	80	45	55	60	8
6	80	95	105	60	75	80	6
4	105	125	140	80	100	110	4
3	120	145	165	95	115	130	3
2	140	170	190	110	135	150	2
1	165	195	220	130	155	175	1
1/0	195	230	260	150	180	205	1/0
2/0	225	265	300	175	210	235	2/0
3/0	260	310	350	200	240	275	3/0
4/0	300	360	405	235	280	315	4/0
250	340	405	455	265	315	355	250
300	375	445	505	290	350	395	300
350	420	505	570	330	395	445	350
400	455	545	615	355	425	480	400
500	515	620	700	405	485	545	500
600	575	690	780	455	540	615	600
700	630	755	855	500	595	675	700
750	655	785	885	515	620	700	750
800	680	815	920	535	645	725	800
900	730	870	985	580	700	785	900
1000	780	935	1055	625	750	845	1000
1250	890	1065	1200	710	855	960	1250
1500	980	1175	1325	795	950	1075	1500
1750	1070	1280	1445	875	1050	1185	1750
2000	1155	1385	1560	960	1150	1335	2000



2008 Edition NATIONAL ELECTRICAL CODE

Copyright National Fire Protection Association
 Provided by IHS under license with NFPA

Licensee=Aramco HQ/9980755100

No reproduction or networking permitted without license from IHS

Not for Resale, 09/23/2007 23:20:41 MDT

CORRECTION FACTORS							
Ambient Temp. (°C)	For ambient temperatures other than 30°C (86°F), multiply the allowable ampacities shown above by the appropriate factor shown below.						Ambient Temp. (°C)
21-25	1.08	1.05	1.04	1.08	1.05	1.04	70-77
26-30	1.00	1.00	1.00	1.00	1.00	1.00	78-86
31-35	0.91	0.94	0.96	0.91	0.94	0.96	87-95
36-40	0.82	0.88	0.91	0.82	0.88	0.91	96-104
41-45	0.71	0.82	0.87	0.71	0.82	0.87	105-113
46-50	0.58	0.75	0.82	0.58	0.75	0.82	114-122
51-55	0.41	0.67	0.76	0.41	0.67	0.76	123-131
56-60		0.58	0.71		0.58	0.71	132-140
61-70		0.33	0.58		0.33	0.58	141-158
71-80			0.41			0.41	159-176



2008 Edition NATIONAL ELECTRICAL CODE

Copyright National Fire Protection Association
 Provided by IHS under license with NFPA
 No reproduction or networking permitted without license from IHS

Licensee=Aramco HQ/9980755100
 Not for Resale, 09/23/2007 23:20:41 MDT

Appendix I: NEC 240.6 Standard Ampere Ratings

Fuses and Fixed-Trip Circuit Breakers. The standard ampere ratings for fuses and inverse time circuit breakers shall be considered 15, 20, 25, 30, 35, 40, 45, 50, 60, 70, 80, 90, 100, 110, 125, 150, 175, 200, 225, 250, 300, 350, 400, 450, 500, 600, 700, 800, 1000, 1200, 1600, 2000, 2500, 3000, 4000, 5000, and 6000 amperes. Additional standard ampere ratings for fuses shall be 1, 3, 6, 10, and 601. The use of fuses and inverse time circuit breakers with nonstandard ampere ratings shall be permitted.



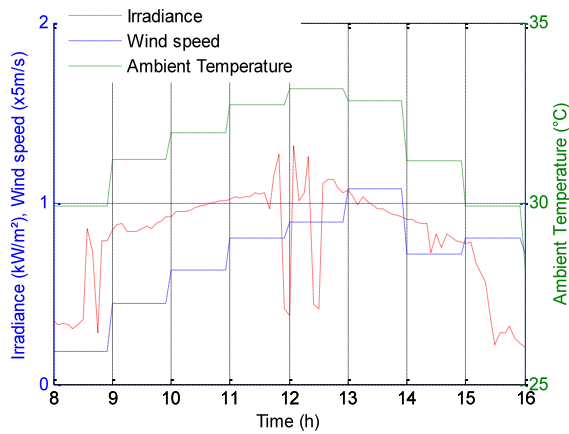
2008 Edition NATIONAL ELECTRICAL CODE

Copyright National Fire Protection Association
Provided by IHS under license with NFPA
No reproduction or networking permitted without license from IHS

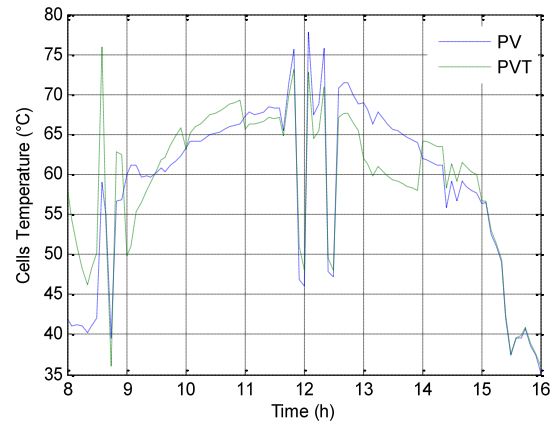
Licensee=Aramco HQ/9980755100
Not for Resale, 09/23/2007 23:20:41 MDT

Appendix J: Graphical results from simulation of PV and PVT arrays systems

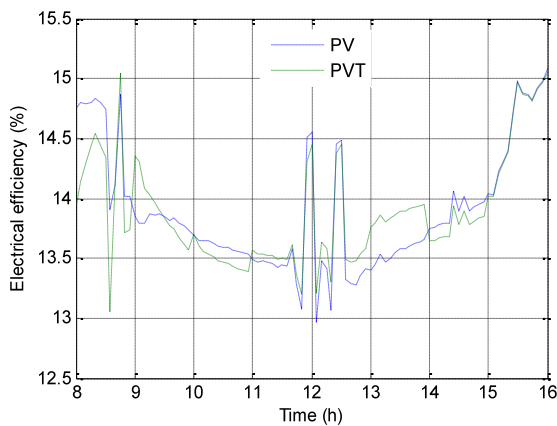
- The following are authors graphical results obtained for *summer day of 29 December 2010*



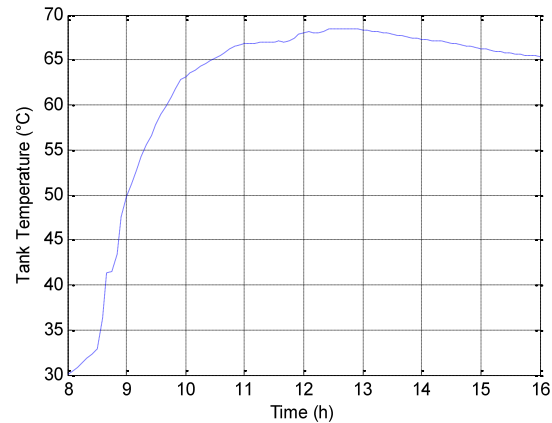
Environmental parameters for summer day of 29/12/2010



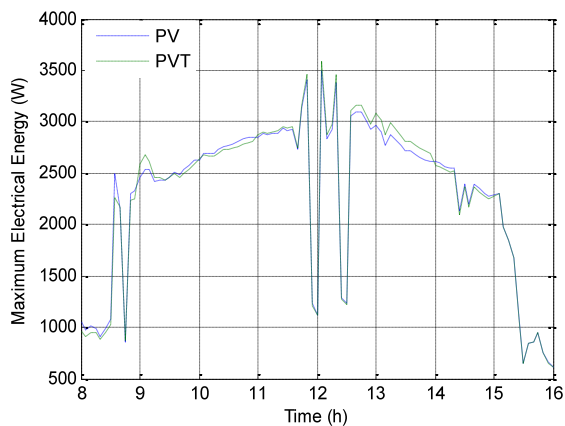
PV and PVT solar cell temperatures for summer day of 29/12/2010



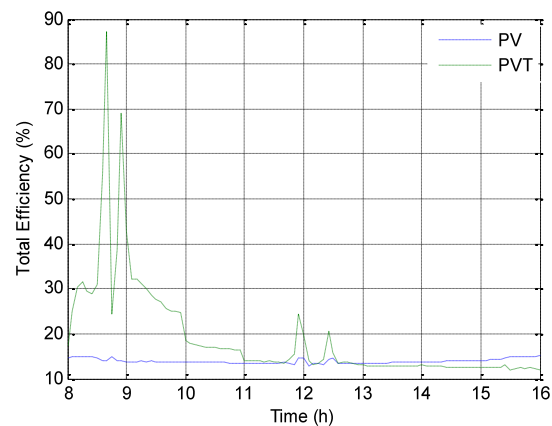
PV and PVT arrays electrical efficiencies for summer day of 29/12/2010



Tank water temperature for summer day of 29/12/2010

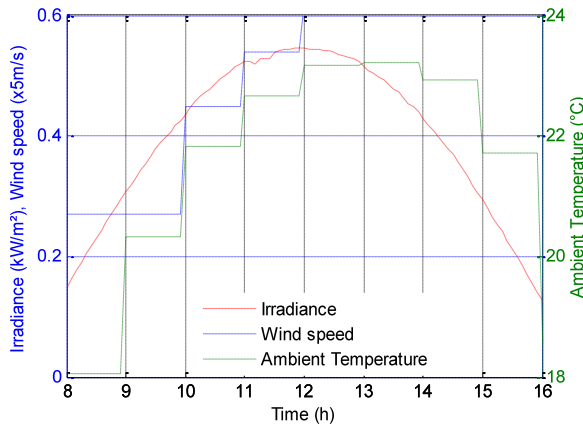


PV and PVT arrays MPP for summer day of 29/12/2010

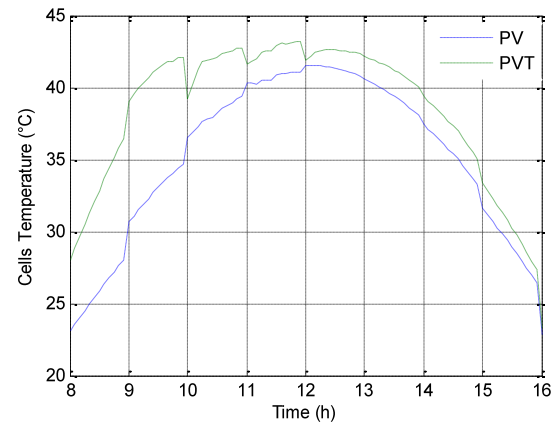


PV and PVT arrays total efficiency for summer day of 29/12/2010

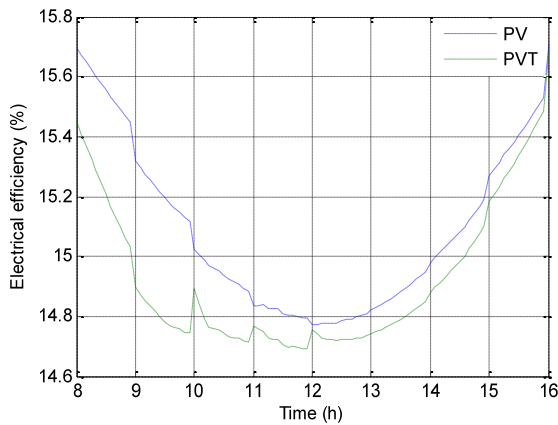
- The following are authors graphical results obtained for winter day of 14 June 2011



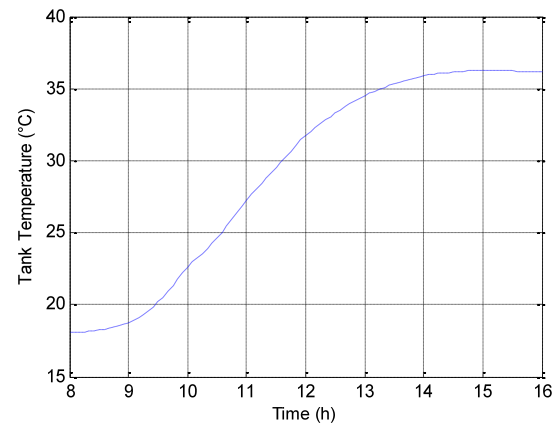
Environmental parameters for summer day of 14/06/2011



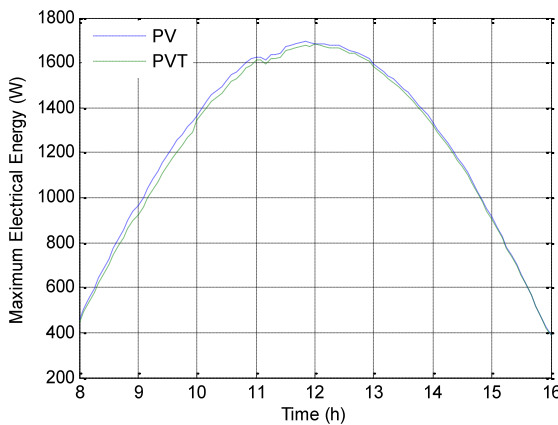
PV and PVT solar cell temperatures for summer day of 14/06/2011



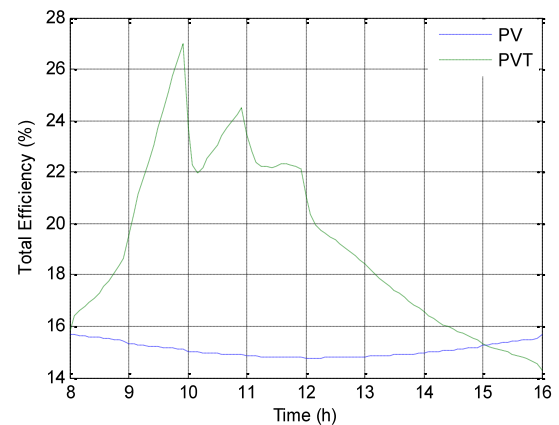
PV and PVT arrays electrical efficiencies for summer day of 14/06/2011



Tank water temperature for summer day of 14/06/2011

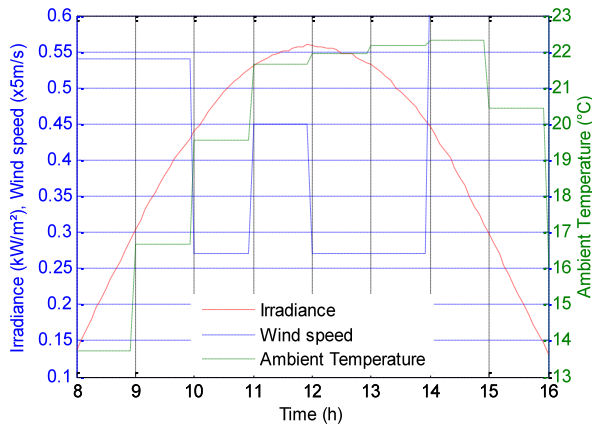


PV and PVT arrays MPP for summer day of 14/06/2011

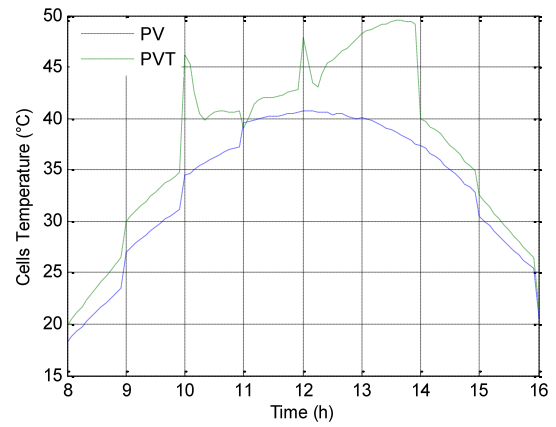


PV and PVT arrays total efficiency for summer day of 14/06/2011

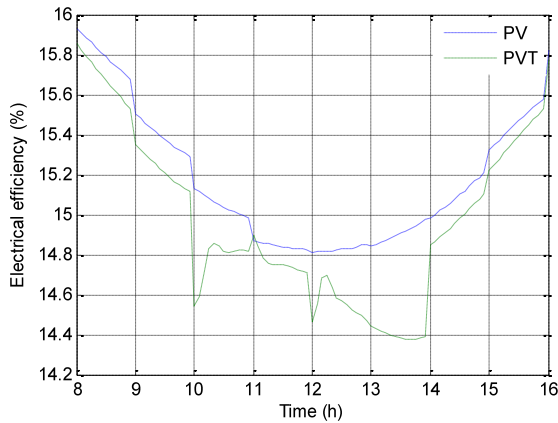
- The following are authors graphical results obtained for *winter day of 28 June 2011*



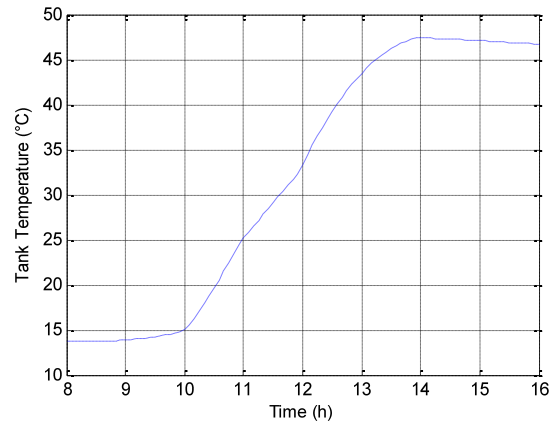
Environmental parameters for summer day of 28/06/2011



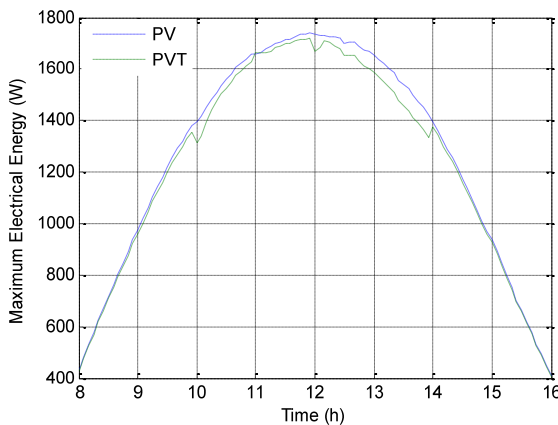
PV and PVT solar cell temperatures for summer day of 28/06/2011



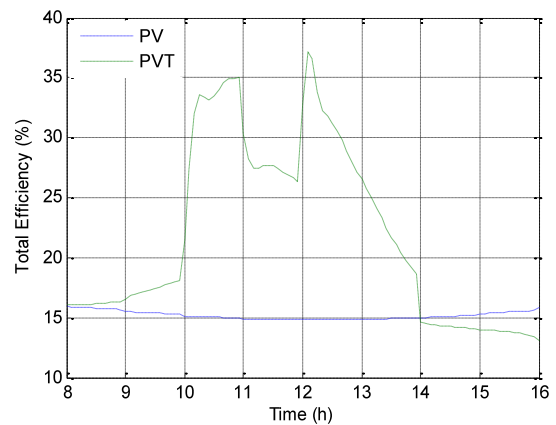
PV and PVT arrays electrical efficiencies for summer day of 28/06/2011



Tank water temperature for summer day of 28/06/2011



PV and PVT arrays MPP for summer day of 28/06/2011



PV and PVT arrays total efficiency for summer day of 28/06/2011

Appendix K: Numerical results from simulation of PV and PVT arrays systems for particular days

- The following *simulation data for the day of 04/12/2010* were obtained by the Author:

<i>Index</i>	<i>t</i>	<i>G</i>	<i>T_a</i>	<i>V_w</i>	<i>T_{pv}</i>	<i>T_{pvt}</i>	<i>E_{mpv}</i>	<i>E_{mpvt}</i>	<i>T_t</i>	<i>η_{pv}</i>	<i>η_{pvt}</i>
1.0e+003 *											
0.0010	0.0080	0.6291	0.0232	0.0032	0.0445	0.0482	1.9327	1.8951	0.0233	0.0146	0.0144
0.0020	0.0081	0.6458	0.0232	0.0032	0.0450	0.0484	1.9811	1.9473	0.0235	0.0146	0.0144
0.0030	0.0082	0.6628	0.0232	0.0032	0.0456	0.0475	2.0299	2.0105	0.0239	0.0146	0.0145
0.0040	0.0083	0.6541	0.0232	0.0032	0.0453	0.0460	2.0050	1.9980	0.0244	0.0146	0.0146
0.0050	0.0083	0.4221	0.0232	0.0032	0.0375	0.0375	1.3114	1.3109	0.0246	0.0150	0.0150
0.0060	0.0084	0.5330	0.0232	0.0032	0.0412	0.0422	1.6490	1.6403	0.0248	0.0148	0.0147
0.0070	0.0085	0.7033	0.0232	0.0032	0.0470	0.0490	2.1458	2.1238	0.0252	0.0145	0.0144
0.0080	0.0086	0.7771	0.0232	0.0032	0.0494	0.0507	2.3522	2.3366	0.0258	0.0144	0.0143
0.0090	0.0087	0.7241	0.0232	0.0032	0.0477	0.0471	2.2043	2.2110	0.0266	0.0145	0.0145
0.0100	0.0088	0.8543	0.0232	0.0032	0.0521	0.0496	2.5621	2.5940	0.0277	0.0142	0.0144
0.0110	0.0088	0.7618	0.0232	0.0032	0.0489	0.0454	2.3097	2.3517	0.0288	0.0144	0.0146
0.0120	0.0089	0.6884	0.0232	0.0032	0.0465	0.0426	2.1033	2.1445	0.0296	0.0145	0.0147
0.0130	0.0090	0.6061	0.0241	0.0032	0.0445	0.0419	1.8575	1.8821	0.0301	0.0146	0.0148
0.0140	0.0091	0.5038	0.0241	0.0032	0.0411	0.0403	1.5541	1.5605	0.0304	0.0148	0.0148
0.0150	0.0092	0.5754	0.0241	0.0032	0.0435	0.0440	1.7674	1.7624	0.0307	0.0147	0.0146
0.0160	0.0092	0.5286	0.0241	0.0032	0.0419	0.0429	1.6286	1.6204	0.0310	0.0148	0.0147
0.0170	0.0093	1.0234	0.0241	0.0032	0.0586	0.0604	2.9867	2.9592	0.0319	0.0139	0.0138
0.0180	0.0094	0.8261	0.0241	0.0032	0.0519	0.0510	2.4754	2.4873	0.0332	0.0143	0.0143
0.0190	0.0095	0.8436	0.0241	0.0032	0.0525	0.0470	2.5225	2.5942	0.0346	0.0142	0.0145
0.0200	0.0096	0.9033	0.0241	0.0032	0.0545	0.0472	2.6804	2.7817	0.0362	0.0141	0.0145
0.0210	0.0097	0.9210	0.0241	0.0032	0.0551	0.0477	2.7266	2.8309	0.0377	0.0141	0.0145
0.0220	0.0098	0.9324	0.0241	0.0032	0.0555	0.0482	2.7562	2.8605	0.0392	0.0141	0.0144
0.0230	0.0098	0.9410	0.0241	0.0032	0.0558	0.0487	2.7783	2.8809	0.0407	0.0141	0.0144
0.0240	0.0099	0.9513	0.0241	0.0032	0.0562	0.0493	2.8047	2.9042	0.0421	0.0140	0.0144
0.0250	0.0100	0.9595	0.0258	0.0036	0.0582	0.0498	2.7998	2.9230	0.0434	0.0139	0.0144
0.0260	0.0101	0.9745	0.0258	0.0036	0.0587	0.0509	2.8376	2.9539	0.0446	0.0139	0.0143
0.0270	0.0102	0.9819	0.0258	0.0036	0.0590	0.0517	2.8562	2.9649	0.0458	0.0139	0.0143
0.0280	0.0103	0.9871	0.0258	0.0036	0.0591	0.0523	2.8691	2.9714	0.0469	0.0139	0.0142
0.0290	0.0103	0.9856	0.0258	0.0036	0.0591	0.0529	2.8656	2.9592	0.0480	0.0139	0.0142
0.0300	0.0104	1.0084	0.0258	0.0036	0.0599	0.0540	2.9223	3.0116	0.0490	0.0139	0.0142
0.0310	0.0105	1.0128	0.0258	0.0036	0.0600	0.0547	2.9330	3.0155	0.0499	0.0139	0.0141
0.0320	0.0106	1.0155	0.0258	0.0036	0.0601	0.0552	2.9398	3.0157	0.0508	0.0138	0.0141
0.0330	0.0107	1.0284	0.0258	0.0036	0.0605	0.0560	2.9715	3.0420	0.0516	0.0138	0.0141
0.0340	0.0107	1.0375	0.0258	0.0036	0.0608	0.0567	2.9939	3.0589	0.0524	0.0138	0.0140
0.0350	0.0108	1.0368	0.0258	0.0036	0.0608	0.0571	2.9921	3.0503	0.0531	0.0138	0.0140
0.0360	0.0109	1.0429	0.0258	0.0036	0.0610	0.0577	3.0071	3.0592	0.0538	0.0138	0.0140
0.0370	0.0110	1.0464	0.0244	0.0032	0.0598	0.0593	3.0376	3.0441	0.0546	0.0139	0.0139
0.0380	0.0111	1.0528	0.0244	0.0032	0.0600	0.0596	3.0534	3.0600	0.0553	0.0139	0.0139
0.0390	0.0112	1.0559	0.0244	0.0032	0.0601	0.0598	3.0610	3.0662	0.0560	0.0138	0.0139
0.0400	0.0113	1.0609	0.0244	0.0032	0.0602	0.0602	3.0732	3.0734	0.0567	0.0138	0.0138
0.0410	0.0113	1.0628	0.0244	0.0032	0.0603	0.0607	3.0778	3.0715	0.0573	0.0138	0.0138
0.0420	0.0114	1.0642	0.0244	0.0032	0.0604	0.0612	3.0811	3.0682	0.0578	0.0138	0.0138

0.0430	0.0115	1.0672	0.0244	0.0032	0.0605	0.0616	3.0886	3.0698	0.0584	0.0138	0.0138
0.0440	0.0116	1.0718	0.0244	0.0032	0.0606	0.0621	3.0996	3.0757	0.0589	0.0138	0.0137
0.0450	0.0117	1.0729	0.0244	0.0032	0.0607	0.0624	3.1023	3.0737	0.0593	0.0138	0.0137
0.0460	0.0118	1.0677	0.0244	0.0032	0.0605	0.0626	3.0898	3.0561	0.0597	0.0138	0.0137
0.0470	0.0118	1.0735	0.0244	0.0032	0.0607	0.0630	3.1039	3.0656	0.0601	0.0138	0.0137
0.0480	0.0119	1.0694	0.0244	0.0032	0.0605	0.0632	3.0939	3.0513	0.0605	0.0138	0.0137
0.0490	0.0120	1.0733	0.0242	0.0032	0.0604	0.0634	3.1068	3.0595	0.0608	0.0138	0.0137
0.0500	0.0121	1.0729	0.0242	0.0032	0.0604	0.0636	3.1058	3.0548	0.0611	0.0138	0.0137
0.0510	0.0122	1.0718	0.0242	0.0032	0.0604	0.0637	3.1032	3.0489	0.0614	0.0138	0.0137
0.0520	0.0123	1.0711	0.0242	0.0032	0.0604	0.0639	3.1015	3.0442	0.0616	0.0138	0.0137
0.0530	0.0123	1.0608	0.0242	0.0032	0.0600	0.0638	3.0764	3.0161	0.0619	0.0139	0.0137
0.0540	0.0124	1.0620	0.0242	0.0032	0.0601	0.0640	3.0793	3.0161	0.0621	0.0138	0.0137
0.0550	0.0125	1.0544	0.0242	0.0032	0.0598	0.0639	3.0608	2.9952	0.0622	0.0139	0.0137
0.0560	0.0126	1.0567	0.0242	0.0032	0.0599	0.0641	3.0664	2.9985	0.0624	0.0139	0.0136
0.0570	0.0127	1.0469	0.0242	0.0032	0.0596	0.0639	3.0423	2.9727	0.0626	0.0139	0.0137
0.0580	0.0127	1.0436	0.0242	0.0032	0.0594	0.0640	3.0341	2.9627	0.0627	0.0139	0.0137
0.0590	0.0128	1.0280	0.0242	0.0032	0.0589	0.0636	2.9958	2.9229	0.0628	0.0139	0.0137
0.0600	0.0129	1.0219	0.0242	0.0032	0.0587	0.0635	2.9806	2.9061	0.0629	0.0139	0.0137
0.0610	0.0130	1.0360	0.0243	0.0036	0.0593	0.0613	3.0138	2.9820	0.0629	0.0139	0.0138
0.0620	0.0131	1.0378	0.0243	0.0036	0.0594	0.0615	3.0182	2.9851	0.0629	0.0139	0.0138
0.0630	0.0132	1.0117	0.0243	0.0036	0.0585	0.0607	2.9536	2.9194	0.0628	0.0139	0.0138
0.0640	0.0133	1.0032	0.0243	0.0036	0.0582	0.0605	2.9323	2.8977	0.0628	0.0139	0.0138
0.0650	0.0133	0.9943	0.0243	0.0036	0.0579	0.0602	2.9099	2.8749	0.0628	0.0140	0.0138
0.0660	0.0134	0.9834	0.0243	0.0036	0.0575	0.0599	2.8825	2.8473	0.0627	0.0140	0.0139
0.0670	0.0135	0.9801	0.0243	0.0036	0.0574	0.0598	2.8741	2.8388	0.0627	0.0140	0.0139
0.0680	0.0136	0.9684	0.0243	0.0036	0.0570	0.0594	2.8444	2.8090	0.0626	0.0140	0.0139
0.0690	0.0137	0.9476	0.0243	0.0036	0.0563	0.0588	2.7914	2.7560	0.0626	0.0140	0.0139
0.0700	0.0138	0.9456	0.0243	0.0036	0.0562	0.0587	2.7861	2.7508	0.0625	0.0140	0.0139
0.0710	0.0138	0.9382	0.0243	0.0036	0.0560	0.0585	2.7672	2.7319	0.0624	0.0141	0.0139
0.0720	0.0139	0.9340	0.0243	0.0036	0.0559	0.0583	2.7563	2.7210	0.0624	0.0141	0.0139
0.0730	0.0140	0.9160	0.0241	0.0036	0.0550	0.0575	2.7134	2.6779	0.0623	0.0141	0.0140
0.0740	0.0141	0.9002	0.0241	0.0036	0.0544	0.0570	2.6724	2.6374	0.0622	0.0141	0.0140
0.0750	0.0142	0.8232	0.0241	0.0036	0.0518	0.0545	2.4676	2.4344	0.0621	0.0143	0.0141
0.0760	0.0143	0.7734	0.0241	0.0036	0.0502	0.0527	2.3319	2.3017	0.0620	0.0143	0.0142
0.0770	0.0143	0.8553	0.0241	0.0036	0.0529	0.0553	2.5537	2.5220	0.0619	0.0142	0.0141
0.0780	0.0144	0.8427	0.0241	0.0036	0.0525	0.0550	2.5200	2.4874	0.0618	0.0142	0.0141
0.0790	0.0145	0.8283	0.0241	0.0036	0.0520	0.0545	2.4812	2.4490	0.0617	0.0143	0.0141
0.0800	0.0146	0.8069	0.0241	0.0036	0.0513	0.0538	2.4233	2.3920	0.0616	0.0143	0.0142
0.0810	0.0147	0.7988	0.0241	0.0036	0.0510	0.0535	2.4014	2.3707	0.0615	0.0143	0.0142
0.0820	0.0147	0.7832	0.0241	0.0036	0.0505	0.0530	2.3588	2.3287	0.0614	0.0143	0.0142
0.0830	0.0148	0.7638	0.0241	0.0036	0.0498	0.0523	2.3054	2.2763	0.0613	0.0144	0.0142
0.0840	0.0149	0.7500	0.0241	0.0036	0.0494	0.0518	2.2671	2.2388	0.0612	0.0144	0.0143
0.0850	0.0150	0.7411	0.0237	0.0036	0.0487	0.0511	2.2470	2.2190	0.0611	0.0144	0.0143
0.0860	0.0151	0.7363	0.0237	0.0036	0.0485	0.0509	2.2334	2.2058	0.0610	0.0144	0.0143
0.0870	0.0152	0.7176	0.0237	0.0036	0.0479	0.0503	2.1812	2.1544	0.0609	0.0145	0.0143
0.0880	0.0153	0.6951	0.0237	0.0036	0.0471	0.0495	2.1176	2.0920	0.0608	0.0145	0.0144
0.0890	0.0153	0.6165	0.0237	0.0036	0.0445	0.0468	1.8915	1.8693	0.0607	0.0146	0.0145
0.0900	0.0154	0.6359	0.0237	0.0036	0.0451	0.0473	1.9479	1.9266	0.0606	0.0146	0.0145
0.0910	0.0155	0.6108	0.0237	0.0036	0.0443	0.0465	1.8750	1.8541	0.0605	0.0146	0.0145
0.0920	0.0156	0.6814	0.0237	0.0036	0.0467	0.0488	2.0787	2.0555	0.0604	0.0145	0.0144
0.0930	0.0157	0.1622	0.0237	0.0036	0.0291	0.0310	0.4885	0.4834	0.0605	0.0154	0.0153
0.0940	0.0158	0.3120	0.0237	0.0036	0.0342	0.0357	0.9648	0.9570	0.0604	0.0151	0.0151
0.0950	0.0158	0.6469	0.0237	0.0036	0.0455	0.0472	1.9796	1.9621	0.0603	0.0146	0.0145
0.0960	0.0159	0.4473	0.0237	0.0036	0.0388	0.0407	1.3857	1.3717	0.0602	0.0149	0.0148
0.0970	0.0160	0.6251	0.0234	0.0032	0.0445	0.0486	1.9187	1.8792	0.0601	0.0146	0.0144

- The following *simulation data for the day of 29/12/2010* were obtained by the Author:

<i>Index</i>	<i>t</i>	<i>G</i>	<i>T_a</i>	<i>V_w</i>	<i>T_{pv}</i>	<i>T_{pvt}</i>	<i>E_{mpv}</i>	<i>E_{mpvt}</i>	<i>T_t</i>	<i>η_{pv}</i>	<i>η_{pvt}</i>
1.0e+003 *											
0.0010	0.0080	0.3535	0.0299	0.0009	0.0419	0.0580	1.0591	0.9665	0.0300	0.0148	0.0140
0.0020	0.0081	0.3272	0.0299	0.0009	0.0410	0.0543	0.9791	0.9080	0.0304	0.0148	0.0141
0.0030	0.0082	0.3369	0.0299	0.0009	0.0413	0.0511	1.0084	0.9548	0.0309	0.0148	0.0143
0.0040	0.0083	0.3292	0.0299	0.0009	0.0410	0.0482	0.9850	0.9467	0.0314	0.0148	0.0144
0.0050	0.0083	0.3057	0.0299	0.0009	0.0403	0.0463	0.9134	0.8832	0.0318	0.0148	0.0145
0.0060	0.0084	0.3283	0.0299	0.0009	0.0410	0.0482	0.9824	0.9437	0.0323	0.0148	0.0144
0.0070	0.0085	0.3584	0.0299	0.0009	0.0420	0.0503	1.0740	1.0261	0.0328	0.0147	0.0143
0.0080	0.0086	0.8614	0.0299	0.0009	0.0590	0.0760	2.4920	2.2678	0.0363	0.0139	0.0131
0.0090	0.0087	0.7361	0.0299	0.0009	0.0548	0.0539	2.1611	2.1712	0.0413	0.0141	0.0142
0.0100	0.0088	0.2876	0.0299	0.0009	0.0396	0.0360	0.8580	0.8753	0.0415	0.0149	0.0151
0.0110	0.0088	0.7910	0.0299	0.0009	0.0566	0.0629	2.3081	2.2320	0.0434	0.0140	0.0137
0.0120	0.0089	0.7966	0.0299	0.0009	0.0568	0.0624	2.3230	2.2544	0.0475	0.0140	0.0137
0.0130	0.0090	0.8537	0.0312	0.0022	0.0600	0.0499	2.4554	2.5882	0.0498	0.0139	0.0144
0.0140	0.0091	0.8856	0.0312	0.0022	0.0611	0.0510	2.5366	2.6741	0.0513	0.0138	0.0143
0.0150	0.0092	0.8871	0.0312	0.0022	0.0612	0.0553	2.5405	2.6195	0.0528	0.0138	0.0141
0.0160	0.0092	0.8419	0.0312	0.0022	0.0596	0.0566	2.4250	2.4646	0.0542	0.0139	0.0140
0.0170	0.0093	0.8463	0.0312	0.0022	0.0598	0.0579	2.4363	2.4604	0.0555	0.0139	0.0140
0.0180	0.0094	0.8428	0.0312	0.0022	0.0597	0.0589	2.4273	2.4370	0.0567	0.0139	0.0139
0.0190	0.0095	0.8565	0.0312	0.0022	0.0601	0.0603	2.4626	2.4599	0.0578	0.0138	0.0138
0.0200	0.0096	0.8769	0.0312	0.0022	0.0608	0.0617	2.5145	2.5020	0.0589	0.0138	0.0138
0.0210	0.0097	0.8632	0.0312	0.0022	0.0604	0.0621	2.4798	2.4567	0.0599	0.0138	0.0137
0.0220	0.0098	0.8856	0.0312	0.0022	0.0611	0.0636	2.5368	2.5035	0.0608	0.0138	0.0137
0.0230	0.0098	0.9034	0.0312	0.0022	0.0617	0.0647	2.5817	2.5398	0.0618	0.0138	0.0136
0.0240	0.0099	0.9226	0.0312	0.0022	0.0624	0.0657	2.6297	2.5820	0.0628	0.0137	0.0136
0.0250	0.0100	0.9283	0.0319	0.0032	0.0633	0.0631	2.6338	2.6363	0.0632	0.0137	0.0137
0.0260	0.0101	0.9522	0.0319	0.0032	0.0641	0.0651	2.6926	2.6781	0.0636	0.0136	0.0136
0.0270	0.0102	0.9536	0.0319	0.0032	0.0641	0.0659	2.6960	2.6700	0.0639	0.0136	0.0136
0.0280	0.0103	0.9540	0.0319	0.0032	0.0641	0.0663	2.6970	2.6660	0.0643	0.0136	0.0135
0.0290	0.0103	0.9658	0.0319	0.0032	0.0645	0.0669	2.7259	2.6919	0.0646	0.0136	0.0135
0.0300	0.0104	0.9801	0.0319	0.0032	0.0650	0.0674	2.7607	2.7249	0.0649	0.0136	0.0135
0.0310	0.0105	0.9850	0.0319	0.0032	0.0652	0.0677	2.7724	2.7352	0.0652	0.0136	0.0135
0.0320	0.0106	0.9896	0.0319	0.0032	0.0653	0.0679	2.7835	2.7445	0.0655	0.0136	0.0135
0.0330	0.0107	0.9983	0.0319	0.0032	0.0656	0.0683	2.8045	2.7637	0.0658	0.0136	0.0134
0.0340	0.0107	1.0093	0.0319	0.0032	0.0660	0.0688	2.8309	2.7886	0.0661	0.0136	0.0134
0.0350	0.0108	1.0141	0.0319	0.0032	0.0662	0.0690	2.8424	2.7988	0.0664	0.0135	0.0134
0.0360	0.0109	1.0174	0.0319	0.0032	0.0663	0.0692	2.8501	2.8048	0.0667	0.0135	0.0134
0.0370	0.0110	1.0243	0.0327	0.0040	0.0673	0.0657	2.8545	2.8792	0.0668	0.0135	0.0136
0.0380	0.0111	1.0370	0.0327	0.0040	0.0677	0.0664	2.8845	2.9058	0.0668	0.0135	0.0135
0.0390	0.0112	1.0303	0.0327	0.0040	0.0675	0.0663	2.8686	2.8875	0.0669	0.0135	0.0135
0.0400	0.0113	1.0361	0.0327	0.0040	0.0677	0.0665	2.8824	2.9012	0.0669	0.0135	0.0135
0.0410	0.0113	1.0405	0.0327	0.0040	0.0678	0.0666	2.8926	2.9114	0.0669	0.0135	0.0135
0.0420	0.0114	1.0599	0.0327	0.0040	0.0685	0.0672	2.9381	2.9587	0.0670	0.0134	0.0135
0.0430	0.0115	1.0522	0.0327	0.0040	0.0682	0.0670	2.9200	2.9395	0.0670	0.0134	0.0135
0.0440	0.0116	1.0563	0.0327	0.0040	0.0684	0.0671	2.9297	2.9492	0.0670	0.0134	0.0135
0.0450	0.0117	0.9715	0.0327	0.0040	0.0655	0.0648	2.7282	2.7383	0.0670	0.0136	0.0136
0.0460	0.0118	1.1444	0.0327	0.0040	0.0713	0.0698	3.1306	3.1573	0.0671	0.0133	0.0134
0.0470	0.0118	1.2714	0.0327	0.0040	0.0756	0.0731	3.4055	3.4541	0.0674	0.0131	0.0132
0.0480	0.0119	0.4201	0.0327	0.0040	0.0469	0.0510	1.2406	1.2131	0.0678	0.0145	0.0143
0.0490	0.0120	0.3816	0.0332	0.0045	0.0460	0.0481	1.1241	1.1116	0.0680	0.0145	0.0144

0.0500	0.0121	1.3189	0.0332	0.0045	0.0777	0.0728	3.4950	3.5902	0.0681	0.0130	0.0132
0.0510	0.0122	1.0165	0.0332	0.0045	0.0675	0.0644	2.8292	2.8767	0.0680	0.0135	0.0136
0.0520	0.0123	1.0560	0.0332	0.0045	0.0688	0.0655	2.9217	2.9749	0.0680	0.0134	0.0136
0.0530	0.0123	1.2618	0.0332	0.0045	0.0758	0.0710	3.3770	3.4658	0.0681	0.0131	0.0133
0.0540	0.0124	0.4361	0.0332	0.0045	0.0479	0.0495	1.2847	1.2731	0.0684	0.0145	0.0144
0.0550	0.0125	0.4175	0.0332	0.0045	0.0473	0.0480	1.2302	1.2255	0.0685	0.0145	0.0145
0.0560	0.0126	1.1125	0.0332	0.0045	0.0707	0.0672	3.0514	3.1109	0.0684	0.0133	0.0135
0.0570	0.0127	1.1322	0.0332	0.0045	0.0714	0.0676	3.0956	3.1594	0.0685	0.0133	0.0135
0.0580	0.0127	1.1342	0.0332	0.0045	0.0714	0.0676	3.1001	3.1664	0.0685	0.0133	0.0135
0.0590	0.0128	1.0893	0.0332	0.0045	0.0699	0.0664	2.9986	3.0568	0.0685	0.0134	0.0135
0.0600	0.0129	1.0563	0.0332	0.0045	0.0688	0.0655	2.9224	2.9747	0.0684	0.0134	0.0136
0.0610	0.0130	1.0715	0.0328	0.0054	0.0690	0.0620	2.9631	3.0768	0.0684	0.0134	0.0138
0.0620	0.0131	1.0467	0.0328	0.0054	0.0682	0.0613	2.9056	3.0149	0.0683	0.0134	0.0138
0.0630	0.0132	0.9913	0.0328	0.0054	0.0663	0.0599	2.7742	2.8710	0.0682	0.0135	0.0139
0.0640	0.0133	1.0360	0.0328	0.0054	0.0678	0.0609	2.8804	2.9881	0.0681	0.0135	0.0138
0.0650	0.0133	1.0101	0.0328	0.0054	0.0669	0.0603	2.8191	2.9203	0.0680	0.0135	0.0138
0.0660	0.0134	0.9898	0.0328	0.0054	0.0662	0.0598	2.7708	2.8677	0.0679	0.0135	0.0139
0.0670	0.0135	0.9697	0.0328	0.0054	0.0656	0.0593	2.7222	2.8150	0.0678	0.0136	0.0139
0.0680	0.0136	0.9691	0.0328	0.0054	0.0655	0.0592	2.7208	2.8136	0.0678	0.0136	0.0139
0.0690	0.0137	0.9523	0.0328	0.0054	0.0650	0.0588	2.6798	2.7691	0.0677	0.0136	0.0139
0.0700	0.0138	0.9428	0.0328	0.0054	0.0646	0.0586	2.6567	2.7443	0.0676	0.0136	0.0139
0.0710	0.0138	0.9324	0.0328	0.0054	0.0643	0.0583	2.6311	2.7165	0.0675	0.0136	0.0139
0.0720	0.0139	0.9234	0.0328	0.0054	0.0640	0.0581	2.6091	2.6928	0.0674	0.0137	0.0139
0.0730	0.0140	0.9146	0.0312	0.0036	0.0620	0.0642	2.6104	2.5805	0.0673	0.0138	0.0136
0.0740	0.0141	0.9094	0.0312	0.0036	0.0619	0.0641	2.5975	2.5665	0.0673	0.0138	0.0136
0.0750	0.0142	0.8977	0.0312	0.0036	0.0615	0.0638	2.5679	2.5364	0.0672	0.0138	0.0137
0.0760	0.0143	0.8882	0.0312	0.0036	0.0611	0.0634	2.5440	2.5126	0.0671	0.0138	0.0137
0.0770	0.0143	0.8904	0.0312	0.0036	0.0612	0.0635	2.5496	2.5184	0.0670	0.0138	0.0137
0.0780	0.0144	0.7291	0.0312	0.0036	0.0558	0.0584	2.1282	2.0987	0.0669	0.0141	0.0139
0.0790	0.0145	0.8293	0.0312	0.0036	0.0592	0.0613	2.3931	2.3653	0.0669	0.0139	0.0138
0.0800	0.0146	0.7555	0.0312	0.0036	0.0567	0.0591	2.1991	2.1709	0.0668	0.0140	0.0139
0.0810	0.0147	0.8296	0.0312	0.0036	0.0592	0.0614	2.3939	2.3654	0.0667	0.0139	0.0138
0.0820	0.0147	0.8120	0.0312	0.0036	0.0586	0.0609	2.3482	2.3189	0.0666	0.0139	0.0138
0.0830	0.0148	0.7959	0.0312	0.0036	0.0580	0.0604	2.3058	2.2770	0.0665	0.0140	0.0138
0.0840	0.0149	0.7850	0.0312	0.0036	0.0577	0.0600	2.2773	2.2490	0.0664	0.0140	0.0139
0.0850	0.0150	0.7815	0.0299	0.0040	0.0563	0.0566	2.2829	2.2792	0.0663	0.0140	0.0140
0.0860	0.0151	0.7876	0.0299	0.0040	0.0565	0.0566	2.2992	2.2976	0.0662	0.0140	0.0140
0.0870	0.0152	0.6696	0.0299	0.0040	0.0525	0.0530	1.9792	1.9742	0.0661	0.0142	0.0142
0.0880	0.0153	0.6239	0.0299	0.0040	0.0510	0.0513	1.8516	1.8488	0.0660	0.0143	0.0143
0.0890	0.0153	0.5643	0.0299	0.0040	0.0490	0.0494	1.6823	1.6786	0.0659	0.0144	0.0144
0.0900	0.0154	0.3590	0.0299	0.0040	0.0421	0.0426	1.0757	1.0724	0.0658	0.0147	0.0147
0.0910	0.0155	0.2200	0.0299	0.0040	0.0374	0.0376	0.6498	0.6490	0.0657	0.0150	0.0150
0.0920	0.0156	0.2829	0.0299	0.0040	0.0395	0.0396	0.8435	0.8428	0.0657	0.0149	0.0149
0.0930	0.0157	0.2873	0.0299	0.0040	0.0396	0.0399	0.8570	0.8560	0.0656	0.0149	0.0149
0.0940	0.0158	0.3175	0.0299	0.0040	0.0407	0.0408	0.9496	0.9486	0.0655	0.0148	0.0148
0.0950	0.0158	0.2554	0.0299	0.0040	0.0386	0.0389	0.7589	0.7576	0.0655	0.0149	0.0149
0.0960	0.0159	0.2222	0.0299	0.0040	0.0374	0.0376	0.6565	0.6558	0.0654	0.0150	0.0150
0.0970	0.0160	0.2055	0.0282	0.0036	0.0351	0.0359	0.6109	0.6080	0.0654	0.0151	0.0151

- The following *simulation data for the day of 14/06/2011* were obtained by the Author:

<i>Index</i>	<i>t</i>	<i>G</i>	<i>T_a</i>	<i>V_w</i>	<i>T_{pv}</i>	<i>T_{pvt}</i>	<i>E_{mpv}</i>	<i>E_{mpvt}</i>	<i>T_t</i>	<i>η_{pv}</i>	<i>η_{pvt}</i>
1.0e+003 *											
0.0010	0.0080	0.1487	0.0181	0.0014	0.0231	0.0280	0.4598	0.4473	0.0181	0.0157	0.0155
0.0020	0.0081	0.1631	0.0181	0.0014	0.0236	0.0289	0.5070	0.4923	0.0181	0.0157	0.0154
0.0030	0.0082	0.1771	0.0181	0.0014	0.0240	0.0296	0.5529	0.5360	0.0181	0.0156	0.0154
0.0040	0.0083	0.1906	0.0181	0.0014	0.0245	0.0305	0.5972	0.5780	0.0181	0.0156	0.0153
0.0050	0.0083	0.2041	0.0181	0.0014	0.0249	0.0313	0.6415	0.6198	0.0182	0.0156	0.0153
0.0060	0.0084	0.2175	0.0181	0.0014	0.0254	0.0321	0.6854	0.6610	0.0182	0.0156	0.0152
0.0070	0.0085	0.2305	0.0181	0.0014	0.0258	0.0329	0.7280	0.7009	0.0182	0.0156	0.0152
0.0080	0.0086	0.2442	0.0181	0.0014	0.0263	0.0336	0.7726	0.7427	0.0183	0.0155	0.0152
0.0090	0.0087	0.2580	0.0181	0.0014	0.0268	0.0344	0.8179	0.7851	0.0184	0.0155	0.0151
0.0100	0.0088	0.2709	0.0181	0.0014	0.0272	0.0351	0.8599	0.8243	0.0184	0.0155	0.0151
0.0110	0.0088	0.2830	0.0181	0.0014	0.0276	0.0358	0.8992	0.8610	0.0185	0.0155	0.0151
0.0120	0.0089	0.2952	0.0181	0.0014	0.0280	0.0364	0.9389	0.8981	0.0186	0.0154	0.0150
0.0130	0.0090	0.3067	0.0203	0.0014	0.0307	0.0391	0.9647	0.9224	0.0188	0.0153	0.0149
0.0140	0.0091	0.3183	0.0203	0.0014	0.0311	0.0396	1.0022	0.9579	0.0189	0.0153	0.0149
0.0150	0.0092	0.3310	0.0203	0.0014	0.0315	0.0399	1.0428	0.9971	0.0191	0.0153	0.0149
0.0160	0.0092	0.3435	0.0203	0.0014	0.0319	0.0403	1.0824	1.0352	0.0193	0.0153	0.0148
0.0170	0.0093	0.3547	0.0203	0.0014	0.0323	0.0407	1.1183	1.0698	0.0196	0.0152	0.0148
0.0180	0.0094	0.3665	0.0203	0.0014	0.0327	0.0411	1.1557	1.1059	0.0199	0.0152	0.0148
0.0190	0.0095	0.3782	0.0203	0.0014	0.0331	0.0414	1.1927	1.1418	0.0202	0.0152	0.0148
0.0200	0.0096	0.3891	0.0203	0.0014	0.0335	0.0416	1.2272	1.1756	0.0205	0.0152	0.0148
0.0210	0.0097	0.3983	0.0203	0.0014	0.0338	0.0418	1.2564	1.2048	0.0209	0.0152	0.0148
0.0220	0.0098	0.4062	0.0203	0.0014	0.0340	0.0418	1.2812	1.2301	0.0213	0.0151	0.0148
0.0230	0.0098	0.4175	0.0203	0.0014	0.0344	0.0421	1.3167	1.2651	0.0218	0.0151	0.0147
0.0240	0.0099	0.4253	0.0203	0.0014	0.0347	0.0421	1.3411	1.2900	0.0223	0.0151	0.0147
0.0250	0.0100	0.4352	0.0218	0.0022	0.0365	0.0392	1.3616	1.3428	0.0226	0.0150	0.0149
0.0260	0.0101	0.4464	0.0218	0.0022	0.0369	0.0402	1.3961	1.3725	0.0229	0.0150	0.0148
0.0270	0.0102	0.4579	0.0218	0.0022	0.0373	0.0413	1.4317	1.4024	0.0232	0.0150	0.0148
0.0280	0.0103	0.4672	0.0218	0.0022	0.0376	0.0418	1.4603	1.4290	0.0236	0.0150	0.0148
0.0290	0.0103	0.4726	0.0218	0.0022	0.0378	0.0419	1.4767	1.4456	0.0239	0.0150	0.0148
0.0300	0.0104	0.4779	0.0218	0.0022	0.0380	0.0419	1.4931	1.4626	0.0243	0.0150	0.0148
0.0310	0.0105	0.4855	0.0218	0.0022	0.0382	0.0421	1.5163	1.4860	0.0246	0.0149	0.0147
0.0320	0.0106	0.4953	0.0218	0.0022	0.0385	0.0424	1.5464	1.5159	0.0250	0.0149	0.0147
0.0330	0.0107	0.5005	0.0218	0.0022	0.0387	0.0424	1.5621	1.5323	0.0255	0.0149	0.0147
0.0340	0.0107	0.5064	0.0218	0.0022	0.0389	0.0425	1.5801	1.5510	0.0259	0.0149	0.0147
0.0350	0.0108	0.5142	0.0218	0.0022	0.0392	0.0427	1.6037	1.5749	0.0264	0.0149	0.0147
0.0360	0.0109	0.5192	0.0218	0.0022	0.0394	0.0428	1.6189	1.5908	0.0268	0.0149	0.0147
0.0370	0.0110	0.5235	0.0227	0.0027	0.0403	0.0417	1.6249	1.6139	0.0273	0.0148	0.0148
0.0380	0.0111	0.5232	0.0227	0.0027	0.0403	0.0418	1.6240	1.6114	0.0277	0.0148	0.0148
0.0390	0.0112	0.5193	0.0227	0.0027	0.0402	0.0420	1.6122	1.5974	0.0280	0.0148	0.0148
0.0400	0.0113	0.5278	0.0227	0.0027	0.0405	0.0425	1.6378	1.6209	0.0284	0.0148	0.0147
0.0410	0.0113	0.5279	0.0227	0.0027	0.0405	0.0426	1.6382	1.6208	0.0288	0.0148	0.0147
0.0420	0.0114	0.5286	0.0227	0.0027	0.0405	0.0426	1.6403	1.6229	0.0291	0.0148	0.0147
0.0430	0.0115	0.5385	0.0227	0.0027	0.0408	0.0430	1.6700	1.6519	0.0295	0.0148	0.0147
0.0440	0.0116	0.5419	0.0227	0.0027	0.0410	0.0431	1.6803	1.6623	0.0299	0.0148	0.0147
0.0450	0.0117	0.5427	0.0227	0.0027	0.0410	0.0430	1.6826	1.6649	0.0303	0.0148	0.0147
0.0460	0.0118	0.5442	0.0227	0.0027	0.0410	0.0431	1.6872	1.6696	0.0307	0.0148	0.0147
0.0470	0.0118	0.5463	0.0227	0.0027	0.0411	0.0432	1.6934	1.6755	0.0311	0.0148	0.0147
0.0480	0.0119	0.5459	0.0227	0.0027	0.0411	0.0432	1.6921	1.6740	0.0314	0.0148	0.0147
0.0490	0.0120	0.5451	0.0232	0.0032	0.0416	0.0419	1.6853	1.6821	0.0318	0.0148	0.0148

0.0500	0.0121	0.5447	0.0232	0.0032	0.0416	0.0422	1.6841	1.6786	0.0320	0.0148	0.0147
0.0510	0.0122	0.5439	0.0232	0.0032	0.0415	0.0424	1.6819	1.6739	0.0323	0.0148	0.0147
0.0520	0.0123	0.5426	0.0232	0.0032	0.0415	0.0425	1.6781	1.6690	0.0326	0.0148	0.0147
0.0530	0.0123	0.5418	0.0232	0.0032	0.0415	0.0426	1.6757	1.6658	0.0328	0.0148	0.0147
0.0540	0.0124	0.5421	0.0232	0.0032	0.0415	0.0427	1.6764	1.6660	0.0331	0.0148	0.0147
0.0550	0.0125	0.5386	0.0232	0.0032	0.0413	0.0426	1.6660	1.6553	0.0333	0.0148	0.0147
0.0560	0.0126	0.5351	0.0232	0.0032	0.0412	0.0425	1.6555	1.6445	0.0335	0.0148	0.0147
0.0570	0.0127	0.5336	0.0232	0.0032	0.0412	0.0425	1.6510	1.6395	0.0337	0.0148	0.0147
0.0580	0.0127	0.5305	0.0232	0.0032	0.0411	0.0425	1.6419	1.6300	0.0339	0.0148	0.0147
0.0590	0.0128	0.5276	0.0232	0.0032	0.0410	0.0424	1.6331	1.6208	0.0341	0.0148	0.0147
0.0600	0.0129	0.5229	0.0232	0.0032	0.0408	0.0423	1.6188	1.6063	0.0343	0.0148	0.0147
0.0610	0.0130	0.5155	0.0232	0.0032	0.0406	0.0422	1.5962	1.5834	0.0345	0.0148	0.0147
0.0620	0.0131	0.5093	0.0232	0.0032	0.0404	0.0420	1.5776	1.5645	0.0347	0.0148	0.0148
0.0630	0.0132	0.5041	0.0232	0.0032	0.0402	0.0419	1.5617	1.5483	0.0348	0.0148	0.0148
0.0640	0.0133	0.4979	0.0232	0.0032	0.0400	0.0417	1.5431	1.5295	0.0350	0.0148	0.0148
0.0650	0.0133	0.4928	0.0232	0.0032	0.0399	0.0416	1.5276	1.5137	0.0351	0.0149	0.0148
0.0660	0.0134	0.4853	0.0232	0.0032	0.0396	0.0414	1.5049	1.4909	0.0352	0.0149	0.0148
0.0670	0.0135	0.4781	0.0232	0.0032	0.0394	0.0412	1.4829	1.4688	0.0354	0.0149	0.0148
0.0680	0.0136	0.4733	0.0232	0.0032	0.0392	0.0411	1.4685	1.4542	0.0355	0.0149	0.0148
0.0690	0.0137	0.4645	0.0232	0.0032	0.0389	0.0408	1.4417	1.4275	0.0356	0.0149	0.0148
0.0700	0.0138	0.4544	0.0232	0.0032	0.0386	0.0405	1.4105	1.3965	0.0357	0.0149	0.0148
0.0710	0.0138	0.4485	0.0232	0.0032	0.0384	0.0403	1.3925	1.3784	0.0357	0.0149	0.0148
0.0720	0.0139	0.4402	0.0232	0.0032	0.0381	0.0400	1.3671	1.3531	0.0358	0.0149	0.0148
0.0730	0.0140	0.4291	0.0229	0.0032	0.0374	0.0394	1.3349	1.3212	0.0359	0.0150	0.0149
0.0740	0.0141	0.4189	0.0229	0.0032	0.0371	0.0391	1.3034	1.2899	0.0359	0.0150	0.0149
0.0750	0.0142	0.4095	0.0229	0.0032	0.0368	0.0388	1.2743	1.2611	0.0360	0.0150	0.0149
0.0760	0.0143	0.3994	0.0229	0.0032	0.0364	0.0384	1.2427	1.2298	0.0360	0.0150	0.0149
0.0770	0.0143	0.3886	0.0229	0.0032	0.0361	0.0380	1.2092	1.1968	0.0361	0.0150	0.0149
0.0780	0.0144	0.3787	0.0229	0.0032	0.0357	0.0377	1.1782	1.1661	0.0361	0.0151	0.0150
0.0790	0.0145	0.3697	0.0229	0.0032	0.0354	0.0374	1.1501	1.1384	0.0362	0.0151	0.0150
0.0800	0.0146	0.3586	0.0229	0.0032	0.0350	0.0370	1.1153	1.1041	0.0362	0.0151	0.0150
0.0810	0.0147	0.3457	0.0229	0.0032	0.0346	0.0365	1.0747	1.0641	0.0362	0.0151	0.0150
0.0820	0.0147	0.3317	0.0229	0.0032	0.0341	0.0360	1.0309	1.0209	0.0362	0.0151	0.0151
0.0830	0.0148	0.3186	0.0229	0.0032	0.0337	0.0355	0.9893	0.9799	0.0362	0.0152	0.0151
0.0840	0.0149	0.3063	0.0229	0.0032	0.0333	0.0350	0.9504	0.9415	0.0362	0.0152	0.0151
0.0850	0.0150	0.2936	0.0217	0.0032	0.0316	0.0334	0.9160	0.9076	0.0362	0.0153	0.0152
0.0860	0.0151	0.2797	0.0217	0.0032	0.0312	0.0328	0.8718	0.8640	0.0362	0.0153	0.0152
0.0870	0.0152	0.2658	0.0217	0.0032	0.0307	0.0323	0.8270	0.8199	0.0362	0.0153	0.0152
0.0880	0.0153	0.2519	0.0217	0.0032	0.0302	0.0318	0.7827	0.7762	0.0362	0.0153	0.0153
0.0890	0.0153	0.2405	0.0217	0.0032	0.0298	0.0313	0.7460	0.7400	0.0362	0.0154	0.0153
0.0900	0.0154	0.2268	0.0217	0.0032	0.0294	0.0308	0.7019	0.6965	0.0362	0.0154	0.0153
0.0910	0.0155	0.2134	0.0217	0.0032	0.0289	0.0303	0.6589	0.6541	0.0362	0.0154	0.0153
0.0920	0.0156	0.2000	0.0217	0.0032	0.0285	0.0297	0.6156	0.6113	0.0362	0.0154	0.0154
0.0930	0.0157	0.1849	0.0217	0.0032	0.0280	0.0291	0.5669	0.5632	0.0362	0.0155	0.0154
0.0940	0.0158	0.1699	0.0217	0.0032	0.0275	0.0286	0.5188	0.5156	0.0362	0.0155	0.0154
0.0950	0.0158	0.1550	0.0217	0.0032	0.0270	0.0280	0.4709	0.4682	0.0362	0.0155	0.0155
0.0960	0.0159	0.1394	0.0217	0.0032	0.0264	0.0273	0.4207	0.4185	0.0362	0.0155	0.0155
0.0970	0.0160	0.1267	0.0186	0.0036	0.0228	0.0233	0.3872	0.3862	0.0361	0.0157	0.0157

- The following *simulation data for the day of 28/06/2011* were obtained by the Author:

<i>Index</i>	<i>t</i>	<i>G</i>	<i>T_a</i>	<i>V_w</i>	<i>T_{pv}</i>	<i>T_{pvt}</i>	<i>E_{mpv}</i>	<i>E_{mpvt}</i>	<i>T_t</i>	<i>η_{pv}</i>	<i>η_{pvt}</i>
1.0e+003 *											
0.0010	0.0080	0.1371	0.0137	0.0027	0.0183	0.0199	0.4324	0.4288	0.0137	0.0159	0.0159
0.0020	0.0081	0.1514	0.0137	0.0027	0.0188	0.0205	0.4801	0.4759	0.0137	0.0159	0.0158
0.0030	0.0082	0.1664	0.0137	0.0027	0.0193	0.0211	0.5301	0.5250	0.0137	0.0159	0.0158
0.0040	0.0083	0.1799	0.0137	0.0027	0.0198	0.0217	0.5753	0.5694	0.0137	0.0159	0.0158
0.0050	0.0083	0.1943	0.0137	0.0027	0.0203	0.0224	0.6236	0.6168	0.0137	0.0158	0.0157
0.0060	0.0084	0.2082	0.0137	0.0027	0.0207	0.0230	0.6701	0.6624	0.0138	0.0158	0.0157
0.0070	0.0085	0.2227	0.0137	0.0027	0.0212	0.0236	0.7185	0.7098	0.0138	0.0158	0.0157
0.0080	0.0086	0.2357	0.0137	0.0027	0.0217	0.0241	0.7619	0.7522	0.0138	0.0158	0.0156
0.0090	0.0087	0.2483	0.0137	0.0027	0.0221	0.0247	0.8041	0.7934	0.0138	0.0157	0.0156
0.0100	0.0088	0.2613	0.0137	0.0027	0.0225	0.0253	0.8476	0.8358	0.0138	0.0157	0.0156
0.0110	0.0088	0.2743	0.0137	0.0027	0.0230	0.0258	0.8906	0.8778	0.0138	0.0157	0.0156
0.0120	0.0089	0.2887	0.0137	0.0027	0.0235	0.0264	0.9385	0.9244	0.0138	0.0157	0.0155
0.0130	0.0090	0.3042	0.0167	0.0027	0.0269	0.0300	0.9752	0.9601	0.0139	0.0155	0.0154
0.0140	0.0091	0.3173	0.0167	0.0027	0.0274	0.0305	1.0178	1.0016	0.0139	0.0155	0.0153
0.0150	0.0092	0.3309	0.0167	0.0027	0.0278	0.0310	1.0621	1.0451	0.0140	0.0155	0.0153
0.0160	0.0092	0.3438	0.0167	0.0027	0.0283	0.0315	1.1042	1.0862	0.0140	0.0154	0.0153
0.0170	0.0093	0.3556	0.0167	0.0027	0.0287	0.0319	1.1423	1.1234	0.0141	0.0154	0.0153
0.0180	0.0094	0.3669	0.0167	0.0027	0.0291	0.0324	1.1788	1.1590	0.0142	0.0154	0.0152
0.0190	0.0095	0.3790	0.0167	0.0027	0.0295	0.0329	1.2178	1.1970	0.0143	0.0154	0.0152
0.0200	0.0096	0.3912	0.0167	0.0027	0.0299	0.0333	1.2570	1.2351	0.0143	0.0154	0.0152
0.0210	0.0097	0.4021	0.0167	0.0027	0.0302	0.0337	1.2920	1.2693	0.0144	0.0153	0.0152
0.0220	0.0098	0.4109	0.0167	0.0027	0.0305	0.0340	1.3202	1.2969	0.0145	0.0153	0.0151
0.0230	0.0098	0.4206	0.0167	0.0027	0.0309	0.0344	1.3512	1.3272	0.0146	0.0153	0.0151
0.0240	0.0099	0.4292	0.0167	0.0027	0.0312	0.0347	1.3786	1.3540	0.0148	0.0153	0.0151
0.0250	0.0100	0.4413	0.0196	0.0014	0.0345	0.0461	1.3964	1.3134	0.0151	0.0151	0.0145
0.0260	0.0101	0.4481	0.0196	0.0014	0.0347	0.0452	1.4175	1.3417	0.0156	0.0151	0.0146
0.0270	0.0102	0.4593	0.0196	0.0014	0.0351	0.0425	1.4526	1.3974	0.0163	0.0151	0.0147
0.0280	0.0103	0.4686	0.0196	0.0014	0.0354	0.0405	1.4815	1.4433	0.0171	0.0151	0.0148
0.0290	0.0103	0.4780	0.0196	0.0014	0.0357	0.0399	1.5107	1.4787	0.0180	0.0151	0.0149
0.0300	0.0104	0.4864	0.0196	0.0014	0.0360	0.0402	1.5368	1.5038	0.0188	0.0151	0.0148
0.0310	0.0105	0.4945	0.0196	0.0014	0.0362	0.0407	1.5617	1.5268	0.0197	0.0150	0.0148
0.0320	0.0106	0.5017	0.0196	0.0014	0.0365	0.0408	1.5838	1.5494	0.0206	0.0150	0.0148
0.0330	0.0107	0.5089	0.0196	0.0014	0.0367	0.0407	1.6061	1.5738	0.0215	0.0150	0.0148
0.0340	0.0107	0.5148	0.0196	0.0014	0.0369	0.0406	1.6241	1.5940	0.0225	0.0150	0.0148
0.0350	0.0108	0.5194	0.0196	0.0014	0.0371	0.0406	1.6384	1.6097	0.0234	0.0150	0.0148
0.0360	0.0109	0.5254	0.0196	0.0014	0.0373	0.0407	1.6566	1.6280	0.0244	0.0150	0.0148
0.0370	0.0110	0.5317	0.0217	0.0022	0.0396	0.0390	1.6579	1.6629	0.0252	0.0149	0.0149
0.0380	0.0111	0.5343	0.0217	0.0022	0.0397	0.0401	1.6659	1.6624	0.0259	0.0149	0.0148
0.0390	0.0112	0.5386	0.0217	0.0022	0.0398	0.0413	1.6788	1.6660	0.0265	0.0149	0.0148
0.0400	0.0113	0.5412	0.0217	0.0022	0.0399	0.0418	1.6868	1.6705	0.0271	0.0149	0.0148
0.0410	0.0113	0.5454	0.0217	0.0022	0.0401	0.0420	1.6993	1.6829	0.0278	0.0148	0.0148
0.0420	0.0114	0.5479	0.0217	0.0022	0.0402	0.0420	1.7068	1.6910	0.0285	0.0148	0.0148
0.0430	0.0115	0.5503	0.0217	0.0022	0.0402	0.0420	1.7139	1.6984	0.0291	0.0148	0.0148
0.0440	0.0116	0.5513	0.0217	0.0022	0.0403	0.0421	1.7171	1.7012	0.0298	0.0148	0.0147
0.0450	0.0117	0.5541	0.0217	0.0022	0.0404	0.0423	1.7255	1.7085	0.0304	0.0148	0.0147
0.0460	0.0118	0.5568	0.0217	0.0022	0.0405	0.0425	1.7335	1.7153	0.0311	0.0148	0.0147
0.0470	0.0118	0.5569	0.0217	0.0022	0.0405	0.0426	1.7338	1.7147	0.0317	0.0148	0.0147
0.0480	0.0119	0.5596	0.0217	0.0022	0.0406	0.0429	1.7418	1.7213	0.0323	0.0148	0.0147
0.0490	0.0120	0.5576	0.0219	0.0014	0.0408	0.0478	1.7336	1.6713	0.0333	0.0148	0.0145

0.0500	0.0121	0.5566	0.0219	0.0014	0.0407	0.0459	1.7305	1.6851	0.0344	0.0148	0.0146
0.0510	0.0122	0.5567	0.0219	0.0014	0.0407	0.0434	1.7309	1.7074	0.0356	0.0148	0.0147
0.0520	0.0123	0.5548	0.0219	0.0014	0.0407	0.0431	1.7251	1.7040	0.0366	0.0148	0.0147
0.0530	0.0123	0.5542	0.0219	0.0014	0.0406	0.0443	1.7235	1.6913	0.0375	0.0148	0.0146
0.0540	0.0124	0.5536	0.0219	0.0014	0.0406	0.0454	1.7215	1.6795	0.0384	0.0148	0.0146
0.0550	0.0125	0.5467	0.0219	0.0014	0.0404	0.0457	1.7010	1.6553	0.0392	0.0148	0.0146
0.0560	0.0126	0.5475	0.0219	0.0014	0.0404	0.0461	1.7032	1.6541	0.0401	0.0148	0.0145
0.0570	0.0127	0.5478	0.0219	0.0014	0.0404	0.0466	1.7042	1.6510	0.0408	0.0148	0.0145
0.0580	0.0127	0.5425	0.0219	0.0014	0.0402	0.0468	1.6883	1.6318	0.0416	0.0148	0.0145
0.0590	0.0128	0.5376	0.0219	0.0014	0.0401	0.0472	1.6736	1.6132	0.0423	0.0148	0.0145
0.0600	0.0129	0.5354	0.0219	0.0014	0.0400	0.0477	1.6669	1.6017	0.0429	0.0149	0.0145
0.0610	0.0130	0.5319	0.0222	0.0014	0.0401	0.0482	1.6544	1.5859	0.0435	0.0148	0.0144
0.0620	0.0131	0.5271	0.0222	0.0014	0.0400	0.0485	1.6399	1.5686	0.0441	0.0149	0.0144
0.0630	0.0132	0.5214	0.0222	0.0014	0.0398	0.0487	1.6227	1.5488	0.0446	0.0149	0.0144
0.0640	0.0133	0.5153	0.0222	0.0014	0.0396	0.0489	1.6042	1.5276	0.0451	0.0149	0.0144
0.0650	0.0133	0.5096	0.0222	0.0014	0.0394	0.0492	1.5870	1.5076	0.0455	0.0149	0.0144
0.0660	0.0134	0.4999	0.0222	0.0014	0.0390	0.0492	1.5576	1.4767	0.0459	0.0149	0.0144
0.0670	0.0135	0.4944	0.0222	0.0014	0.0389	0.0494	1.5407	1.4575	0.0462	0.0149	0.0144
0.0680	0.0136	0.4887	0.0222	0.0014	0.0387	0.0496	1.5236	1.4386	0.0465	0.0149	0.0144
0.0690	0.0137	0.4808	0.0222	0.0014	0.0384	0.0495	1.4995	1.4139	0.0468	0.0149	0.0144
0.0700	0.0138	0.4728	0.0222	0.0014	0.0381	0.0495	1.4747	1.3889	0.0470	0.0149	0.0144
0.0710	0.0138	0.4653	0.0222	0.0014	0.0379	0.0494	1.4518	1.3657	0.0472	0.0150	0.0144
0.0720	0.0139	0.4549	0.0222	0.0014	0.0375	0.0492	1.4200	1.3348	0.0474	0.0150	0.0144
0.0730	0.0140	0.4468	0.0223	0.0032	0.0374	0.0400	1.3938	1.3752	0.0474	0.0150	0.0149
0.0740	0.0141	0.4364	0.0223	0.0032	0.0371	0.0397	1.3616	1.3428	0.0474	0.0150	0.0149
0.0750	0.0142	0.4220	0.0223	0.0032	0.0366	0.0392	1.3171	1.2993	0.0474	0.0150	0.0149
0.0760	0.0143	0.4129	0.0223	0.0032	0.0363	0.0389	1.2889	1.2716	0.0473	0.0150	0.0149
0.0770	0.0143	0.4030	0.0223	0.0032	0.0359	0.0385	1.2579	1.2413	0.0473	0.0151	0.0149
0.0780	0.0144	0.3893	0.0223	0.0032	0.0355	0.0380	1.2153	1.1997	0.0473	0.0151	0.0150
0.0790	0.0145	0.3752	0.0223	0.0032	0.0350	0.0374	1.1711	1.1564	0.0473	0.0151	0.0150
0.0800	0.0146	0.3643	0.0223	0.0032	0.0346	0.0370	1.1369	1.1229	0.0473	0.0151	0.0150
0.0810	0.0147	0.3508	0.0223	0.0032	0.0342	0.0365	1.0942	1.0811	0.0472	0.0151	0.0150
0.0820	0.0147	0.3353	0.0223	0.0032	0.0336	0.0359	1.0456	1.0335	0.0472	0.0152	0.0151
0.0830	0.0148	0.3249	0.0223	0.0032	0.0333	0.0354	1.0124	1.0010	0.0472	0.0152	0.0151
0.0840	0.0149	0.3116	0.0223	0.0032	0.0328	0.0349	0.9705	0.9599	0.0471	0.0152	0.0151
0.0850	0.0150	0.2982	0.0204	0.0032	0.0305	0.0325	0.9370	0.9270	0.0471	0.0153	0.0152
0.0860	0.0151	0.2840	0.0204	0.0032	0.0300	0.0320	0.8915	0.8823	0.0471	0.0153	0.0153
0.0870	0.0152	0.2706	0.0204	0.0032	0.0296	0.0314	0.8482	0.8398	0.0470	0.0154	0.0153
0.0880	0.0153	0.2547	0.0204	0.0032	0.0290	0.0308	0.7971	0.7896	0.0470	0.0154	0.0153
0.0890	0.0153	0.2402	0.0204	0.0032	0.0285	0.0302	0.7502	0.7436	0.0470	0.0154	0.0153
0.0900	0.0154	0.2253	0.0204	0.0032	0.0280	0.0296	0.7020	0.6961	0.0469	0.0154	0.0154
0.0910	0.0155	0.2142	0.0204	0.0032	0.0277	0.0292	0.6658	0.6604	0.0469	0.0155	0.0154
0.0920	0.0156	0.1997	0.0204	0.0032	0.0272	0.0286	0.6188	0.6141	0.0469	0.0155	0.0154
0.0930	0.0157	0.1865	0.0204	0.0032	0.0267	0.0280	0.5761	0.5719	0.0468	0.0155	0.0154
0.0940	0.0158	0.1728	0.0204	0.0032	0.0263	0.0275	0.5318	0.5283	0.0468	0.0155	0.0155
0.0950	0.0158	0.1609	0.0204	0.0032	0.0259	0.0270	0.4932	0.4901	0.0468	0.0156	0.0155
0.0960	0.0159	0.1470	0.0204	0.0032	0.0254	0.0264	0.4484	0.4457	0.0467	0.0156	0.0155
0.0970	0.0160	0.1312	0.0161	0.0032	0.0205	0.0215	0.4072	0.4050	0.0467	0.0158	0.0158

Appendix L: Annual Cash Flow for Systems

The annual cash flow for each system for the PV system with the utility cost of electricity increasing by 5% each year over twenty years:

Year	Loan Balance	Loan Payment	Loan Interest	Delta Pay	Delta tax	Annual Cost	PV cost (R/kWh)	Utility (R/kWh)	Savings (R/yr)
0	83160.78	8787.68	7068.67	1719.01	1571.36	7216.32	0.85	0.94	756.67
1	81441.77	8787.68	6922.55	1865.13	1538.88	7248.80	0.85	0.98	1122.84
2	79576.64	8787.68	6764.01	2023.67	1503.64	7284.04	0.86	1.03	1506.18
3	77552.97	8787.68	6592.00	2195.68	1465.40	7322.28	0.86	1.08	1907.45
4	75357.29	8787.68	6405.37	2382.31	1423.91	7363.77	0.87	1.14	2327.45
5	72974.98	8787.68	6202.87	2584.81	1378.90	7408.78	0.87	1.20	2766.99
6	70390.17	8787.68	5983.16	2804.52	1330.06	7457.62	0.88	1.26	3226.94
7	67585.66	8787.68	5744.78	3042.90	1277.06	7510.62	0.88	1.32	3708.18
8	64542.76	8787.68	5486.13	3301.55	1219.57	7568.11	0.89	1.38	4211.62
9	61241.21	8787.68	5205.50	3582.18	1157.18	7630.50	0.90	1.45	4738.22
10	57659.03	8787.68	4901.02	3886.66	1089.50	7698.18	0.90	1.53	5288.97
11	53772.37	8787.68	4570.65	4217.03	1016.06	7771.62	0.91	1.60	5864.89
12	49555.34	8787.68	4212.20	4575.48	936.37	7851.31	0.92	1.68	6467.03
13	44979.86	8787.68	3823.29	4964.39	849.92	7937.76	0.93	1.77	7096.49
14	40015.47	8787.68	3401.31	5386.37	756.11	8031.57	0.94	1.86	7754.40
15	34629.10	8787.68	2943.47	5844.21	654.33	8133.35	0.96	1.95	8441.92
16	28784.90	8787.68	2446.72	6340.96	543.91	8243.78	0.97	2.05	9160.26
17	22443.93	8787.68	1907.73	6879.95	424.09	8363.59	0.98	2.15	9910.64
18	15563.99	8787.68	1322.94	7464.74	294.09	8493.59	1.00	2.26	10694.35
19	8099.24	8787.68	688.44	8099.24	153.04	8634.64	1.01	2.37	11512.70
20	0.00	0.00	0.00	0.00	0.00	0.00	0.00	2.49	21154.71

The annual cash flow for each system for the PVT system with the utility cost of electricity increasing by 5% each year over twenty years:

Year	Loan Balance	Loan Payment	Loan Interest	Delta Pay	Delta tax	Annual Cost	PV cost (R/kWh)	Utility (R/kWh)	Savings (R/yr)
0	127250.88	13446.72	10816.32	2630.40	2404.47	11042.26	0.91	0.94	304.30
1	124620.48	13446.72	10592.74	2853.98	2354.77	11091.96	0.92	0.98	821.94
2	121766.50	13446.72	10350.15	3096.57	2300.84	11145.89	0.92	1.03	1363.72
3	118669.92	13446.72	10086.94	3359.78	2242.33	11204.40	0.93	1.08	1930.71
4	115310.14	13446.72	9801.36	3645.36	2178.84	11267.88	0.93	1.14	2523.99
5	111664.78	13446.72	9491.51	3955.22	2109.96	11336.76	0.94	1.20	3144.72
6	107709.56	13446.72	9155.31	4291.41	2035.23	11411.50	0.94	1.26	3794.07
7	103418.15	13446.72	8790.54	4656.18	1954.14	11492.59	0.95	1.32	4473.27
8	98761.97	13446.72	8394.77	5051.96	1866.16	11580.57	0.96	1.38	5183.60
9	93710.01	13446.72	7965.35	5481.37	1770.70	11676.03	0.96	1.45	5926.36
10	88228.64	13446.72	7499.43	5947.29	1667.12	11779.60	0.97	1.53	6702.92
11	82281.35	13446.72	6993.91	6452.81	1554.75	11891.98	0.98	1.60	7514.69
12	75828.54	13446.72	6445.43	7001.30	1432.82	12013.91	0.99	1.68	8363.10
13	68827.24	13446.72	5850.32	7596.41	1300.53	12146.20	1.00	1.77	9249.68
14	61230.83	13446.72	5204.62	8242.10	1156.99	12289.74	1.01	1.86	10175.94
15	52988.73	13446.72	4504.04	8942.68	1001.25	12445.48	1.03	1.95	11143.50
16	44046.05	13446.72	3743.91	9702.81	832.27	12614.45	1.04	2.05	12153.99
17	34343.24	13446.72	2919.17	10527.55	648.93	12797.79	1.06	2.15	13209.08
18	23815.69	13446.72	2024.33	11422.39	450.01	12996.72	1.07	2.26	14310.52
19	12393.29	13446.72	1053.43	12393.29	234.18	13212.55	1.09	2.37	15460.06
20	0.00	0.00	0.00	0.00	0.00	0.00	0.00	2.49	30106.64